# Three-Dimensional Study of Annular Chamber Mufflers using Green's Function Method

Harshad Nitin Keskar

A Thesis Submitted to

Indian Institute of Technology Hyderabad

In Partial Fulfillment of the Requirements for

The Degree of Master of Technology



भारतीय प्रौद्योगिकी संस्थान हैदराबाद
Indian Institute of Technology Hyderabad

Department of Mechanical and Aerospace Engineering

June 2016

# Declaration

I declare that this written submission represents my ideas in my own words, and where ideas or words of others have been included, I have adequately cited and referenced the original sources. I also declare that I have adhered to all principles of academic honesty and integrity and have not misrepresented or fabricated or falsified any idea/data/fact/source in my submission. I understand that any violation of the above will be a cause for disciplinary action by the Institute and can also evoke penal action from the sources that have thus not been properly cited, or from whom proper permission has not been taken when needed.
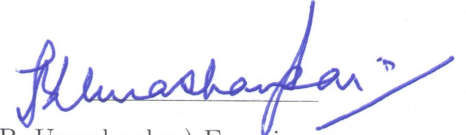
(Signature)

HARSHAD . N . KESKAR

(Harshad Nitin Keskar)

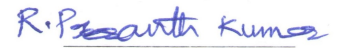MEI4MTECH11027

(Roll No.)

# Approval Sheet

This Thesis entitled Three-Dimensional Study of Annular Chamber Mufflers using Green's Function Method by Harshad Nitin Keskar is approved for the degree of Master of Technology from IIT Hyderabad

(Dr. B. Umashankar) Examiner
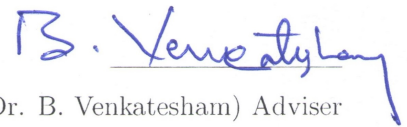Dept. of Civil Engg.
IITH

(Dr. R. Prasanth Kumar) Examiner
Dept. of Mechanical and Aerospace Engg.
IITH

(Dr. B. Venkatesham) Adviser
Dept. of Mechanical and Aerospace Engg.
IITH

# Acknowledgements

*Dedicated to my loving parents*

# Abstract

A major area of interest in a muffler design is in its acoustic and flow performance. Other parameters in design are weight, availability of space and reliability of operation. Transmission Loss (TL) and Insertion Loss (IL) of a muffler are good indicators of acoustical performance. These values are computed by using methods such as one-dimensional transfer matrix, two-dimensional mode matching method, Green's function method, Finite-Element Method (FEM) and Boundary Element Method (BEM). Pressure drops across muffler influence its functioning. It is known that acoustic and flow performance parameters are contradicting. An efficient muffler design should have a minimum pressure drop and as high transmission loss as possible. Extended Inlet and Extended Outlet (EIEO) muffler has a wider frequency band acoustical performance as compared to a Simple Expansion Chamber (SEC). A methodology is developed for EIEO muffler to optimize both acoustic and flow parameters using one-dimensional study.

This study works well for low to medium operating frequencies. As the chamber parameters change, one-dimensional analysis is not alone sufficient. The high-frequency waves, due to their short wavelength, tend to travel in all the three directions. The plane-wave assumption does not hold for short chamber mufflers. To get more accurate results, a three-dimensional methodology is more suitable. An EIEO muffler can be considered as a combination of circular and annular cavities. Literature to estimate the transmission loss of circular cavity, analytically using Green's function has already been deveoped. Thus, an analytical approach for the transmission loss characteristics of an annular cavity with arbitrary locations of inlet and outlet ports has been established in this thesis. The analytically obtained results for various configurations are validated numerically using FEM software. The analytical resluts were found to be in good agreement with those obtained using fininte element method.

# Contents

# List of Figures

# List of Tables

1

# Nomenclature

**Chapter 1**

$\lambda$      Wavelength in m

$c$      Speed of sound in m/s

$f$      Frequency in Hz

$k$      Waveumber in m$^{-1}$

$M$      Mach number

$T$      Absolute temperature

$W_i$      Incident power in W

$W_t$      Transmitted power in W

$Y_a, Y_b$   Characteristic impedance in m$^{-1}$s$^{-1}$

**Chapter 2**

$a, b$      Constants relating $C_1$ and $C_2$

$C_1$      Constant used for $x/d$

$C_2$      Constant used for $y/x$

$D$      Chamber diameter in mm

$d$      Pipe diameter in mm

$l_a$      Extended inlet length in mm

$l_b$      Extended outlet length in mm

$l_g$      Acoustic gap length in mm

$p_1$      Acoustic pressure at the inlet

$p_2$      Acoustic pressure at the outlet

$q$      Velocity ratio

$U_0$      Mean flow velocity in m/s

$v_1$       Volume velocity at the inlet

$v_2$       Volume velocity at the outlet

$x$       Axial position

$x_{max}$       Maximum core jet length in mm

$y$       Normalized jet height

**Chapter 3**

$\delta$       Face port location

$\omega$       Natural frequency in rad/s

$\phi$       Velocity potential

$\Psi$       Mode function

$a$       Inner diameter of cavity

$a_1$       Half major axis length of inlet port

$a_2$       Half major axis length of outlet port

$b$       Outer diameter of cavity

$b_1$       Half minor axis length of inlet port

$b_2$       Half minor axis length of outlet port

$k_{zp}$       Axial wavenumber

$L$       Cavity length

$m$       Circumferential mode order

$n$       Radial mode order

$P$       Acoustic pressure

$p$       Axial mode order

$u_1$       Hypothetical velocity of inlet piston

$u_2$       Hypothetical velocity of outlet piston

# Chapter 1

# Introduction

## 1.1 Basic concepts of acoustics

A few basic terms and concepts that will be useful throughout the thesis are defined in this section. An acoustic wave can be typically described using five variables. They are wavelength, speed of propagation, amplitude, frequency and wavenumber. The speed of propagation is the speed at which an acoustic wave propagates through a medium. The speed of propagation depends only on the medium through which it propagates and the environmental conditions. The wavelength is the spatial period of the wave. The frequency is defined as the number of oscillations occurring in one second. The frequency, speed of propagation and wavelength are related to one another. This relation is given in Eq. 1.1. The amplitude is the magnitude of oscillation of the wave. The wavenumber is the spatial periodicity of the wave. It is expressed in units of reciprocal of meters. The wavenumber can be calculated from Eq. 1.2.

$$c = f\lambda \qquad \text{(m/s)} \tag{1.1}$$

$$k = \frac{2\pi}{\lambda} \qquad (\text{m}^{-1}) \tag{1.2}$$

where $c$ is the speed of sound, $f$ is the frequency and $k$ is the wavenumber.

The speed of sound in air varies with temperature given by Eq. 1.3

$$c = 20.05\sqrt{T} \qquad \text{(m/s)} \tag{1.3}$$

## 1.2 Measurement of muffler acoustic performance

Mufflers are well known noise control solution along the path. The acoustical performance of a muffler is measured in three ways: insertion loss, transmission loss and noise reduction. Insertion loss is the difference of sound pressure levels before and after a muffler is installed in the system. Transmission loss gives the loss of acoustic power of a wave as it travels through a muffler. Noise reduction is the comparison of the sound pressure levels of a point upstream of the muffler and a point downstream of the muffler. Each of these performance standards will be explained in more

detail in further sections. Two more terms that are useful to define are acoustic impedance and characteristic acoustic impedance. Acoustic systems may be analysed as an equivalent impedance circuits, same as done for electrical circuits. Acoustic impedance represents the pressure change created by a wave divided by the volume velocity that is imparted to the medium by the same wave. Acoustic impedance is a property of the device that a wave is travelling in. The characteristic acoustic impedance is the ratio of the acoustic pressure to the acoustic mass velocity of a progressive wave.

### 1.2.1  Insertion loss

Insertion loss is defined as the reduction in sound power transmitted through a duct compared to that transmitted with no muffler in place [1].

$$IL = 20 \log_{10} \left( \frac{P_r}{P_m} \right) \qquad \text{(dB)} \tag{1.4}$$

where $IL$ is the insertion loss, $P_m$ is the measured sound pressure with the muffler installed and $P_r$ is the measured sound pressure without the muffler.

There are two main advantages in using IL as the standard of performance. The first advantage is that, for a given system, conceptually, IL is the actual performance of a muffler. It is the comparison of the duct system before and after the muffler is installed. It is simple to measure. The second advantage is that IL measurement is comparatively easy, and only requires one microphone [2].

The disadvantage of IL is that it is system dependent. Both the source impedance and the load impedance must be taken into consideration when predicting IL. This system dependence causes another disadvantage which is for the same muffler is used, the insertion loss can be different for different systems, different sources, and different loads.

### 1.2.2  Transmission loss

Transmission loss is defined as the ratio of incident sound power and transmitted sound power. Transmission loss does not depend on the source parameters and an anechoic termination at the downstream end is assumed [3].

$$TL = 10 \log_{10} \left( \frac{W_i}{W_t} \right) \qquad \text{(dB)} \tag{1.5}$$

where $TL$ is transmission loss, $W_i$ is the incident sound power and $W_t$ is the transmitted sound power.

Transmission loss can be easily calculated as it is independent of the source and load characteristics unlike insertion loss. This makes TL much more popular in the research area, because performance of mufflers and muffler elements can be easily estimated. The fact that though TL is source-independent, its measurement is much more complex than that of IL. Incident and transmitted waves must be properly isolated so that calculation of transmission loss can be done easily.

### 1.2.3  Noise reduction

The level difference between the sound pressure between two points in a system is known as noise reduction [1]. For a muffler, one point should be upstream and the other point should be downstream. Noise reduction is similar to insertion loss and it can be measured very easily. The disadvantage of noise reduction is that it is load dependent thus making it hard to predict and calculate. The formula for noise reduction is:

$$NR = 20 \log_{10} \left( \frac{P_u}{P_d} \right) \qquad \text{(dB)} \tag{1.6}$$

where $NR$ is noise reduction, $P_u$ and $P_d$ are the sound pressures at the upstream and downstream points respectively.

## 1.3  One-dimensional analysis

One dimensional plane wave theory is used for analysis of acoustic mufflers since the past few decades. In this theory, it is assumed that the pressure remains constant in a given cross-section perpendicular to the direction of propagation. Thus, there exists an acoustic pressure variation only along the longitudinal direction. This assumption holds for small mufflers installed on the car engines [3]. However, as the size of the duct increases with respect to the acoustic wave, the wave is allowed to propagate in all the three directions. The following sections will explain this phenomenon of three-dimensional propagation, its effects, and the difficulties that arise in analyzing and predicting these effects.

## 1.4  The need for multi-dimensional analysis

A plane wave assumption is valid for frequencies below cut-on frequency. Higher order modes will propagate above the cut-on frequency. At low frequencies, one-dimensional analysis is appropriate for muffler analysis. Each mode has a particular cut-on frequency above which it is allowed to propagate. The cut-on frequency for a rectangular duct is given as [3]:

$$f_c = \frac{c\sqrt{1 - M^2}}{2\pi} \sqrt{\left( \frac{m\pi}{a} \right)^2 + \left( \frac{n\pi}{b} \right)^2} \qquad \text{(Hz)} \tag{1.7}$$

where $f_c$ is the cut-on frequency in Hz, $c$ is the speed of sound in the duct medium in m/s, $M$ is the Mach number, $a$ and $b$ are the duct dimensions in metre. while $m$ and $n$ are the number of cross nodes along the duct dimensions $a$ and $b$ respectively.

Fig 1.1 describes the mode shapes for a rectangular duct cross-section. In this figure, the solid lines represent the walls of the duct while the dotted lines represent the nodes of acoustic pressure in the corresponding direction. The area in between the lines represents the alternating maximum and minimum pressure regions of the wave as denoted by the "+" and the "−" signs respectively [3].

The cut-on frequencies for a circular duct are similar to that of a rectangular duct. Only in this case, diameter is the measurement of interest and instead of cross modes in two directions there are circumferential and radial modes. The cut-on frequencies for a circular duct are given by [3]:
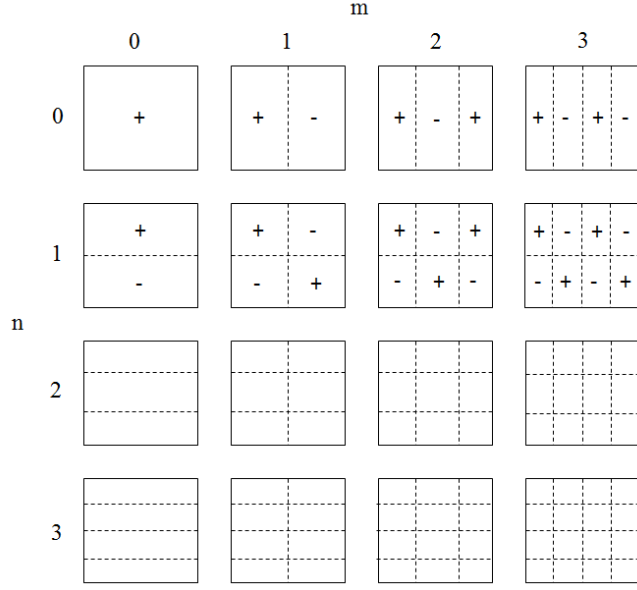
Figure 1.1: The mode shapes of the first three cut-on frequencies of rectangular duct
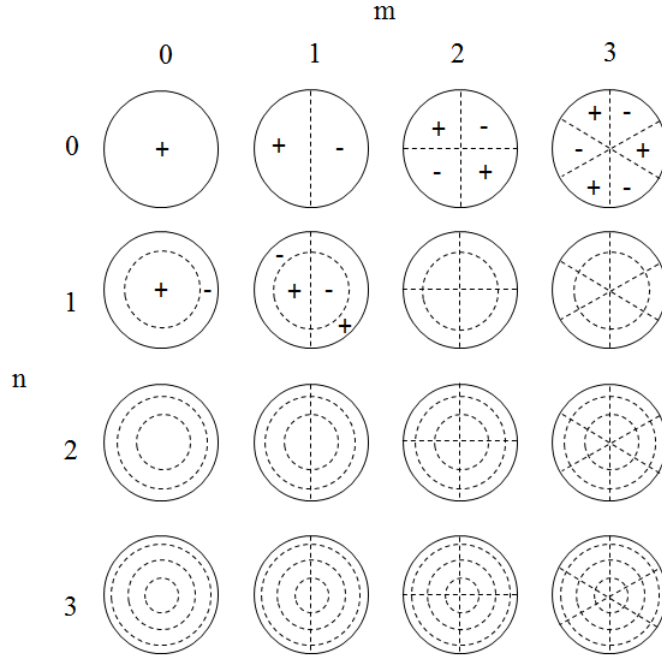


Figure 1.2: The mode shapes of the first three cut-on frequencies of circular duct

$$f_c = J_{mn} \times \frac{c}{\pi D}\sqrt{1 - M^2} \qquad \text{(Hz)} \tag{1.8}$$

where $D$ is the diameter of the duct, and $J_{mn}$ is the zero of a Bessel function for the mode of interest, $m$ is the order of the Bessel function or the circumferential modes and $n$ is the number of radial nodes. This labeling scheme is shown in Fig. 1.2. Plus and minus signs are added to the antinodes

in the first few modes.

## 1.5 Motivation

Acoustic mufflers are used in a number of applications requiring the suppression or attenuation of sound. Acoustic mufflers make everyday life much more pleasant. Many common appliances, such as refrigerators and air conditioners, use acoustic mufflers to produce a minimal working noise. The application of acoustic mufflers is mostly directed to machine components or areas where there is a large amount of radiated sound such as high pressure exhaust pipes, gas turbines, and rotary pumps. Although there are a number of applications for acoustic mufflers, there are really only two main types which are used. These are absorptive and reactive mufflers. Absorptive mufflers incorporate sound absorbing materials to attenuate the radiated energy in gas flow. Reactive mufflers work on the principle of impedance mismatch. It uses a series of complex passages to maximize sound attenuation while meeting set specifications, such as pressure drop and volume flow.

The design and analysis work for these mufflers has been mostly done with one-dimensional plane wave theory in terms of transfer matrix approach. However, when the size of the muffler is in the order of cut off wavelength, the higher order modes will also propagate. So, it requires a multi-dimensional approach. The main goal of this research is to optimise the flow and acoustic performance of a short chamber muffler.

Green's function is one of the methods used to evaluate the transmission loss of mufflers by developing a three-dimensional transfer matrix method as this gives a practical insight into the performance of mufflers.

## 1.6 Literature overview

One-dimensional transfer matrix modeling (Sec. 2.1) has been the one of the most common methods used for analysis of mufflers. Based on this theory, the TL curve for a simple expansion chamber can be obtained. Due to the extensions of the inlet and outlet pipes, the TL curve is improved. Although, these relations do not hold true in reality because they fail to consider the effect of three-dimensional (3-D) evanescent waves due to area discontinuities. This effect is rectified by the use of end corrections [4, 5]. Different analytical [4] and numerical [5] methods have been used in the past to estimate the end-corrections of sudden expansion and sudden contraction. Expression for the end correction were derived after extensive parametric studies [6]. P. Chaitanya et. al. [7] studied the effect of wall thickness on the end corrections and established a correlation between the geometric and the acoustic lengths.

One also needs to consider the fluid flow requirement in the design. In case of an extended inlet and outlet, higher back pressure happens because of flow expansion of the fluid inside the chamber. The flow exhausting from the inlet pipe forms the jet from inlet pipe to outlet pipe in the slow moving air-stream. The jet structure formation strictly depends on the respective inlet flow conditions. An analysis of flow inside the EIEO muffler by using computational fluid dynamics model gives an insight of the flow expansion behaviour. Various parameters are considered for parametric study such as inlet flow velocity, inlet pipe dimensions, chamber dimensions and fluid properties. The extended pipe lengths are decided considering the constant flow conditions which should establish a

continuous jet structure from inlet to outlet pipe.

It is important to study fluid flow behaviour in an extended inlet and outlet muffler to reduce pressure loss between two ends. A lot of strategies are put forth in the CFD domain to calculate back pressure. The perforated and cross-flow type reactive mufflers were studied using CFD by S. N. Panigrahi et al. [8]. Fang et al. [9] discussed the influence of an inlet velocity on pressure distribution inside the muffler by using CFD and experiments. D. C. Wilcox [10] developed a numerical procedure to compute the velocity profiles of an axisymmetric plane jet. Aliakbar et al. [11] performed CFD simulations on SEC mufflers and devised a methodology for the EIEO muffler by making use of acoustics and fluid dynamics along with optimization tools. An optimum design was established which is found to be suitable for short-chamber mufflers.

In this case, the length and the diameter are of comparable magnitude. Thus, the acoustic pressure variation takes place in all the three directions. Hence, a one-dimensional analysis is not alone sufficient to get a complete idea of the performance of the mufflers. This prompted the use of advanced three-dimensional methods like finite element method, boundary element method using simulation software.

The transmission loss characteristics of an annular cavity give insights for the designing of mechanical systems like the exhaust mufflers of automobiles and refrigerator compressors. Au-Yang [12] discussed about the analytical method for the acoustic pressure distribution inside an annular-like water reactor induced by a coolant pump. The model includes variations due to minor differences in the blade passing frequency of the pump. Experimental method was used to verify the model.

Kim and Soedel [13] developed an analytical method to establish the pressure response of the system for three-dimensional wave propagation by utilizing modal expansion. A point source model was proposed to formulate the pressure response. An idea of formulation of the four pole parameters based on this pressure response was introduced. The results were applied for an annular cavity so that it can be later used in combination for a complete system.

Zhou and Kim [14] later revised the above point source model by investigating the shortcomings of a singularity arising at the source point in the model. A new surface model was put forth instead along with a new definition of input point impedance.

Kim Hann [15] used the Green's function method to study the acoustic characteristics of a circular chamber with arbitrary inlet and outlet locations. Homogeneous boundary conditions were used for the solution of Green's function. Chamber walls were considered as rigid and the acoustic source location was assumed to be of uniform volume. Theses solutions were compared with experimental results and modal expansion techniques.

B. Venkatesham et al. [16] performed a transmission loss analysis using Green's function method. This was done using a rectangular expansion chamber with arbitrary inlet/outlet locations. Piston analogy approach was used to model the ports with a plane wave excitation. Average pressure on each of the ports is estimated and transfer matrix is derived for calculation of transmission loss.

## 1.7 Thesis outline

The thesis is divided into six chapters. The first chapter gives a brief introduction about the general concepts of acoustics and various performance measurement techniques for mufflers. Chapter 2 talks about the optimum design methodology used for analysis of EIEO muffler.

An EIEO muffler can be considered as a combination of annular and circular cavities. The literature for circular cavities already exists. Thus, it is required to develop an analytical approach for the estimation of transmission loss of an annular cavity. It is discussed in chapter 3. Chapter 4 is about the finite element analysis. It also explains about the software LMS Virtual.Lab and its use in estimation of transmission loss. The analytical results and its comparison with the numerical results are a part of Chapter 5. The sixth chapter summarizes the conclusions of the thesis work. The last chapter discusses about the future scope of the research.

# Chapter 2

# Optimum design methodology

## 2.1 Transfer matrix modeling

One dimensional plane wave theory assumes constant pressure in a given cross-section perpendicular to the direction of propagation. Thus, there exists an acoustic pressure variation only along the longitudinal direction. This assumption holds good for low frequency analysis. This also implies that each subsystem is a two-port system with two unknown parameters, which are the two interfering waves traveling in opposite directions. Such systems can be described by a transfer matrix. The elements of this matrix are known as four pole parameters [2, 17].

$$\begin{Bmatrix} p_1 \\ v_1 \end{Bmatrix} = \begin{bmatrix} T_{11} & T_{12} \\ T_{21} & T_{22} \end{bmatrix} \begin{Bmatrix} p_2 \\ v_2 \end{Bmatrix} \tag{2.1}$$

where $p_1$ and $p_2$ is the acoustic pressure; $v_1$ and $v_2$ are the volume velocities; at upstream and downstream respectively, and $T_{11}$, $T_{12}$, $T_{21}$, $T_{22}$ are the four pole parameters.

The transfer matrix for a uniform area tube or a pipe with rigid walls is given by [18]
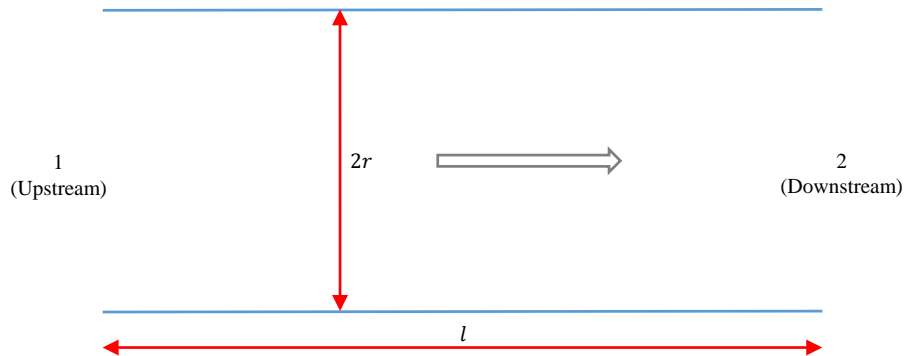


Figure 2.1: A rigid wall tube with uniform diameter

$$\begin{Bmatrix} p_1 \\ v_1 \end{Bmatrix} = \begin{bmatrix} \cos kl & jZ_0 \sin kl \\ \frac{j}{Z_0} \sin kl & \cos kl \end{bmatrix} \begin{Bmatrix} p_2 \\ v_2 \end{Bmatrix} \tag{2.2}$$

where $Z_0$ is the acoustic impedance of the tube.

The expression for TL is given by [2]:

$$TL = 20 \log_{10} \left[ \sqrt{\frac{Z_2}{Z_1}} \left| \frac{T_{11} + T_{12}/Z_2 + T_{21}Z_1 + T_{22}Z_1/Z_2}{2} \right| \right] \tag{2.3}$$

**Simple expansion chamber (SEC)**

The simplest muffler configuration is a simple expansion chamber. It can be considered as analogous to a low pass filter correlating to electrical network theory. A schematic of SEC is shown in Fig. 2.2
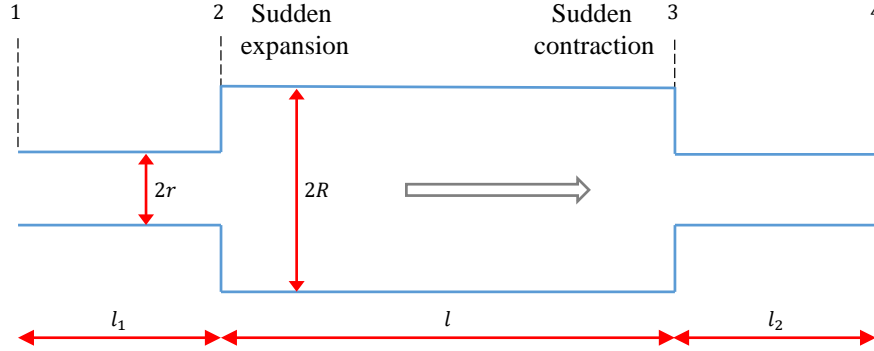


Figure 2.2: A simple expansion chamber

The transfer matrix for the SEC muffler can be written by multiplying the transfer matrices of the inlet, the chamber and the outlet.

$$\begin{aligned} \begin{Bmatrix} p_1 \\ v_1 \end{Bmatrix} &= [TM_{1\to2}] \, [TM_{2\to3}] \, [TM_{3\to4}] \begin{Bmatrix} p_4 \\ v_4 \end{Bmatrix} \\ &= \begin{bmatrix} \cos kl_1 & jZ_1 \sin kl_1 \\ \frac{j}{Z_1} \sin kl_1 & \cos kl_1 \end{bmatrix} \begin{bmatrix} \cos kl & jZ_0 \sin kl \\ \frac{j}{Z_0} \sin kl & \cos kl \end{bmatrix} \begin{bmatrix} \cos kl_2 & jZ_2 \sin kl_2 \\ \frac{j}{Z_2} \sin kl_2 & \cos kl_2 \end{bmatrix} \begin{Bmatrix} p_4 \\ v_4 \end{Bmatrix} \end{aligned} \tag{2.4}$$

where $l_1$, $l_2$ are the lengths; and $Z_1$, $Z_2$ are the acoustic impedances of the inlet and the outlet pipes. By making use of distributed element transfer matrix for chamber length $l$ and combining with Eq. 2.3, the formula for TL of a simple expansion chamber can be written as [2]:

$$TL = 10 \log_{10} \left[ 1 + \left\{ \left( \frac{m - 1/m}{2} \right) \sin(kl) \right\}^2 \right] \tag{2.5}$$

where m is the area expansion ratio, $m = (R/r)^2$, and the product of $kl$ is called Helmholtz number or non-dimensional frequency.
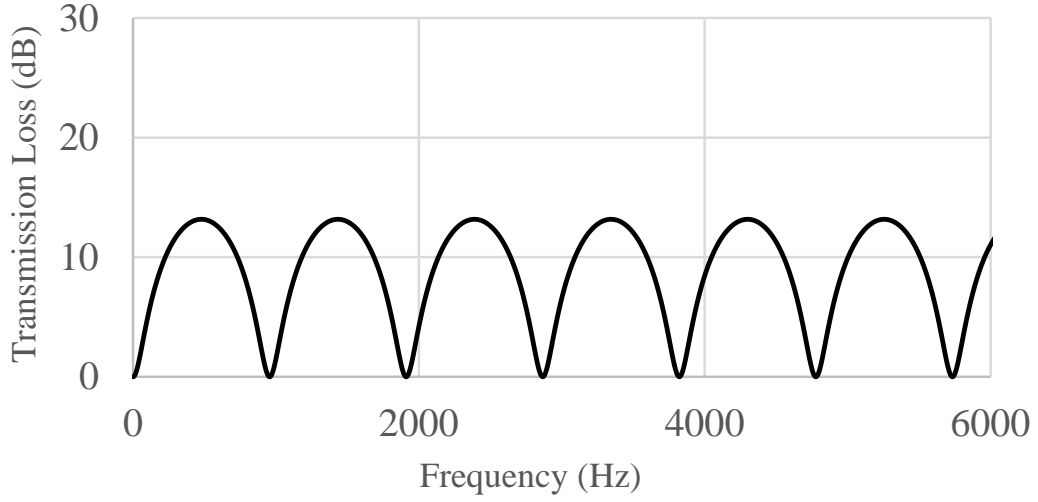
Figure 2.3: Transmission loss curve for SEC with $r = 15$ mm, $R = 45$ mm for $l/D = 2$

The TL curve for SEC is shown in Fig. 2.3. It is observed that troughs in transmission loss of a simple expansion chamber occur at a Helmholtz number of $kl = n\pi$ and peaks at $kl = n\pi/2$.

**Extended inlet extended outlet (EIEO) chamber**
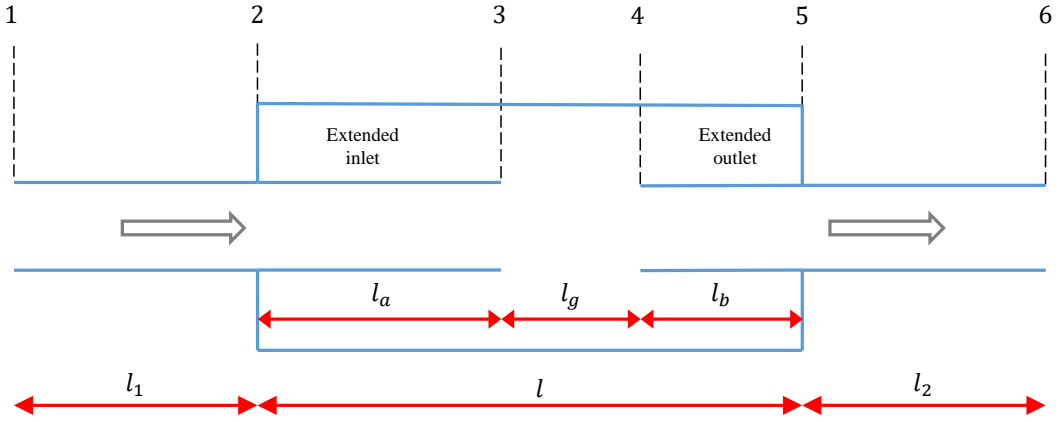


Figure 2.4: An extended inlet extended outlet chamber

Schematic of an EIEO chamber is shown in Fig. 2.4. The inlet and outlet pipe of an SEC when extended into the chamber, form the EIEO chamber. The extended lengths of the inlet and the outlet are denoted by $l_a$ and $l_b$ respectively. The extended lengths act like shunt impedances analogous to the electrical network. The two branch impedances are given by [18]

$$Z_a = -jY_a \cot(kl_a) \quad \text{and} \quad Z_b = -jY_b \cot(kl_b) \tag{2.6}$$

13

where $Y_a = Y_b = c/S_{ann}$ is the characteristic impedance of the annulus; and $S_{ann}$ is the annular cross-section area.
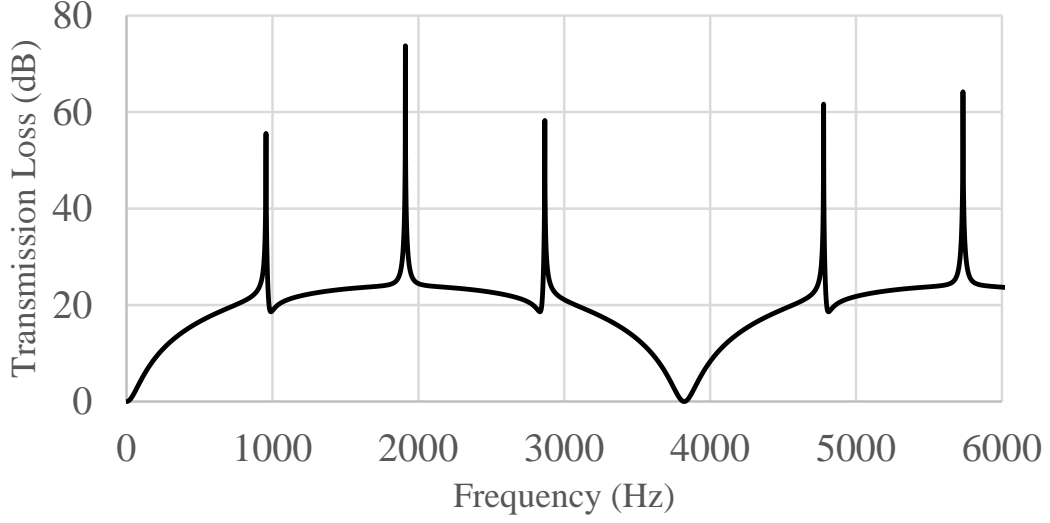


Figure 2.5: Transmission loss curve for EIEO chamber $l_a = 90$ mm; $l_b = 45$ mm for $l/D = 2$

$$\begin{Bmatrix} p_1 \\ v_1 \end{Bmatrix} = [TM_{1\to2}] [TM_{1\to2\to3}] [TM_{3\to4}] [TM_{3\to4\to5}] [TM_{5\to6}] \begin{Bmatrix} p_6 \\ v_6 \end{Bmatrix}$$

$$= \begin{bmatrix} \cos kl_1 & jZ_1 \sin kl_1 \\ \frac{j}{Z_1} \sin kl_1 & \cos kl_1 \end{bmatrix} \begin{bmatrix} 1 & 0 \\ \frac{1}{Z_a} & 1 \end{bmatrix} \begin{bmatrix} \cos kl_g & jZ_2 \sin kl_g \\ \frac{j}{Z_0} \sin kl_g & \cos kl_g \end{bmatrix} \begin{bmatrix} 1 & 0 \\ \frac{1}{Z_b} & 1 \end{bmatrix} \tag{2.7}$$

$$\begin{bmatrix} \cos kl_2 & jZ_2 \sin kl_2 \\ \frac{j}{Z_2} \sin kl_2 & \cos kl_2 \end{bmatrix} \begin{Bmatrix} p_6 \\ v_6 \end{Bmatrix}$$

Transmission loss of EIEO chamber becomes infinity if $Z_a$ and $Z_b$ tend to zero. This happens when

$$kl_a = (2m-1)\,\pi/2 \qquad \text{and} \qquad kl_b = (2n-1)\,\pi/2 \tag{2.8}$$

where $m$ and $n$ are integers $(m, n = 1, 2, 3 \dots)$

This property can be used to cancel out some of the troughs in the TL curve of SEC. It can be shown that [19] if $l_a = l/2$ then troughs 1, 3, 5, 7 ... and so on would be canceled out, and if $l_b = l/4$ then troughs 2, 6, 10, 14 ... and so on would be nullified. This is shown in Fig. 2.5. Thus except 4, 8, 12, ... all the troughs are tuned. Also, the overall TL curve has been lifted. This is the basic principle of an EIEO chamber.

## 2.2   Formulation for optimized design

It is important to study fluid flow behaviour in an Extended Inlet Extended Outlet muffler to reduce the pressure loss between two ends. An EIEO muffler with dimensions $D = 153$ mm, $d_1 = d_2 = 48.59$ mm is considered for flow analysis. An axial velocity of 10 m/s is given as inlet condition.
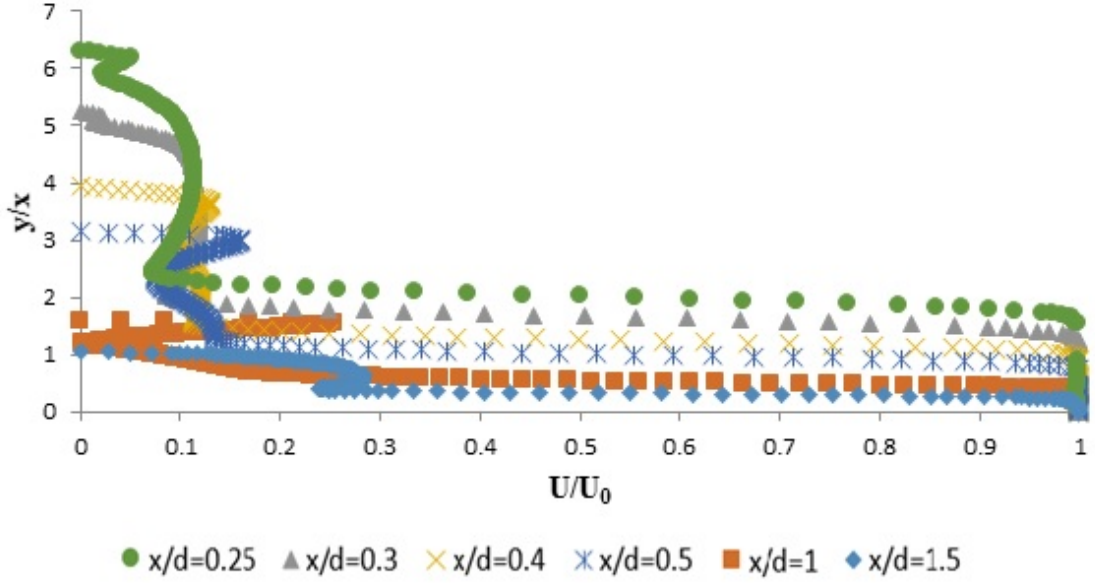
Figure 2.6: Normalized jet height w.r.t. velocity ratio at different axial locations in SEC muffler

Table 2.1 gives the details of the computational model and boundary conditions used for numerical simulation. [11].

Table 2.1: Computational model details and boundary conditions

| Sr. No. | Solution Variables | |
|---|---|---|
| 1. | Model | K-$\epsilon$ Turbulence |
| 2. | Solver | Axisymmetric, $2^{nd}$ Order implicit |
| 3. | Pressure-Velocity coupling | PISO |
| 4. | Discretization technique | Second Order UPWIND |
| 5. | Fluid | Air(Ideal) |
| 6. | Operating Pressure | 101325 Pa |
| | Boundary Conditions | |
| 7. | Inlet velocity | 10 m/s |
| 8. | Outlet gauge pressure | 0 Pa |
| 9. | Turbulent Intensity | 3% |
| 10. | Hydraulic Diameter | Diameter of inlet/outlet pipe |

Velocity ratio is defined as a ratio of velocity at a particular position to the mean flow velocity of the jet ($U/U_0$). It is symbolized as $q$ and is decided based on allowable back pressure. Fig. 2.6 represents velocity ratio $U/U_0$ in a non-dimensional form and normalized jet height dimensions with respect to axial positions $y/x$. Axial location $x$ is normalized with pipe diameter $d$ which can be used to describe the required core jet formation length $x/d$. Higher values of $x/d$ means longer core jet length, and these values are varied from 0.25 to 1.5 in the current study. It is observed that the potential core is decreasing with the axial distance. For designing the extended pipe length, one needs to fix the $U/U_0$ value and $y$ value to get an axial dimension $x$. Fig. 2.6 is redrawn for a constant velocity ratio $q$ and it provides relationship between $x/d$ and $y/x$. A simple representation

15

is assumed for $x/d$ and $y/x$ as $C_1$ and $C_2$, respectively. $C_1$ and $C_2$ are called as characteristic parameters.

For different values of L/D, flow curves are plotted as $C_2$ vs $C_1$. $C_1$ and $C_2$ are called as characteristic parameters. As shown in Fig. 2.7, $y$ is the radial distance from the centre axis whereas $x$ is the axial length. It is proposed to keep $y$ constant for a given inlet jet speed $q$ for $x$ varying from 0 to $L/D$. This will ensure that a maximum portion of the fluid jet is passed on to the extended outlet with very less or without expansion in the chamber of a muffler. For this ideal case, it is assumed that the jet diameter is same as diameter of the extended lengths (i.e. $y = d/2$). The ideal equation can be written as:

$$C_1 C_2 = 0.5 \tag{2.9}$$

The relationship between characteristic parameters $C_1$ and $C_2$ is expressed in a generalised form of equations as:

$$C_2 = a C_1^{-b} \tag{2.10}$$

where $a$ and $b$ are constants for a particular $L/D$ ratio.
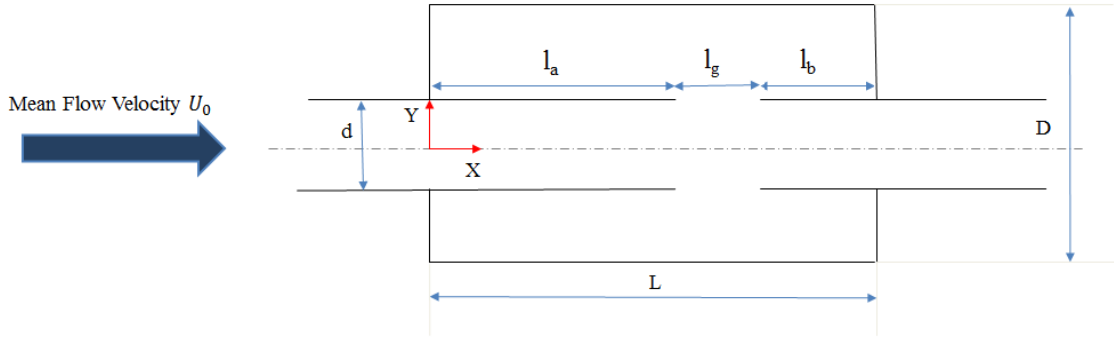


Figure 2.7: Representation of terminology for $C_1$ vs $C_2$ curves

Practically, it is not possible to get the jet core diameter as $d$. Thus $y = g \times d$ is considered, where $g$ is the ratio of jet core radius to inlet diameter and it is less than 0.5. Flow simulation data is collected for velocity ratios from $q = 0.5$ up to $q = 0.9$ and the constants $a$ and $b$ are determined as functions of $q$. Fig. 2.8 shows the curve equations for the constants $a$ and $b$ as functions of velocity ratio for different $L/D$. To find a more generalized equation, these constants are assumed as functions of parameter $L/D$. The generalized equation obtained is:

$$C_2 = [Aq + B] \times C_1^{[Eq^2 + Fq + G]} \tag{2.11}$$

where $A$, $B$, $E$, $F$ and $G$ are functions of $L/D$.

The back pressure is minimized by avoiding flow expansion inside the chamber. It is achieved with jet height dimensions as close as possible to the radius of extended inlet and outlet pipe. So it leads to a condition as:

$$C_2 \geq C_{2(ideal)} \tag{2.12}$$
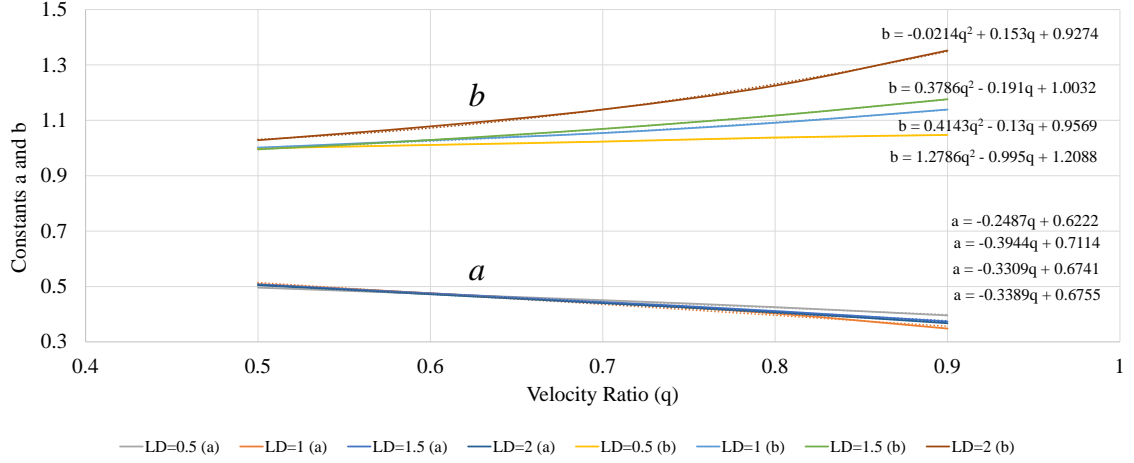
Figure 2.8: Empirically formulated curves for constants $a$ and $b$

Using Eqs. 2.10 and 2.12, the constraint to be satisfied is obtained as:

$$x \geq l_g \tag{2.13}$$

Eq. 2.11 was used to find values of $C_2$ for available simulation parameters i.e. $C_1$, $q$ and $L/D$. A MATLAB® code [20] was written to do a regression fit analysis and a linear model with regression coefficient $R^2 = 0.975$ was obtained as:

$$C_2 = -0.1426 + 0.55886 C_1 - 0.02843q + 0.037828 \left( \frac{L}{D} \right) \tag{2.14}$$

## 2.3 Results

A regression analysis was implemented for the one-dimensional study of EIEO muffler. Eq. 2.14 was obtained as a linear fit equation. It was used to estimate the maximum core jet length $x_{max}$ and then compared with acoustic gap length $l_g$.

Table 2.2: Comparison between acoustic gap length $l_g$ and maximum core jet length $x_{max}$

| $L/D$ Ratio | $l_a$ (mm) | $l_b$ (mm) | $l_g$ (mm) | $x_{max}$ (mm) |
|---|---|---|---|---|
| 0.5 | 21.4 | 6.4 | 32.2 | 41.6 |
| 1.0 | 51.4 | 21.4 | 47.2 | 40.9 |
| 1.5 | 81.4 | 36.4 | 62.2 | 40.1 |
| 2.0 | 111.4 | 51.4 | 77.2 | 39.4 |
| 2.5 | 141.4 | 66.4 | 92.2 | 38.6 |

An EIEO muffler with dimensions of $d = 40$ mm, $D = 120$ mm, $q = 0.9$ and $g = 0.45$ was considered for the study. The required acoustic gap length $l_g$ was calculated using the end correction. The expression for end correction is given as [7]:

$$\frac{\delta}{d} = a_0 + a_1 \left( \frac{D}{d} \right) + a_2 \left( \frac{t_w}{d} \right) + a_3 \left( \frac{D}{d} \right)^2 + a_4 \left( \frac{D}{d} \frac{t_w}{d} \right) + a_5 \left( \frac{t_w}{d} \right)^2 \tag{2.15}$$

where $a_0$=0.005177, $a_1$=0.0909, $a_2$=0.537, $a_3$=-0.008594, $a_4$=0.002616, $a_5$=-5.425; $d$ and $t_w$ are diameter and wall thickness of the extended inlet and outlet.

The acoustic gap length was then compared with the maximum core jet length $x_{max}$ for a given velocity ratio.
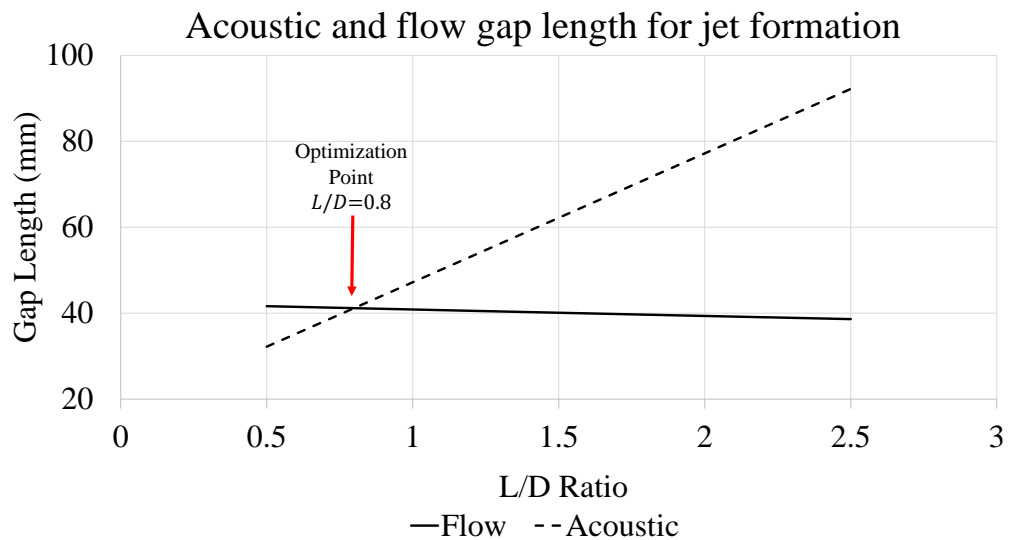


Figure 2.9: Variation of acoustic gap length and maximum core jet length

The $l_g$ and $x_{max}$ values for different $L/D$ ratios are given in Table 2.2. These results are presented in graphical form in Fig. 2.9. If $l_g$ is less than $x_{max}$, a jet core is formed between the inlet and outlet extensions of the muffler. It is evident from this study that the jet formation concept to reduce back pressure is ideal for short chamber EIEO muffler design.

# Chapter 3

# Three-dimensional analysis

As discussed in Chapter 2, one-dimensional analysis is used to analyze the performance of EIEO muffler. But, as transverse mode propagation is significant in short chamber length mufflers, a three-dimensional analysis is required for estimating the transmission loss characteristics. The EIEO muffler can be considered as a combination of annular and circular cavities. The literature for circular cavities already exists [13]. The methodology for calculating the transmission loss of an annular cavity is discussed in this chapter.

The step-by-step procedure involves the following steps:

- Mode shape function
- Green's function derivation
- Velocity potential
- Piston analogy approach
- Four pole parameters
- Calculation of transmission loss

### 3.0.1  Mode shape function

The three-dimensional homogeneous wave equation [13] is given as:

$$\nabla^2 P - \frac{1}{c^2} \frac{\partial^2 P}{\partial t^2} = 0 \tag{3.1}$$

The above equation is solved by using separation of variables. The basic idea behind this technique is to assume, initially, that the variable of interest can be separated into factors which depend separately on the coordinates. The above differential equation can be solved by assuming a solution in the cylindrical co-ordinate system as:

$$P(r, \theta, z, t) = R(r) \, \Theta(\theta) \, Z(z) \, e^{j\omega t} \tag{3.2}$$

Substituting Eq. 3.2 in 3.1, we get

$$\frac{R''}{R} + \frac{1}{r} \frac{R'}{R} + \frac{1}{r^2} \frac{\Theta''}{\Theta} + \frac{Z''}{Z} + \frac{\omega^2}{c^2} = 0 \tag{3.3}$$

Since the $\Theta$ function has to satisfy continuity condition, it takes the form of trigonometric cosine function.

$$\Theta(\theta) = \cos(m\theta - \alpha) \tag{3.4}$$

where $\alpha$ is an arbitrary angle.

Therefore,

$$\frac{\Theta''}{\Theta} = -m^2 \tag{3.5}$$

Substituting in Eq. 3.3,

$$\frac{R''}{R} + \frac{1}{r}\frac{R'}{R} - \frac{m^2}{r^2} + \frac{Z''}{Z} + \frac{\omega^2}{c^2} = 0 \tag{3.6}$$

Rewriting Eq. 3.6 as a function of $r$ and $z$ only,

$$\left(\frac{R''}{R} + \frac{1}{r}\frac{R'}{R} - \frac{m^2}{r^2}\right) + \left(\frac{Z''}{Z}\right) = -\frac{\omega^2}{c^2} \tag{3.7}$$

Now, the differential equation has been separated into a sum of two differential equations, each of which depend on a different variable. Making a substitution for function $Z$ as given below, it is simplified as:

$$\frac{Z''}{Z} = -k_{zp}{}^2 \tag{3.8}$$

Boundary conditions used for $z$ co-ordinate are:

$$\left.\frac{d}{dz}Z(z)\right|_{z=0} = 0, \qquad \left.\frac{d}{dz}Z(z)\right|_{z=L} = 0 \tag{3.9}$$

Solving Eq. 3.8 we get

$$\sin(k_{zp}L) = 0 \tag{3.10}$$

Therefore,

$$k_{zp}L = p\pi \qquad i.e. \qquad k_{zp} = \frac{p\pi}{L} \qquad (p = 0, 1, 2 \ldots) \tag{3.11}$$

Thus, the solution for $Z$ is given as:

$$Z(z) = \cos\left(\frac{p\pi z}{L}\right) \tag{3.12}$$

The wavenumber is given by Eq. 3.13

$$k^2 = \frac{\omega^2}{c^2} \tag{3.13}$$

Substituting Eqs. 3.8 and 3.13 in Eq. 3.7, we get

$$r^2 R'' + rR' + \left[\left(k^2 - \frac{p^2\pi^2}{L^2}\right)r^2 - m^2\right]R = 0 \tag{3.14}$$

Solution of Eq. 3.14 is given by making use of Bessel functions as below.

$$R(r) = A_m J_m(\kappa r) + B_m Y_m(\kappa r) \tag{3.15}$$

where

$$\kappa = \sqrt{\left(k^2 - \frac{p^2\pi^2}{L^2}\right)} \tag{3.16}$$

Function $R$ will be equal to 0 at the inner radius $(a/2)$ and the outer radius $(b/2)$. Thus, the boundary conditions for function $R$ can be written as:

$$\frac{d}{dr}R(r)\bigg|_{r=a/2} = 0 \qquad \frac{d}{dr}R(r)\bigg|_{r=b/2} = 0 \tag{3.17}$$

Applying the above boundary conditions to Eq. 3.15

$$J_m'\left(\frac{\kappa a}{2}\right)Y_m'\left(\frac{\kappa b}{2}\right) - J_m'\left(\frac{\kappa b}{2}\right)Y_m'\left(\frac{\kappa a}{2}\right) = 0 \tag{3.18}$$

Eq. 3.18 can be rewritten as follows using the recurrence relationship for Bessel functions.

$$\left[mJ_m\left(\frac{\kappa a}{2}\right) - \frac{\kappa a}{2}J_{m+1}\left(\frac{\kappa a}{2}\right)\right]\left[mY_m\left(\frac{\kappa b}{2}\right) - \frac{\kappa b}{2}Y_{m+1}\left(\frac{\kappa b}{2}\right)\right]$$
$$- \left[mY_m\left(\frac{\kappa a}{2}\right) - \frac{\kappa a}{2}Y_{m+1}\left(\frac{\kappa a}{2}\right)\right]\left[mJ_m\left(\frac{\kappa b}{2}\right) - \frac{\kappa b}{2}J_{m+1}\left(\frac{\kappa b}{2}\right)\right] = 0 \tag{3.19}$$

Different values of $m$ are used to find the roots of Eq. 3.19. For selected values of $m$, a $\kappa$ is sought for, which satisfies the above equation. There will be an infinite number of them. Each value is designated as $\kappa_{mn}$, where $n = 0, 1, 2 \ldots$

The natural frequencies are then obtained from Eq. 3.20.

$$\omega_{mnp} = c\sqrt{\kappa_{mn}^2 + k_{zp}^2} \tag{3.20}$$

The mode function $R$ thus becomes:

$$R(r) = J_m(\kappa_{mn}r) + C_{mn}Y_m(\kappa_{mn}r) \tag{3.21}$$

where

$$C_{mn} = \frac{\left[mJ_m\left(\frac{\kappa_{mn}a}{2}\right) - \frac{\kappa_{mn}a}{2}J_{m+1}\left(\frac{\kappa_{mn}a}{2}\right)\right]}{\left[mY_m\left(\frac{\kappa_{mn}a}{2}\right) - \frac{\kappa_{mn}a}{2}Y_{m+1}\left(\frac{\kappa_{mn}a}{2}\right)\right]} \tag{3.22}$$

Thus, two sets of mutually independent natural modes can be used for determination of mode shapes. This is done by considering the $\Theta$ function as $\cos\theta$ and $\sin\theta$. This gives the following two mode shape functions which are obtained from Eqs. 3.4, 3.12 and 3.21.

$$P_{mnp(1)}(r, \theta, z) = [J_m(\kappa_{mn}r) + C_{mn}Y_m(\kappa_{mn}r)]\cos(m\theta)\cos\left(\frac{p\pi z}{L}\right)$$
$$P_{mnp(2)}(r, \theta, z) = [J_m(\kappa_{mn}r) + C_{mn}Y_m(\kappa_{mn}r)]\sin(m\theta)\cos\left(\frac{p\pi z}{L}\right) \tag{3.23}$$

### 3.0.2 Green's function derivation

A Green's function is the impulse response of an inhomogeneous differential equation defined on a domain, with specified initial conditions or boundary conditions. The acoustic wave equation for arbitrary space which has distributed sources $Q(\vec{r})$ can be represented in terms of velocity potential

$\phi(r)$ as [21]:

$$\nabla^2 \phi + k^2 \phi = Q(\vec{r}) \tag{3.24}$$

Thus acoustic pressure is:

$$p(\vec{r}, t) = -\rho \frac{\partial \phi(\vec{r}, t)}{\partial t} = -\rho j \omega \phi(\vec{r}) \tag{3.25}$$

and particle velocity:

$$u(\vec{r}) = grad\phi(\vec{r}) = \nabla \phi(\vec{r}) \tag{3.26}$$

The acoustic field for the whole space can be obtained by superposition principle. That is, if $G(\vec{r}|\vec{r_0})$ is the field at the observer point $\vec{r}$ caused by a unit point source $\vec{r_0}$, it is governed by:

$$\nabla^2 G(\vec{r}|\vec{r_0}) + k^2 G(\vec{r}|\vec{r_0}) = \delta^3(\vec{r} - \vec{r_0}) \tag{3.27}$$

We assume that the eigenfunctions $\Psi_{mnp}(\vec{r})$ form a single set. Thus the Green's function can be expressed in a series of $\Psi_{mnp}(\vec{r})$, satisfying the homogeneous boundary conditions [21].

$$G(\vec{r}|\vec{r_0}) = 4\pi \sum_{mnp} \frac{\bar{\Psi}_{mnp}(\vec{r}) \cdot \Psi_{mnp}(\vec{r_0})}{k_{mnp}^2 - k^2} \tag{3.28}$$

The mode shape of an annular cavity is given as:

$$\Psi_{mnp}(\vec{r}) = [J_m(\kappa_{mn}r) + C_{mn}Y_m(\kappa_{mn}r)]\cos(m\theta)\cos\left(\frac{p\pi z}{L}\right) \tag{3.29}$$

and the corresponding wavenumber is:

$$k_{mnp} = \left[\kappa_{mn}^2 + k_{zp}^2\right]^{1/2} \tag{3.30}$$

The orthonormal function $\bar{\Psi}_{mnp}(\vec{r})$ is written as:

$$\bar{\Psi}_{mnp}(\vec{r}) = (e_r e_\theta e_z)^{-1} \Psi_{mnp}(\vec{r}) \tag{3.31}$$

Here, $r$ and $r_0$ are the response vector and source vector respectively; $m$, $n$ and $p$ are integers; $e_r$, $e_\theta$ and $e_z$ are known as normalizing factors. They are as follows:

$$e_r = \int_{a/2}^{b/2} r \left[J_m(\kappa_{mn}r) + C_{mn}Y_m(\kappa_{mn}r)\right]^2 dr \tag{3.32}$$

$$e_\theta = \int_0^{2\pi} \left[\cos(m\theta)\right]^2 d\theta \tag{3.33}$$

$$e_z = \int_0^L \left[\cos\left(\frac{p\pi z}{L}\right)\right]^2 dz \tag{3.34}$$

The expression for $e_r$ can be calculated using Mathematica as [22]:

$$e_r = e_{r1} + e_{r2} + e_{r3}$$
$$= \int_{\frac{a}{2}}^{\frac{b}{2}} r J_m(\kappa_{mn}r)^2 dr + e_{r2} + C_{mn}^2 \int_{\frac{a}{2}}^{\frac{b}{2}} r Y_m(\kappa_{mn}r)^2 dr \tag{3.35}$$

The integral solution of $e_{r1}$ and $e_{r3}$ can be obtained easily.

$$e_{r1} = \frac{1}{8\kappa_{mn}} \left( b \left( b\kappa_{mn} \left( J_{m-1} \left( \frac{b\kappa_{mn}}{2} \right)^2 + J_m \left( \frac{b\kappa_{mn}}{2} \right)^2 \right) - 4m J_{m-1} \left( \frac{b\kappa_{mn}}{2} \right) J_m \left( \frac{b\kappa_{mn}}{2} \right) \right) \right)$$
$$- \frac{1}{8\kappa_{mn}} \left( a \left( a\kappa_{mn} \left( J_{m-1} \left( \frac{a\kappa_{mn}}{2} \right)^2 + J_m \left( \frac{a\kappa_{mn}}{2} \right)^2 \right) - 4m J_{m-1} \left( \frac{a\kappa_{mn}}{2} \right) J_m \left( \frac{a\kappa_{mn}}{2} \right) \right) \right)$$
$$(3.36)$$

$$e_{r3} = \frac{C_{mn}^2}{8\kappa_{mn}} \left( b \left( b\kappa_{mn} \left( Y_{m-1} \left( \frac{b\kappa_{mn}}{2} \right)^2 + Y_m \left( \frac{b\kappa_{mn}}{2} \right)^2 \right) - 4m Y_{m-1} \left( \frac{b\kappa_{mn}}{2} \right) Y_m \left( \frac{b\kappa_{mn}}{2} \right) \right) \right)$$
$$- \frac{C_{mn}^2}{8\kappa_{mn}} \left( -a \left( a\kappa_{mn} \left( Y_{m-1} \left( \frac{a\kappa_{mn}}{2} \right)^2 + Y_m \left( \frac{a\kappa_{mn}}{2} \right)^2 \right) - 4m Y_{m-1} \left( \frac{a\kappa_{mn}}{2} \right) Y_m \left( \frac{a\kappa_{mn}}{2} \right) \right) \right)$$
$$(3.37)$$

The integral $e_{r2}$ can be evaluated numerically as no complete solution can be obtained for it. Mathematica [22] is used to evaluate this integral.

The integrals $e_\theta$ and $e_z$ are calculated as:

$$e_\theta = \begin{cases} 2\pi, & m = 0, \\ \pi, & \text{otherwise} \end{cases}$$

$$e_z = \begin{cases} 2L, & p = 0, \\ L, & \text{otherwise} \end{cases}$$

The Green's function can be obtained by substituting Eqs. 3.31, 3.32, 3.33 and 3.34 in Eq. 3.28

$$G\left(\vec{r}|\vec{r_0}\right) = 4\pi \sum_{mnp} G_{mnp}(k) \Psi_{mnp}\left(\vec{r}\right) \Psi_{mnp}\left(\vec{r_0}\right) \tag{3.38}$$

where

$$G_{mnp}(k) = \frac{(e_r e_\theta e_z)^{-1}}{k_{mnp}^2 - k^2} \tag{3.39}$$

$$\Psi_{mnp}\left(\vec{r}\right) = [J_m\left(\kappa_{mn} r\right) + C_{mn} Y_m\left(\kappa_{mn} r\right)] \cos(m\theta) \cos\left(\frac{p\pi z}{L}\right) \tag{3.40}$$

$$\Psi_{mnp}\left(\vec{r_0}\right) = [J_m\left(\kappa_{mn} r_0\right) + C_{mn} Y_m\left(\kappa_{mn} r_0\right)] \cos(m\theta_0) \cos\left(\frac{p\pi z_0}{L}\right) \tag{3.41}$$

## 3.1 Side-Inlet-Side-Outlet (SISO) configuration

As seen in Fig. 3.1, the surfaces of the annular cavity are defined as $S_A$, $S_B$ and $S_C$. The inlet port is located on surface $S_A$ at a distance $l_1$ from surface $S_B$ and at 0°. The outlet port is at a distance $l_2$ and at 180°. Both the ports are of elliptical cross-section. The half major axis length is $a_1$ and $a_2$ whereas the half minor axis length is $b_1$ and $b_2$ for the inlet and outlet ports respectively. The hypothetical velocities of pistons at the inlet and outlet ports are assumed as $u_1$ and $u_2$ respectively.
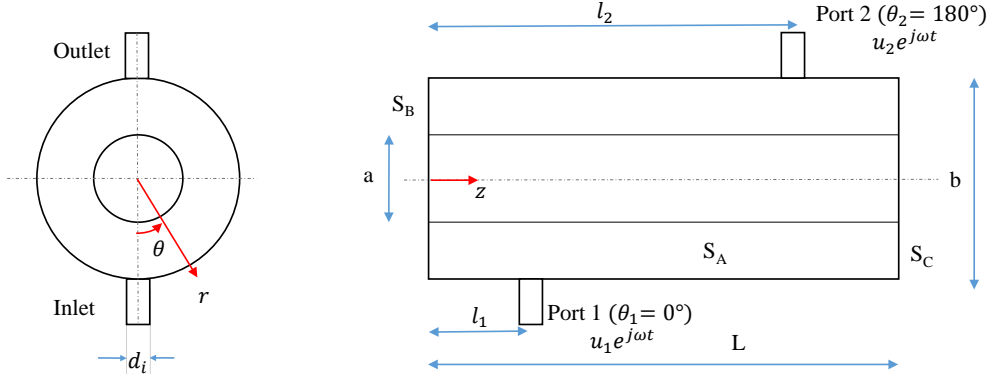
Figure 3.1: Annular cavity with Side-Inlet-Side-Outlet configuration

The boundary conditions on the surfaces of the annular cavity can be defined as follows:

$$S_A \;\; : \;\; \left.\frac{\partial \phi}{\partial r}\right|_{r=b/2} = u_1 \cos\theta_1 f_1(z,\theta) + u_2 \cos\theta_2 f_2(z,\theta) = N_1(z,\theta) + N_2(z,\theta) \tag{3.42}$$

$$S_B \;\; : \;\; \left.\frac{\partial \phi}{\partial z}\right|_{z=0} = 0 \tag{3.43}$$

$$S_C \;\; : \;\; \left.\frac{\partial \phi}{\partial z}\right|_{z=L} = 0 \tag{3.44}$$

### 3.1.1 Velocity potential

Assuming harmonic behaviour, the velocity potential may be written as $\phi(\vec{r},t) = \phi(\vec{r})e^{j\omega t}$.
Total velocity potential inside the chamber is expressed by superimposing the velocity potentials generated due to the inlet and outlet piston sources. Thus, the expression for total velocity potential can be written as:

$$\begin{aligned}
\phi(\vec{r}) &= -\frac{1}{4\pi} \iint G(\vec{r}|\vec{r_0}) \, N(r_0^S) dS_0 \\
&= -\frac{1}{4\pi} \left[ \iint G(\vec{r}|\vec{r_0}) \, N_1(z,\theta) \, dS_A + \iint G(\vec{r}|\vec{r_0}) \, N_2(z,\theta) \, dS_A \right]
\end{aligned} \tag{3.45}$$

Let us assume:

$$\phi_1(\vec{r}) = -\frac{1}{4\pi} \iint_{\text{port 1}} G(\vec{r}|\vec{r_0}) \, N_1(z,\theta) \, dS_A \tag{3.46}$$

$$\phi_2(\vec{r}) = -\frac{1}{4\pi} \iint_{\text{port 2}} G(\vec{r}|\vec{r_0}) \, N_2(z,\theta) \, dS_A \tag{3.47}$$

The velocity potential caused by port 1 can be obtained by substituting Green's function (3.38) into Eq. 3.46

$$\phi_1(\vec{r}) = (-)\frac{1}{4\pi} \iint 4\pi \sum_{mnp} G_{mnp}(k)\Psi_{mnp}(\vec{r})\,\Psi_{mnp}(\vec{r_0})N_1(z,\theta)\,dS_A$$

$$= (-)\sum_{mnp} G_{mnp}(k)\Psi_{mnp}(\vec{r}) \iint \Psi_{mnp}(\vec{r_0})\,u_1\cos\theta_1 f_1(z,\theta)\,dS_A \qquad (3.48)$$

$$= (-)\sum_{mnp} G_{mnp}(k)\Psi^{(1)}_{mnp}(\vec{r})u_1 x_1$$

where $\Psi^{(1)}_{mnp}(\vec{r})$ is the mode shape function corresponding to port 1.

$$\Psi^{(1)}_{mnp}(\vec{r}) = \left[J_m\left(\frac{\kappa_{mn}b}{2}\right) + C_{mn}Y_m\left(\frac{\kappa_{mn}b}{2}\right)\right]\cos(m\theta_1)\cos(k_{zp}l_1) \qquad (3.49)$$

and,

$$x_1 = \left[J_m\left(\frac{\kappa_{mn}b}{2}\right) + C_{mn}Y_m\left(\frac{\kappa_{mn}b}{2}\right)\right]\iint_{\text{port 1}}\cos(\theta)\cos(m\theta)\cos(k_{zp}z)\,dS_A$$

$$= \pi a_1 b_1\left[J_m\left(\frac{\kappa_{mn}b}{2}\right) + C_{mn}Y_m\left(\frac{\kappa_{mn}b}{2}\right)\right]\cos(k_{zp}l_1) \qquad (3.50)$$

$$\left[F_{mp}\left(\frac{1}{2}, \cos[(m-1)\theta_1] \times \frac{J_1(b_2\beta_{m-1,1})}{b_2\beta_{m-1,1}}\right) + \cos[(m-1)\theta_1] \times \frac{J_1(b_1\beta_{m+1,1})}{b_1\beta_{m+1,1}}\right]$$

The evaluation of the above integral is explained in Appendix A.1.

Similarly, the velocity potential for piston 2 can be written as:

$$\phi_2(\vec{r}) = (-)\sum_{mnp} G_{mnp}(k)\Psi^{(2)}_{mnp}(\vec{r})u_2 x_2 \qquad (3.51)$$

where $\Psi^{(2)}_{mnp}(\vec{r})$ is the mode shape function corresponding to port 2.

$$\Psi^{(2)}_{mnp}(\vec{r}) = \left[J_m\left(\frac{\kappa_{mn}b}{2}\right) + C_{mn}Y_m\left(\frac{\kappa_{mn}b}{2}\right)\right]\cos(m\theta_2)\cos(k_{zp}l_2) \qquad (3.52)$$

and,

$$x_2 = \left[J_m\left(\frac{\kappa_{mn}b}{2}\right) + C_{mn}Y_m\left(\frac{\kappa_{mn}b}{2}\right)\right]\iint_{\text{port 2}}\cos(\theta)\cos(m\theta)\cos(k_{zp}z)\,dS_A$$

$$= \pi a_2 b_2\left[J_m\left(\frac{\kappa_{mn}b}{2}\right) + C_{mn}Y_m\left(\frac{\kappa_{mn}b}{2}\right)\right]\cos(k_{zp}l_2) \qquad (3.53)$$

$$\left[F_{mp}\left(\frac{1}{2}, \cos[(m-1)\theta_2] \times \frac{J_1(b_2\beta_{m-1,2})}{b_2\beta_{m-1,2}}\right) + \cos[(m-1)\theta_2] \times \frac{J_1(b_2\beta_{m+1,2})}{b_2\beta_{m+1,2}}\right]$$

The evaluation of the above integral is explained in Appendix A.1.

### 3.1.2 Piston analogy approach

The equations for derived velocity potentials in the above section are used to estimate the four pole parameters of the transfer matrix. It is further used to evaluate the transmission loss, which expresses the performance of the cavity.

The average sound pressure acting on piston $i$ with cross-sectional area $A_i$ caused by the velocity field which is generated by elliptic piston $j$, can be written as:

$$\bar{p}_{ij} = (-)\frac{j\omega\rho}{A_i} \iint_{\text{piston i}} \phi_j(\vec{r})dS_i = v_i E_{ij} \tag{3.54}$$

where $v_i$ is the volume velocity; $v_i = A_i u_i$.

If the geometry of the ports is identical, then $A_i = A_j$, implying $E_{ij} = E_{ji}$, which shows that these values are independent of inlet and outlet port positions. Hence, the reciprocity relation is satisfied. Accordingly, the total sound pressure acting on the inlet and outlet ports can be expressed as:

$$\bar{p}_1 = \bar{p}_{11} + \bar{p}_{12} = v_1 E_{11} + v_2 E_{12} \tag{3.55}$$

$$\bar{p}_2 = \bar{p}_{21} + \bar{p}_{22} = v_1 E_{21} + v_2 E_{22} \tag{3.56}$$

According to Eq. 3.54, the average sound pressure acting on output piston 2 due to input piston 1 can be written as:

$$\begin{aligned}
\bar{p}_{21}(\vec{r}) &= (-)\frac{j\omega\rho}{A_2} \int_{\text{piston 2}} \phi_1(\vec{r})\, dS_2 \\
&= (-)\frac{j\omega\rho}{A_2} \int_{\text{piston 2}} (-)\sum_{mnp} G_{mnp}(k)\, u_1 x_1 \Psi_{mnp}^{(1)}(\vec{r})\, dS_2 \\
&= \frac{j\omega\rho}{A_2} \sum_{mnp} G_{mnp}(k)\, u_1 x_1 y_2
\end{aligned} \tag{3.57}$$

where

$$\begin{aligned}
y_2 &= \left[ J_m\left(\frac{\kappa_{mn}b}{2}\right) + C_{mn} Y_m\left(\frac{\kappa_{mn}b}{2}\right) \right] \iint_{\text{port 2}} \cos(m\theta)\cos(k_{zp}z)\, dS_A \\
&= 2\pi a_2 b_2 \left[ J_m\left(\frac{\kappa_{mn}b}{2}\right) + C_{mn} Y_m\left(\frac{\kappa_{mn}b}{2}\right) \right] \cos(k_{zp}l_2)\cos(m\theta_2) Q_{mp}\left(\frac{1}{2}, \frac{J_1(b_2\beta_{m,2})}{b_2\beta_{m,2}}\right)
\end{aligned} \tag{3.58}$$

The solution for the above integral has been explained in Appendix A.2

Thus, the E-function $E_{21}$ can be written as:

$$E_{21} = \frac{\bar{p}_{21}(\vec{r})}{A_1 u_1} = \frac{j\omega\rho}{A_1 A_2} \sum_{mnp} G_{mnp}(k)\, y_2 x_1 \tag{3.59}$$

Similarly,

$$E_{11} = \frac{\bar{p}_{11}(\vec{r})}{A_1 u_1} = \frac{j\omega\rho}{A_1^2} \sum_{mnp} G_{mnp}(k)\, y_1 x_1 \tag{3.60}$$

$$E_{12} = \frac{\bar{p}_{12}\left(\vec{r}\right)}{A_2 u_2} = (-)\frac{j\omega\rho}{A_1 A_2} \sum_{mnp} G_{mnp}\left(k\right) y_1 x_2 \tag{3.61}$$

$$E_{22} = \frac{\bar{p}_{21}\left(\vec{r}\right)}{A_2 u_2} = (-)\frac{j\omega\rho}{A_2{}^2} \sum_{mnp} G_{mnp}\left(k\right) y_2 x_2 \tag{3.62}$$

### 3.1.3 Four pole parameters

The transfer matrix relating the acoustic state variables at the inlet and outlet is written as:

$$\begin{Bmatrix} \bar{p}_1 \\ v_1 \end{Bmatrix} = \begin{bmatrix} T_{11} & T_{12} \\ T_{21} & T_{22} \end{bmatrix} \begin{Bmatrix} \bar{p}_2 \\ v_2 \end{Bmatrix} \tag{3.63}$$

where, $\bar{p}_1$ and $\bar{p}_2$ are acoustic pressures; $v_1$ and $v_2$ are volume velocities at the inlet and the outlet respectively.

Using Eqs. 3.55 and 3.56 the four pole parameters $T_{ij}$ can be written in terms of E-functions as follows:

$$T_{11} = \left.\left|\frac{\bar{p}_1}{\bar{p}_2}\right|\right|_{v_2=0} = \frac{E_{11}}{E_{21}} \tag{3.64}$$

$$T_{12} = \left.\left|\frac{\bar{p}_1}{v_2}\right|\right|_{\bar{p}_2=0} = \left(E_{12} - \frac{E_{11} E_{22}}{E_{21}}\right) \tag{3.65}$$

$$T_{21} = \left.\left|\frac{v_1}{\bar{p}_2}\right|\right|_{v_2=0} = (E_{21})^{-1} \tag{3.66}$$

$$T_{22} = \left.\left|\frac{v_1}{v_2}\right|\right|_{\bar{p}_2=0} = (-)\frac{E_{22}}{E_{21}} \tag{3.67}$$

### 3.1.4 Calculation of transmission loss

The transmission loss can be expressed in terms of four pole parameters as:

$$TL = 20\log_{10}\left\{\left(\frac{Z_2}{Z_1}\right)^{1/2} \left|\frac{T_{11} + \frac{T_{12}}{Z_2} + T_{21}Z_1 + T_{22}\left(\frac{Z_1}{Z_2}\right)}{2}\right|\right\} \tag{3.68}$$

where $Z_1$ is the acoustic impedance of the inlet, $Z_2$ is the acoustic impedance of the outlet.

## 3.2 Face-Inlet-Face-Outlet (FIFO) configuration

As seen in Fig. 3.2, the surfaces of the annular cavity are defined as $S_A$, $S_B$ and $S_C$. The inlet port is located on surface $S_B$ at a distance $\delta$ from the $z$ axis at 0°. Both the ports are of elliptical cross-section. The half major axis length is $a_1$ and $a_2$ whereas the half minor axis length is $b_1$ and $b_2$ for the inlet and outlet ports respectively. The outlet port is on the surface $S_C$, also at a distance $\delta$ and at 180°. The hypothetical velocities of pistons at the inlet and outlet ports are assumed as $u_1$ and $u_2$ respectively.
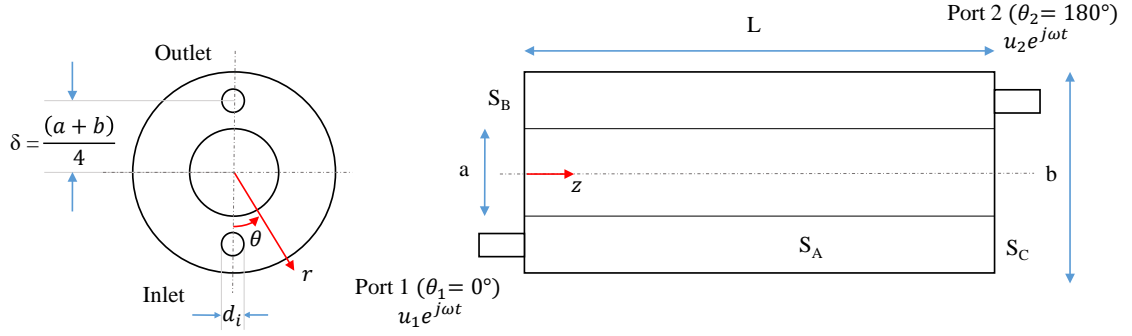
Figure 3.2: Annular cavity with Face-Inlet-Face-Outlet configuration

The boundary conditions on the surfaces of the annular cavity can be defined as follows:

$$S_A \; : \; \left.\frac{\partial \phi}{\partial r}\right|_{r=b/2} = 0 \tag{3.69}$$

$$S_B \; : \; \left.\frac{\partial \phi}{\partial z}\right|_{z=0} = u_1 f_1(r,\theta) = N_1(r,\theta) \tag{3.70}$$

$$S_C \; : \; \left.\frac{\partial \phi}{\partial z}\right|_{z=L} = u_2 f_2(r,\theta) = N_2(r,\theta) \tag{3.71}$$

### 3.2.1   Velocity potential

Assuming harmonic behaviour, the velocity potential may be written as $\phi(\vec{r},t) = \phi(\vec{r})e^{j\omega t}$.
Total velocity potential inside the chamber is expressed by superimposing the velocity potentials generated due to the inlet and outlet piston sources. Thus, the expression for total velocity potential can be written as:

$$
\begin{aligned}
\phi(\vec{r}) &= -\frac{1}{4\pi} \iint G\left(\vec{r}|\vec{r_0}\right) N(r_0^S) dS_0 \\
&= -\frac{1}{4\pi} \left[ \iint G\left(\vec{r}|\vec{r_0}\right) N_1\left(r,\theta\right) dS_B + \iint G\left(\vec{r}|\vec{r_0}\right) N_2\left(r,\theta\right) dS_C \right]
\end{aligned}
\tag{3.72}
$$

Let us assume:

$$\phi_1(\vec{r}) = -\frac{1}{4\pi} \iint_{\text{port 1}} G\left(\vec{r}|\vec{r_0}\right) N_1\left(r,\theta\right) dS_B \tag{3.73}$$

$$\phi_2(\vec{r}) = -\frac{1}{4\pi} \iint_{\text{port 2}} G\left(\vec{r}|\vec{r_0}\right) N_2\left(r,\theta\right) dS_C \tag{3.74}$$

The velocity potential caused by port 1 can be obtained by substituting Green's function (3.38) into Eq. 3.73

$$\phi_1(\vec{r}) = (-)\frac{1}{4\pi} \iint 4\pi \sum_{mnp} G_{mnp}(k)\Psi_{mnp}(\vec{r})\, \Psi_{mnp}(\vec{r_0})N_1(r,\theta)\, dS_B$$

$$= (-)\sum_{mnp} G_{mnp}(k)\Psi_{mnp}(\vec{r}) \iint \Psi_{mnp}(\vec{r_0})\, u_1 f_1(r,\theta)\, dS_B \qquad (3.75)$$

$$= (-)\sum_{mnp} G_{mnp}(k)\Psi_{mnp}^{(1)}(\vec{r})u_1 x_1$$

where $\Psi_{mnp}^{(1)}(\vec{r})$ is the mode shape function corresponding to port 1.

$$\Psi_{mnp}^{(1)}(\vec{r}) = \left[ J_m\left(\frac{\kappa_{mn}b}{2}\right) + C_{mn}Y_m\left(\frac{\kappa_{mn}b}{2}\right) \right] \cos(m\theta_1)\cos(k_{zp}l_1) \qquad (3.76)$$

and,

$$x_1 = \iint_{\text{port 1}} J_m(\kappa_{mn}r)\cos(m\theta)f_1(r,\theta)rdrd\theta$$

$$= \frac{2\pi a_1{}^2}{(\kappa_{mn}a_1 + 2\mu_{mn})}\left(J_1(\kappa_{mn}a_1) + \mu_{mn}\right)J_m(\kappa_{mn}\delta)\cos(m\theta_1)\cos(k_{zp}l_1) \qquad (3.77)$$

Similarly, the velocity potential for piston 2 can be written as:

$$\phi_2(\vec{r}) = (-)\sum_{mnp} G_{mnp}(k)\Psi_{mnp}^{(2)}(\vec{r})u_2 x_2 \qquad (3.78)$$

where $\Psi_{mnp}^{(2)}(\vec{r})$ is the mode shape function corresponding to port 2.

$$\Psi_{mnp}^{(2)}(\vec{r}) = \left[ J_m\left(\frac{\kappa_{mn}b}{2}\right) + C_{mn}Y_m\left(\frac{\kappa_{mn}b}{2}\right) \right] \cos(m\theta_2)\cos(k_{zp}l_2) \qquad (3.79)$$

and,

$$x_2 = \iint_{\text{port 2}} J_m(\kappa_{mn}r)\cos(m\theta)f_2(r,\theta)rdrd\theta$$

$$= \frac{2\pi a_2{}^2}{(\kappa_{mn}a_2 + 2\mu_{mn})}\left(J_1(\kappa_{mn}a_2) + \mu_{mn}\right)J_m(\kappa_{mn}\delta)\cos(m\theta_2)\cos(k_{zp}l_2) \qquad (3.80)$$

The solution for integration over the port area has been explained in Appendix A.3

## 3.2.2   Piston analogy approach

As described in Sec. 3.1.2, the average sound pressure acting on output piston 2 due to input piston 1 can be written as:

$$\bar{p}_{21}(\vec{r}) = (-)\frac{j\omega\rho}{A_2} \int\limits_{\text{piston 2}} \phi_1(\vec{r})\, dS_2$$

$$= (-)\frac{j\omega\rho}{A_2} \int\limits_{\text{piston 2}} (-)\sum_{mnp} G_{mnp}(k)\, u_1 x_1 \Psi_{mnp}^{(1)}(\vec{r})\, dS_2 \tag{3.81}$$

$$= \frac{j\omega\rho}{A_2} \sum_{mnp} G_{mnp}(k)\, u_1 x_1 x_2$$

Thus, the E-function $E_{21}$ can be written as:

$$E_{21} = \frac{\bar{p}_{21}(\vec{r})}{A_1 u_1} = \frac{j\omega\rho}{A_1 A_2} \sum_{mnp} G_{mnp}(k)\, x_2 x_1 \tag{3.82}$$

Similarly,

$$E_{11} = \frac{\bar{p}_{11}(\vec{r})}{A_1 u_1} = \frac{j\omega\rho}{A_1{}^2} \sum_{mnp} G_{mnp}(k)\, x_1{}^2 \tag{3.83}$$

$$E_{12} = \frac{\bar{p}_{12}(\vec{r})}{A_2 u_2} = (-)\frac{j\omega\rho}{A_1 A_2} \sum_{mnp} G_{mnp}(k)\, x_1 x_2 \tag{3.84}$$

$$E_{22} = \frac{\bar{p}_{21}(\vec{r})}{A_2 u_2} = (-)\frac{j\omega\rho}{A_2{}^2} \sum_{mnp} G_{mnp}(k)\, x_2{}^2 \tag{3.85}$$

### 3.2.3  Four pole parameters

The four pole parameters can be estimated in the same way as described in Sec. 3.1.3

### 3.2.4  Calculation of transmission loss

The transmission loss can be estimated in a similar way as described in Sec. 3.1.4

## 3.3  Face-Inlet-Side-Outlet (FISO) configuration

As shown in Fig. 3.3, the surfaces of the annular cavity are defined as $S_A$, $S_B$ and $S_C$. The inlet port is located on surface $S_B$ at a distance $\delta$ from the $z$ axis at 180°. The outlet port is on the curved surface $S_A$, and is at a distance $l_2$ at 0°from surface $S_B$. Both the ports are of elliptical cross-section. The half major axis length is $a_1$ and $a_2$ whereas the half minor axis length is $b_1$ and $b_2$ for the inlet and outlet ports respectively. The hypothetical velocities of pistons at the inlet and outlet ports are assumed as $u_1$ and $u_2$ respectively as shown in the diagram.
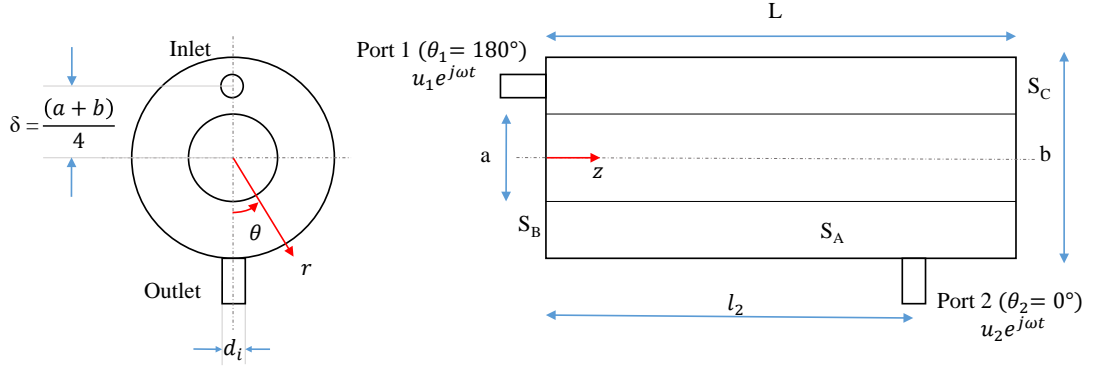
Figure 3.3: Annular cavity with Face-Inlet-Side-Outlet configuration

The boundary conditions on the surfaces of the annular cavity can be defined as follows:

$$S_A \; : \; \left.\frac{\partial \phi}{\partial r}\right|_{r=b/2} = u_2 \cos \theta_2 f_2(z,\theta) = N_2(z,\theta) \tag{3.86}$$

$$S_B \; : \; \left.\frac{\partial \phi}{\partial z}\right|_{z=0} = u_1 f_1(r,\theta) = N_1(r,\theta) \tag{3.87}$$

$$S_C \; : \; \left.\frac{\partial \phi}{\partial z}\right|_{z=L} = 0 \tag{3.88}$$

### 3.3.1 Velocity potential

Assuming harmonic behaviour, the velocity potential may be written as $\phi(\vec{r}, t) = \phi(\vec{r})e^{j\omega t}$.
Total velocity potential inside the chamber is expressed by superimposing the velocity potentials generated due to the inlet and outlet piston sources. Thus, the expression for total velocity potential can be written as:

$$\begin{aligned}
\phi(\vec{r}) &= -\frac{1}{4\pi} \iint G\left(\vec{r}|\vec{r_0}\right) N(r_0^S) dS_0 \\
&= -\frac{1}{4\pi} \left[ \iint G\left(\vec{r}|\vec{r_0}\right) N_1\left(r,\theta\right) dS_B + \iint G\left(\vec{r}|\vec{r_0}\right) N_2\left(z,\theta\right) dS_A \right]
\end{aligned} \tag{3.89}$$

Let us assume:

$$\phi_1(\vec{r}) = -\frac{1}{4\pi} \iint_{\text{port 1}} G\left(\vec{r}|\vec{r_0}\right) N_1\left(r,\theta\right) dS_B \tag{3.90}$$

$$\phi_2(\vec{r}) = -\frac{1}{4\pi} \iint_{\text{port 2}} G\left(\vec{r}|\vec{r_0}\right) N_2\left(z,\theta\right) dS_A \tag{3.91}$$

31

The velocity potential caused by port 1 can be obtained by substituting Green's function (3.38) into Eq. 3.90

$$\phi_1(\vec{r}) = (-)\frac{1}{4\pi} \iint 4\pi \sum_{mnp} G_{mnp}(k)\Psi_{mnp}(\vec{r})\,\Psi_{mnp}(\vec{r_0})N_1(r,\theta)\,dS_B$$

$$= (-)\sum_{mnp} G_{mnp}(k)\Psi_{mnp}(\vec{r}) \iint \Psi_{mnp}(\vec{r_0})\,u_1 f_1(r,\theta)\,dS_B \qquad (3.92)$$

$$= (-)\sum_{mnp} G_{mnp}(k)\Psi_{mnp}^{(1)}(\vec{r})u_1 x_1$$

where $\Psi_{mnp}^{(1)}(\vec{r})$ is the mode shape function corresponding to port 1.

$$\Psi_{mnp}^{(1)}(\vec{r}) = \left[J_m\left(\frac{\kappa_{mn}b}{2}\right) + C_{mn}Y_m\left(\frac{\kappa_{mn}b}{2}\right)\right]\cos(m\theta_1)\cos(k_{zp}l_1) \qquad (3.93)$$

and,

$$x_1 = \iint_{\text{port 1}} J_m(\kappa_{mn}r)\cos(m\theta)f_1(r,\theta)r\,dr\,d\theta$$

$$= \frac{2\pi a_1{}^2}{(\kappa_{mn}a_1 + 2\mu_{mn})}\left(J_1(\kappa_{mn}a_1) + \mu_{mn}\right)J_m(\kappa_{mn}\delta)\cos(m\theta_1)\cos(k_{zp}l_1) \qquad (3.94)$$

Similarly, the velocity potential for piston 2 can be written as:

$$\phi_2(\vec{r}) = (-)\frac{1}{4\pi} \iint 4\pi \sum_{mnp} G_{mnp}(k)\Psi_{mnp}(\vec{r})\,\Psi_{mnp}(\vec{r_0})N_2(z,\theta)\,dS_A$$

$$= (-)\sum_{mnp} G_{mnp}(k)\Psi_{mnp}(\vec{r}) \iint \Psi_{mnp}(\vec{r_0})\,u_2 \cos\theta_2 f_2(z,\theta)\,dS_A \qquad (3.95)$$

$$= (-)\sum_{mnp} G_{mnp}(k)\Psi_{mnp}^{(2)}(\vec{r})u_2 y_2$$

where $\Psi_{mnp}^{(2)}(\vec{r})$ is the mode shape function corresponding to port 2.

$$\Psi_{mnp}^{(2)}(\vec{r}) = \left[J_m\left(\frac{\kappa_{mn}b}{2}\right) + C_{mn}Y_m\left(\frac{\kappa_{mn}b}{2}\right)\right]\cos(m\theta_2)\cos(k_{zp}l_2) \qquad (3.96)$$

and,

$$y_2 = \left[J_m\left(\frac{\kappa_{mn}b}{2}\right) + C_{mn}Y_m\left(\frac{\kappa_{mn}b}{2}\right)\right] \iint_{\text{port 2}} \cos(m\theta)\cos(k_{zp}z)\,dS_A$$

$$= \pi a_2 b_2 \left[J_m\left(\frac{\kappa_{mn}b}{2}\right) + C_{mn}Y_m\left(\frac{\kappa_{mn}b}{2}\right)\right] \qquad (3.97)$$

$$\cos(k_{zp}l_2)\left[F_{mp}\left(\frac{1}{2}, \cos[(m-1)\theta_2] \times \frac{J_1(b_2\beta_{m-1,2})}{b_2\beta_{m-1,2}}\right) + \cos[(m-1)\theta_2] \times \frac{J_1(b_2\beta_{m+1,2})}{b_2\beta_{m+1,2}}\right]$$

### 3.3.2 Piston analogy approach

The average sound pressure acting on input piston 1 due to input piston 1 can be derived using the same formulation as described in Sec. 3.1.2.

$$
\begin{aligned}
\bar{p}_{11}\left(\vec{r}\right) &= (-)\frac{j\omega\rho}{A_1}\int_{\text{piston 1}}\phi_1\left(\vec{r}\right)dS_1 \\
&= (-)\frac{j\omega\rho}{A_1}\int_{\text{piston 1}}(-)\sum_{mnp}G_{mnp}\left(k\right)u_1x_1\Psi_{mnp}^{(1)}\left(\vec{r}\right)dS_1 \\
&= \frac{j\omega\rho}{A_1}\sum_{mnp}G_{mnp}\left(k\right)u_1{x_1}^2
\end{aligned}
\tag{3.98}
$$

Thus, the E-function $E_{11}$ can be written as:

$$
E_{11} = \frac{\bar{p}_{11}\left(\vec{r}\right)}{A_1u_1} = \frac{j\omega\rho}{{A_1}^2}\sum_{mnp}G_{mnp}\left(k\right){x_1}^2
\tag{3.99}
$$

Similarly, the sound pressure $\bar{p}_{21}\left(\vec{r}\right)$ can be derived as:

$$
\begin{aligned}
\bar{p}_{21}\left(\vec{r}\right) &= (-)\frac{j\omega\rho}{A_2}\int_{\text{piston 2}}\phi_1\left(\vec{r}\right)dS_2 \\
&= (-)\frac{j\omega\rho}{A_2}\int_{\text{piston 2}}(-)\sum_{mnp}G_{mnp}\left(k\right)u_1x_1\Psi_{mnp}^{(1)}\left(\vec{r}\right)dS_2 \\
&= \frac{j\omega\rho}{A_2}\sum_{mnp}G_{mnp}\left(k\right)u_1x_1y_2
\end{aligned}
\tag{3.100}
$$

The corresponding E-function is

$$
E_{21} = \frac{\bar{p}_{21}\left(\vec{r}\right)}{A_1u_1} = \frac{j\omega\rho}{A_1A_2}\sum_{mnp}G_{mnp}\left(k\right)x_1y_2
\tag{3.101}
$$

Similarly,

$$
E_{12} = \frac{\bar{p}_{12}\left(\vec{r}\right)}{A_2u_2} = (-)\frac{j\omega\rho}{A_1A_2}\sum_{mnp}G_{mnp}\left(k\right)x_1y_2
\tag{3.102}
$$

$$
E_{22} = \frac{\bar{p}_{21}\left(\vec{r}\right)}{A_2u_2} = (-)\frac{j\omega\rho}{{A_2}^2}\sum_{mnp}G_{mnp}\left(k\right){y_2}^2
\tag{3.103}
$$

### 3.3.3 Four pole parameters

The four pole parameters can be estimated in the same way as described in Sec. 3.1.3

### 3.3.4 Calculation of transmission loss

The transmission loss can be calculated from Sec. 3.1.4

# Chapter 4

# Finite element analysis

## 4.1 Introduction to FEA

Finite element analysis (FEA) also known as finite element method (FEM) is one of the most common method in practice. A large and complex system, which is governed by a partial differential equation(s) is broken down into a discrete system of algebraic linear equations. These linear equations represent the behaviour of the discretised portions of the system, known as elements. Smaller the element area of the system, more accurate will the model be. The simple equations that model these finite elements are then assembled together to model the entire system. The general form of the consequent linear equations is usually represented as $[K]\{u\} = \{F\}$. Generally, a structure is divided into several hundred elements, generating a very large number of equations that can only be solved with the help of a computer.

The term finite element stems from the procedure in which a structure is divided into small but finite size elements (as opposed to an infinite size, generally used in mathematical integration). The endpoints or corner points of the element are called nodes. Each element possesses its own geometric and elastic properties. Spring, Truss, and Beams elements, called line elements, are usually divided into small sections with nodes at each end. Plane and solid elements require more than two nodes and can have over 8 nodes for a 3 dimensional element.

A line element has an exact theoretical solution, e.g., truss and beam elements are governed by their respective theories of deflection. But when it comes to complex engineering systems with stress concentration points like holes and other discontinuities, it becomes impossible to use standard equations. This is where the finite element method comes into picture.The following section explains the use of 'LMS Virtual.Lab' to estimate the transmission loss of the annular cavity.

## 4.2 LMS Virtual.Lab

LMS Virtual.Lab is a software which integrates 3D FEM and multi-body simulation and optimizes the performance of mechanical systems for structural integrity, noise and vibration, system dynamics and durability.

LMS Virtual.Lab Finite Element Acoustics offers an advanced method for predicting and improving the noise and sound performance of a broad range of systems.

The major steps involved in performing a 3D FEM simulation on this software are:

- Creating a CAD model
- Meshing the model
- Importing the model in LMS Virtual.Lab
- Assigning proper boundary conditions
- Post-processing the results
- Calculation of transmission loss

### 4.2.1 Creating a CAD model

The CAD model is a geometrical representation of the flow domain inside the annular muffler cavity. Different types of CAD software can be used to create the model according to ease to the user.
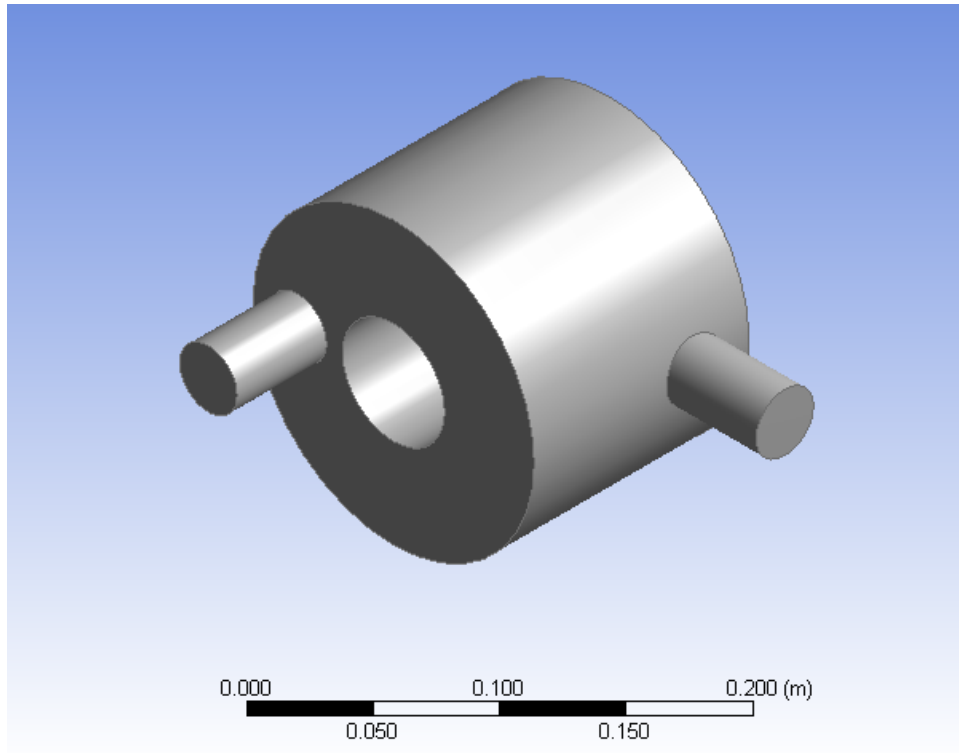


Figure 4.1: CAD geometry of Face-Inlet-Side-Outlet (FISO) annular cavity

Fig. 4.1 shows the geometry of an annular cavity with Face-Inlet-Side-Outlet configuration. ANSYS Workbench was used to create the geometry. The geometry depicts the volume which will be used for simulation.

### 4.2.2 Meshing the model

Meshing is probably the most important part in any of the computer simulations, because it can show drastic changes in the obtained results. Meshing simply means creating a mesh of some grid-points called 'nodes'. It is done with a variety of tools and options available in the software. The

results are calculated by solving the relevant governing equations numerically at each of the nodes of the mesh. The governing equations are almost always partial differential equations. The pattern and relative positioning of the nodes also affect the solution, computational efficiency and time. This is why good meshing is very essential for a computer simulation to give satisfactory results.
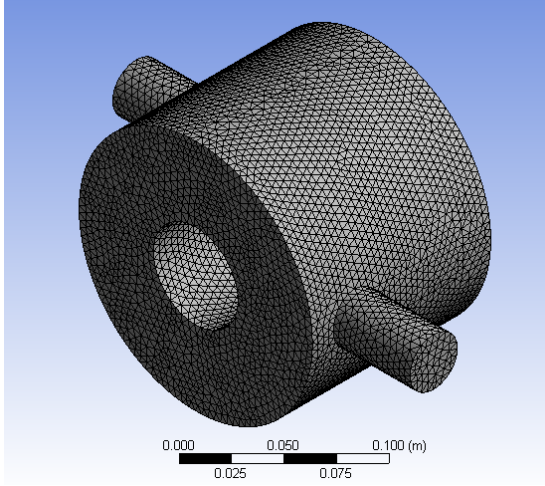


Figure 4.2: Tetrahedral Mesh
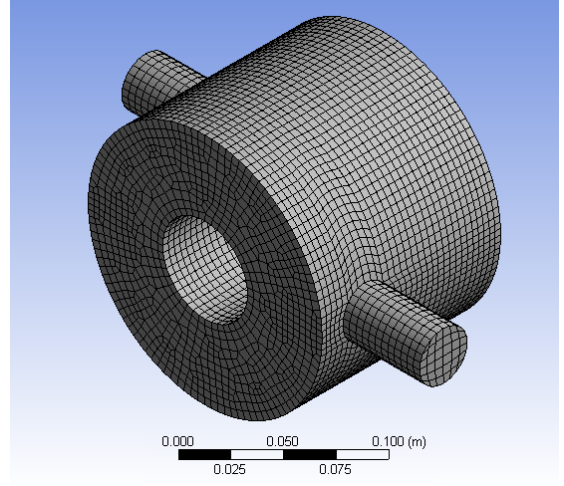


Figure 4.3: Hexahedral Mesh

Fig. 4.2 shows a tetrahedral mesh created using the meshing module of ANSYS®Workbench. A tetrahedral mesh being an unstructured mesh, can be created easily. Although, it is computationally expensive as it takes more time for simulation.

An hexahedral mesh is shown in Fig. 4.3. It consists of hexahedrons which are arranged in regular patterns across the whole volume. This type of mesh can be easily created for simple pre-defined geometry shapes. But when it comes to complex geometries, it takes some manipulations thus consuming more time. An hexahedral mesh is a structured mesh. Hence, it is computationally better than a tetrahedral mesh as solving the linear equations becomes much easier and faster.

### 4.2.3   Importing the model in LMS Virtual.Lab

After creating the meshed model, it can be imported into the software in various compatible formats such as *.cdb*, *.nas*, *.stp*, etc.

### 4.2.4   Assigning proper boundary conditions

After importing the model into the software, materials and properties for the flow domain are defined. In case of a muffler cavity, an inlet and outlet is defined for the sound wave propagation. A unit velocity of 1 m/s is applied as the inlet boundary condition while the outlet is considered as anechoic termination.

### 4.2.5   Post-processing the results

After the simulation is complete, the acoustic pressure values at the inlet and outlet are estimated by the software for the specified frequency range.

### 4.2.6 Calculation of transmission loss

The transmission loss can be estimated in two different ways:

1. *Exporting the acoustic pressure data from the software into a Microsoft®Excel file.*
   The acoustic pressure comprises of the real and imaginary component. Both components of the inlet and outlet acoustic pressures are exported and transmission loss is calculated according to the formula as:

$$TL = 20 \log_{10} \left| \frac{P_{in} + \rho c V_{in}}{2 P_{out}} \right| \tag{4.1}$$

   where $P_{in}$ is the acoustic pressure at the inlet, $P_{out}$ is the acoustic pressure at the outlet, $V_{in}$ is the velocity at the inlet (1 m/s)

2. *Post-processing the acoustic pressure data in the software itself.*
   The detailed procedure regarding the steps involved in transmission loss calculation are mentioned in appendix C.

# Chapter 5

# Results

## 5.1 Numerical model

A numerical model was developed to validate the analytical methodology described in the previous section. The numerical simulation was carried out under the 'Acoustic Harmonic FEM' module of the commercial simulation software LMS Virtual.Lab [23]. Each configuration was considered with a short-length and a long-length model. The following table gives the number of nodes and elements for each long-length configuration, and the maximum frequency up to which the model is valid. The numerical simulation was done for a frequency range of 5 to 3000 Hz in steps of 5 Hz.

Table 5.1: Numerical model details

| Type | Configuration | Nodes | Elements | Maximum frequency (Hz) |
| --- | --- | --- | --- | --- |
| | SISO | 22981 | 19576 | 3685 |
| Long | FIFO | 23026 | 20302 | 3920 |
| | FISO | 20701 | 17852 | 3616 |
| | SISO | 8296 | 6816 | 4378 |
| Short | FIFO | 8318 | 7016 | 4175 |
| | FISO | 9900 | 8346 | 4361 |

## 5.2 Analytical model

The analytical methodology described in Chapter 3 was used to develop a MATLAB® code to calculate the transmission loss of the annular cavity for the three different types of configurations. Two types of models were considered, one with short length and the other with long length for each of the three configurations. For these TL curves, the modal series was summed up to m=3, n=3 and p=7.

The parameters and constants used in the code are given below in Table 5.2.

Table 5.2: Dimensions and constants

| Description | Symbol and value |
|---|---|
| Outer diameter of the cavity | $b = 0.157$ m |
| Inner diameter of the cavity | $a = 0.057$ m |
| Long-length cavity | $L = 0.44$ m |
| Short-length cavity | $L = 0.12$ m |
| Location of side inlet | $l_1 = 0.25L$ |
| Location of side outlet | $l_2 = 0.75L$ |
| Location of face inlet | $\delta_1 = 0.0535$ m |
| Location of face outlet | $\delta_2 = 0.0535$ m |
| Diameter of inlet and outlet ports | $d_1 = d_2 = 0.032$ m |
| Density of air | $\rho = 1.225$ kg/m$^3$ |
| Speed of sound | $c = 340$ m/s |

## 5.3 Validation

### 5.3.1 Side-Inlet-Side-Outlet (SISO) configuration

Fig. 5.1 shows the comparison between transmission loss curves calculated analytically and numerically. The plot is taken up to a frequency range of 5 to 3000 Hz. The cut-on frequency in this case is estimated to be 1037 Hz which corresponds to the first circumferential mode. The maximum value to TL occurs at close to 700 Hz, which is 79 dB. At, low frequencies, modes appear to be well separated. Whereas, at medium frequencies, they are close to each other.
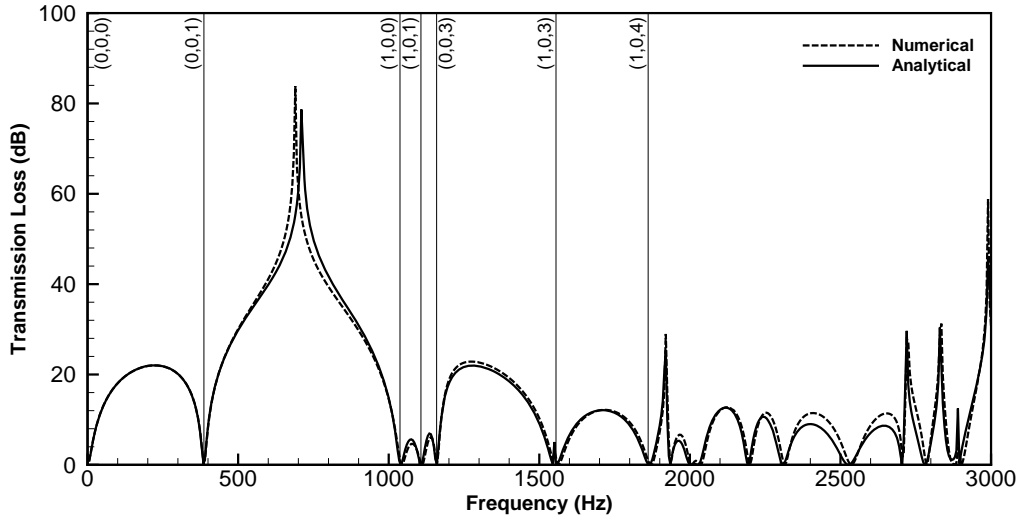


Figure 5.1: Transmission loss of SISO long-length cavity

Table 5.3: Mode shapes of SISO long-length annular cavity
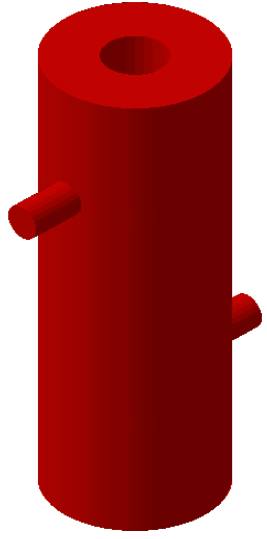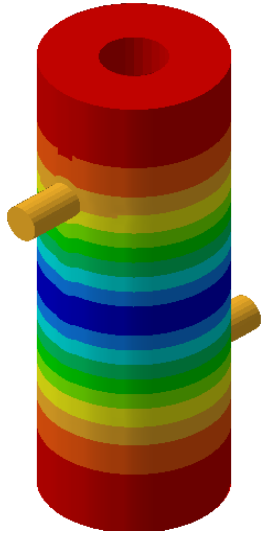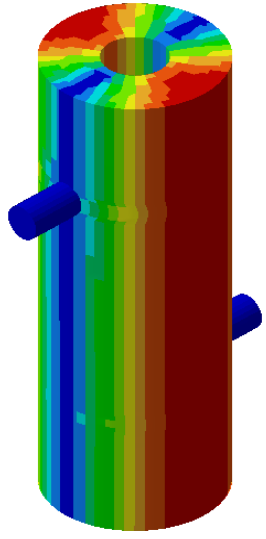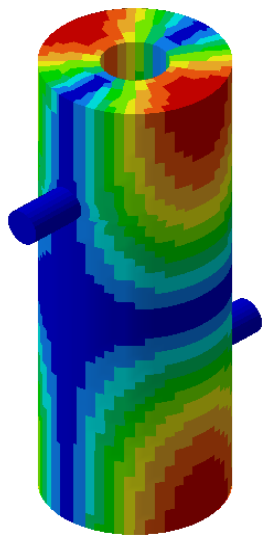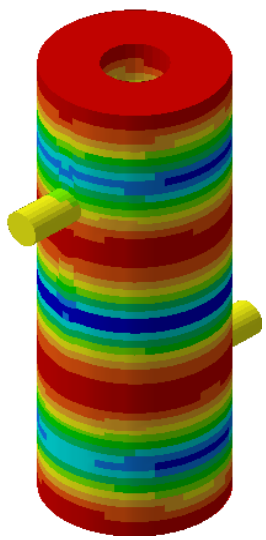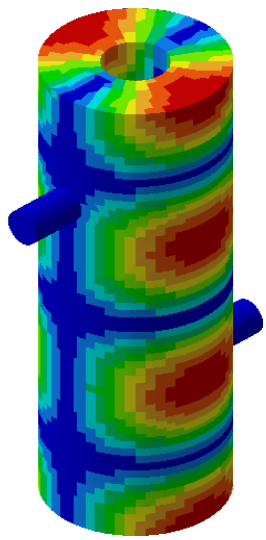
| Mode | (0, 0, 0) | (0, 0, 1) | (1, 0, 0) |
|------|-----------|-----------|-----------|
| Frequency | 0 Hz | 386 Hz | 1037 Hz |
| Mode Shape |  |  |  |
| Mode | (1, 0, 1) | (0, 0, 3) | (1, 0, 3) |
| Frequency | 1107 Hz | 1160 Hz | 1555 Hz |
| Mode Shape |  |  |  |

Table 5.3 depicts the first six modal indices (values corresponding to m, n and p) of an SISO long-length annular cavity and the corresponding acoustic natural frequencies and mode shapes. The images denote the acoustic modeshape of the annular cavity.

Fig. 5.2 shows the comparison of analytical and numerical transmission loss of an SISO annular cavity. The maximum value of TL predicted by the analytical method is 46 dB, which occurs at a frequency of 1325 Hz. The L/b ratio for this short-length cavity is approximately 0.76. Due to a short length, the modes of the TL graph are well spread over the range of 3000 Hz.
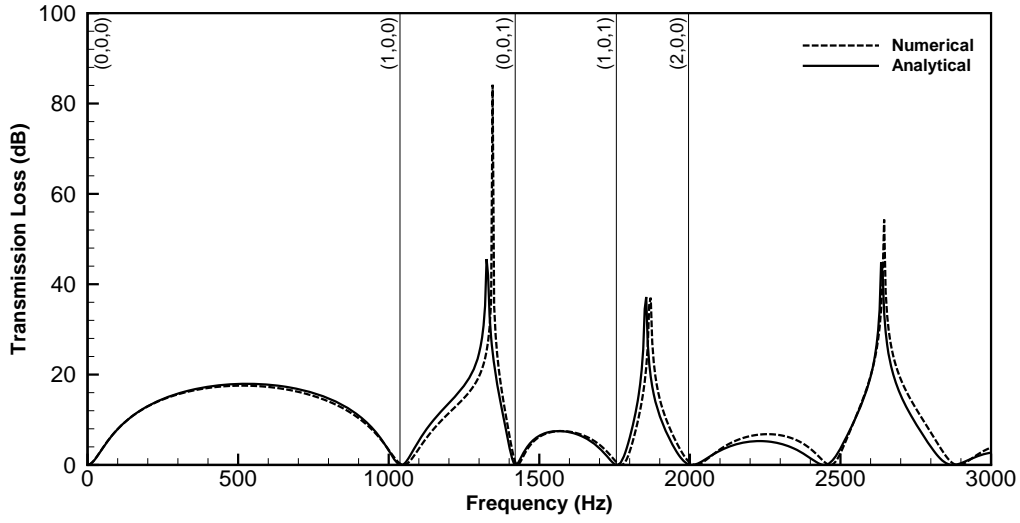
Figure 5.2: Transmission loss of SISO short-length cavity

## 5.3.2 Face-Inlet-Face-Outlet (FIFO) configuration
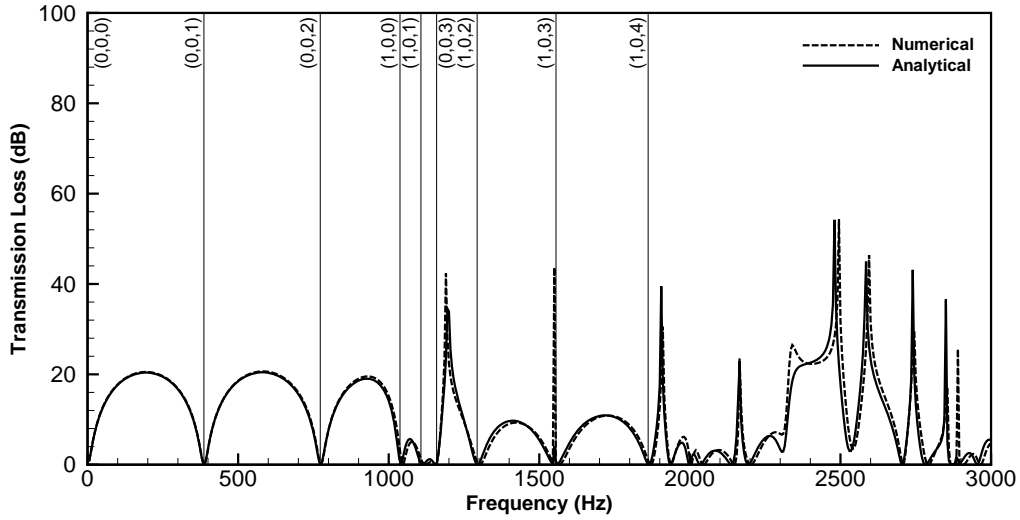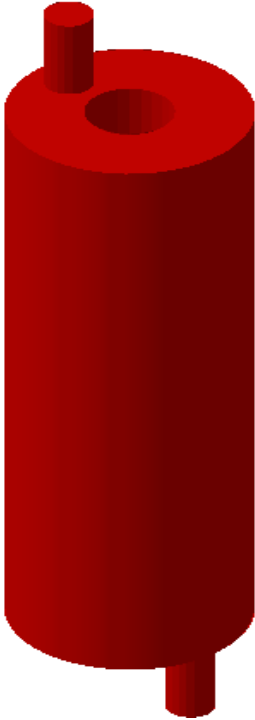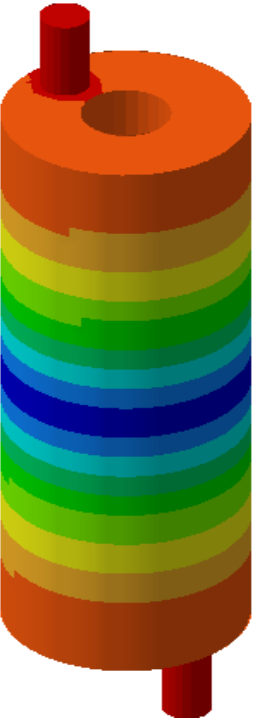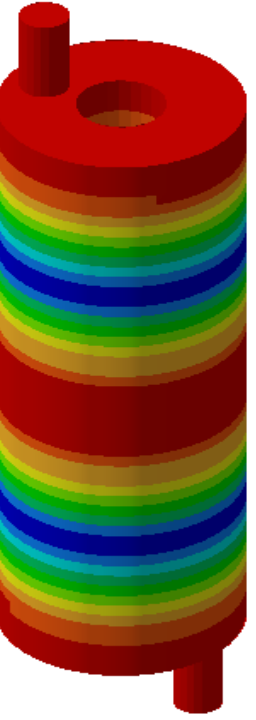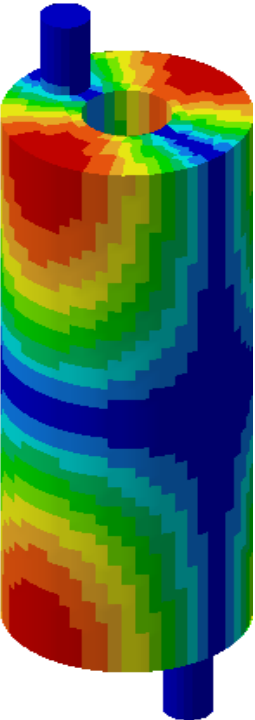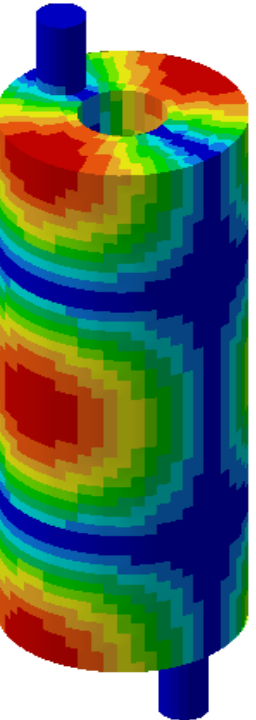


Figure 5.3: Transmission loss of FIFO long-length cavity

Fig. 5.3 shows the plot of analytical and numerical transmission loss for an FIFO annular cavity. The plot range for frequency is from 5 to 3000 Hz. This being a long-length cavity, the L/b ratio is approximately 2.78. The cut-on frequency for this cavity is also 1037 Hz, as the diameters remain the same. The maximum value of TL is 54 dB occurring at 2480 Hz. Up to the cut-on frequency, the FIFO long-length cavity has similar characteristics as that of an SEC muffler.

Table 5.4 shows some of the mode shapes and the corresponding acoustic natural frequencies of the FIFO long-length annular cavity. The images denote the acoustic modeshape of the cavity.

Table 5.4: Mode shapes of FIFO long-length annular cavity

| Mode | (0, 0, 0) | (0, 0, 1) | (0, 0, 2) |
|---|---|---|---|
| Frequency | 0 Hz | 386 Hz | 772 Hz |
| Mode Shape | | | |

| Mode | (1, 0, 0) | (1, 0, 1) | (1, 0, 2) |
|---|---|---|---|
| Frequency | 1037 Hz | 1107 Hz | 1295 Hz |
| Mode Shape | | | |
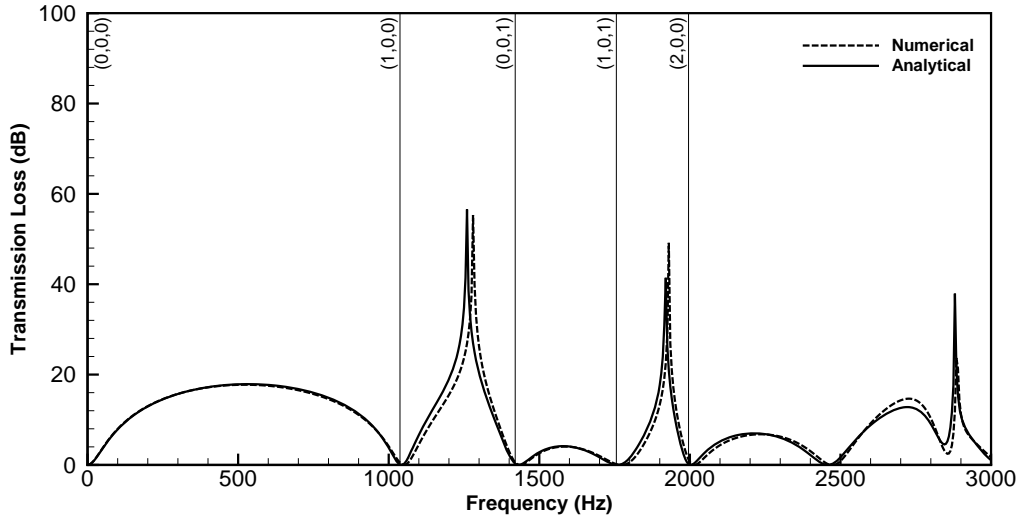
Figure 5.4: Transmission loss of FIFO short-length cavity

The analytical and numerical transmission loss graph for an FIFO short-length cavity is shown in Fig. 5.4. The TL curve has well separated modes since the L/b ratio is less than 1. The cut-on frequency occurs at the first circumferential mode. (m=1, n=0, p=0). The maximum TL occurs at 1260 Hz with a magnitude of 56 dB.

### 5.3.3   Face-Inlet-Side-Outlet (FISO) configuration
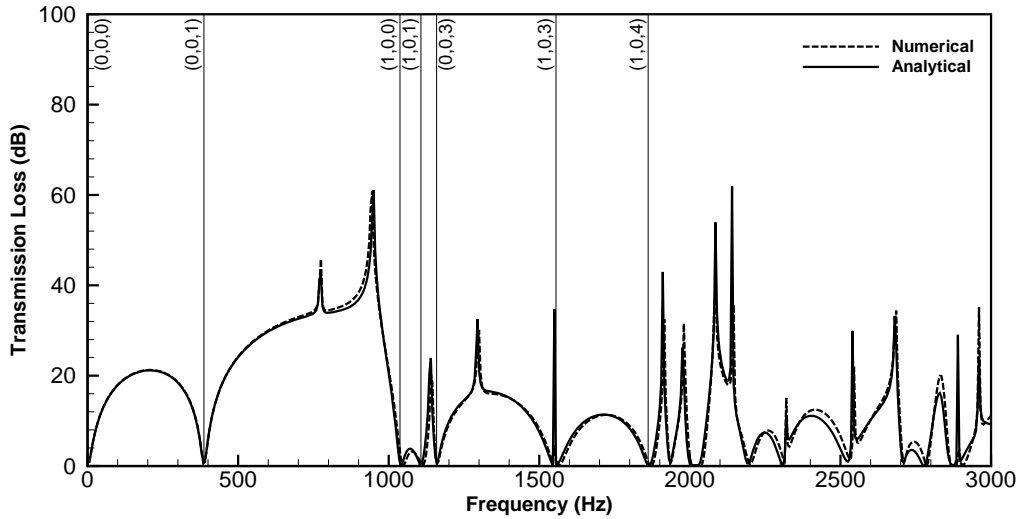


Figure 5.5: Transmission loss of FISO long-length cavity

An FISO annular cavity has its inlet on the face and the outlet port on its side. The TL comparison of analytical and numerical methods is shown in Fig. 5.5. There is a good agreement between the two results. Again, in this case, the cut-on frequency is 1037 Hz. Thereafter, higher order modes

43

start to propagate. As we move towards 3000 Hz, the modes appear to be closely spaced. The maximum values of TL is 61 dB which occurs at two frequencies of 950 Hz and 2140 Hz.

Table 5.5: Mode shapes of FISO long-length annular cavity
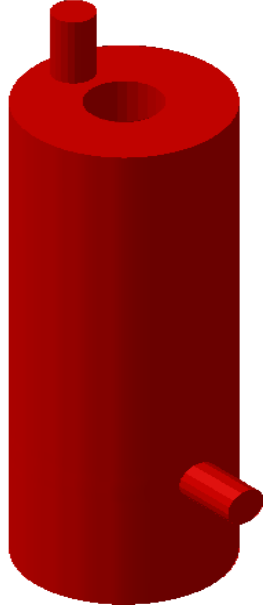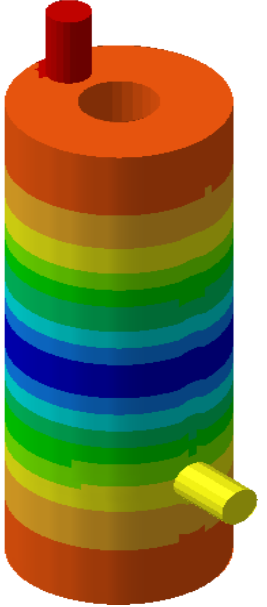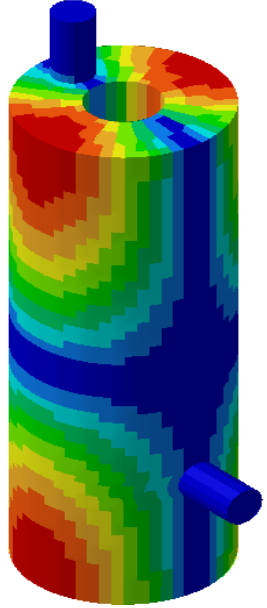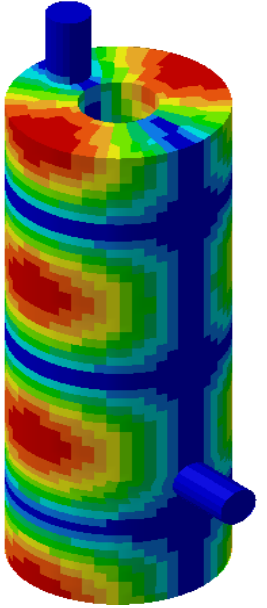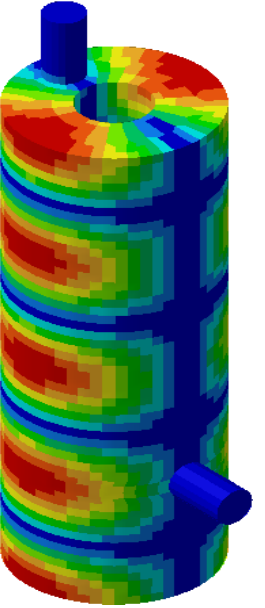
| Mode | (0, 0, 0) | (0, 0, 1) | (1, 0, 0) |
|---|---|---|---|
| Frequency | 0 Hz | 386 Hz | 1037 Hz |
| Mode Shape |  |  |  |
| Mode | (1, 0, 1) | (1, 0, 3) | (1, 0, 4) |
| Frequency | 1107 Hz | 1555 Hz | 1861 Hz |
| Mode Shape |  |  |  |

Table 5.5 shows some of the mode shapes of the FISO long-length annular cavity. The mode index for each mode shape is represented as a combination of m, n and p. The corresponding acoustic natural frequencies are also mentioned.
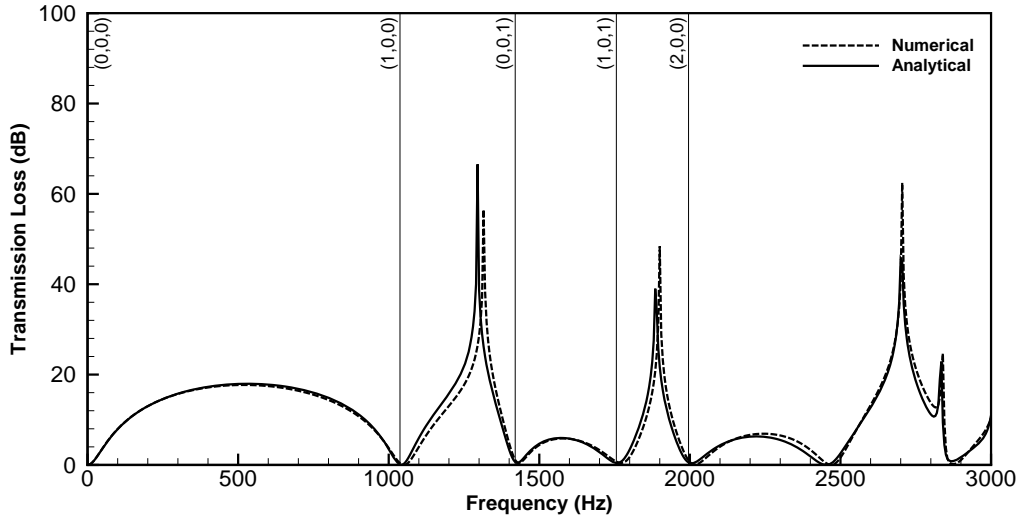
Figure 5.6: Transmission loss of FISO short-length cavity

For the short-length FISO annular cavity, the plot of transmission loss is plotted for a frequency range up to 3000 Hz as shown in Fig. 5.6. The TL curve for a short-length has well separated modes due to its L/b ratio being less than 1. The cut-on frequency in this case is also 1037 Hz, same as the long-length cavity. The peak of TL occurs at 1295 Hz which is 66 dB.
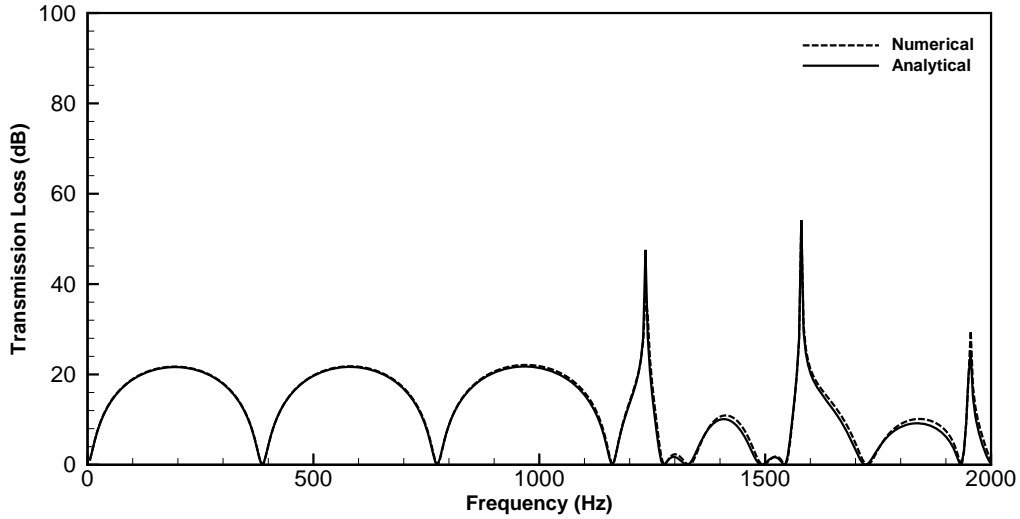
## 5.4   Transmission loss of a circular duct



Figure 5.7: Transmission loss of FIFO long-length circular duct

An annular cavity with no inner diameter resembles a circular duct. The same formulation can be used to estimate the transmission loss of a circular duct by making the inner diameter as zero. Due

to this, the radial mode shape function for a circular duct becomes to Eq. 5.1

$$R(r) = J_m(\kappa_{mn}r) \tag{5.1}$$

This equation is same as that for an annular cavity with the term $C_{mn} = 0$. (Refer Eq. 3.21)
A comparison of analytical and numerical TL for a Face-Inlet-Face-Outlet (FIFO) circular duct is shown in this section. All the remaining parameters are kept same as that of the annular cavity. Fig. 5.7 shows the comparison between the numerical and analytical TL of a long-length FIFO circular duct. The graph is plotted for a range of 5 to 2000 Hz. Both, the numerical and the analytical results are in good agreement with each other and are found to be consistent with the existing literature [15].

## 5.5 Comparison of 3D and 1D plane wave analysis
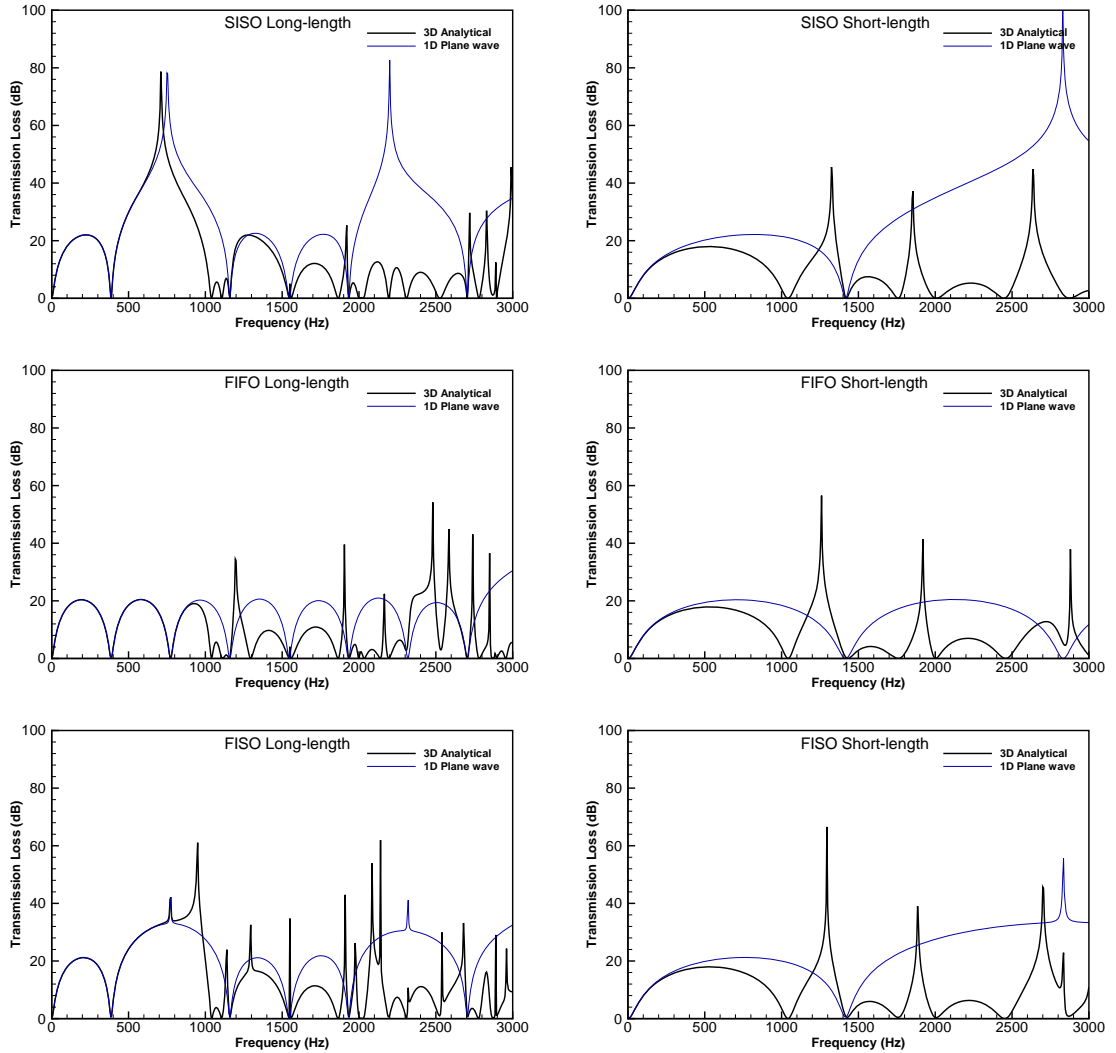


Figure 5.8: TL comparison of 3D analytical method and 1D plane wave for an annular cavity

The 1D plane wave propagation considers the acoustic pressure variation only in the longitudinal direction. Th acoustic pressure remains constant at any given cross-section of the annular cavity. A plane wave can be obtained by setting the radial mode order (m) and circumferential mode order (n) to zero in the Green's function.

Fig. 5.8 shows the comparison of 3D analytical and 1D plane wave transmission loss of an annular cavity with arbitrary port locations. Three different configurations viz. SISO, FIFO and FISO with long and short lengths are compared in the above figure. The 3D analytical TL is shown in black color whereas the 1D plane wave TL is in blue colour. It is observed that the 1D analysis results are in good agreement with 3D analysis predictions up to the cut-on frequency of higher order modes. These higher order modes, which propagate through the annular cavity, cannot be captured using a plane wave propagation.

The proposed formulation for calculating transmission loss of an annular chamber can also be used for a circular duct and one-dimensional plane wave analysis.

## 5.6 Parametric study

### 5.6.1 Inner diameter

The inlet diameter (a) affects the performance of the annular cavity. The cross-sectional area and the volume of the cavity are dependent on it. This prompts the investigation of the variation in the TL curves according to the change in the inlet diameter. For this parametric study, four different values of inner diameter are considered viz. 0.2b, 0.4b, 0.6b, and 0.8b. Frequency range for the parametric study is changed to 5 to 2000 Hz as the results are validated with the numerical method. Fig. 5.9 shows the analytical transmission loss for these four variations for the SISO configuration. The rest of the parameters are kept same as described in the previous section.
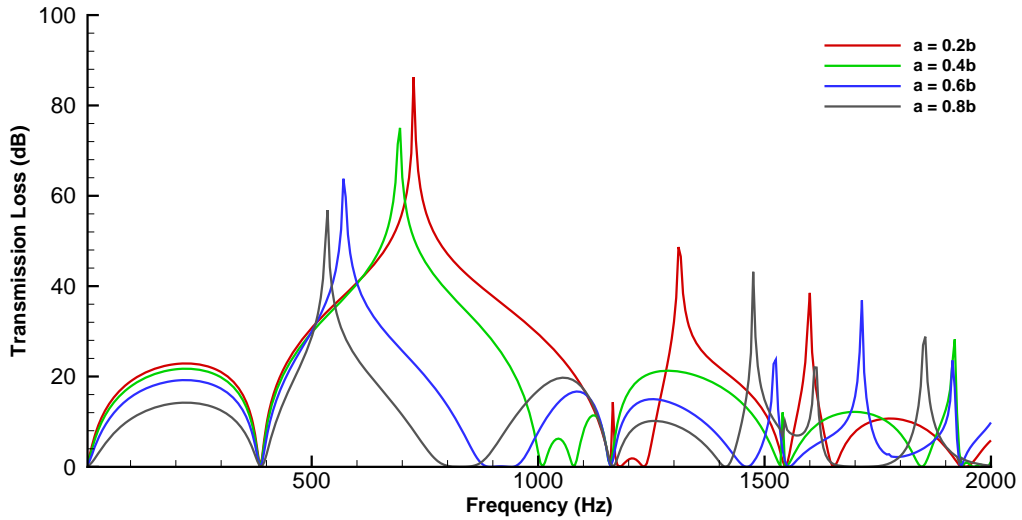


Figure 5.9: Analytical transmission loss for inner diameter variation

Table 5.6: Cut-on frequency variation with inner diameter

| Inner diameter (a) | Cut-on frequency (Hz) |
|---|---|
| 0.2b | 1160 |
| 0.4b | 1010 |
| 0.6b | 895 |
| 0.8b | 830 |

Form Fig. 5.9, it is seen that the inner diameter has a significant effect on the transmission loss of the cavity. The acoustic natural frequency is a function of the inner diameter. As, the inner diameter increases, the acoustic natural frequency decreases. Table 5.6 gives the cut-on frequencies for different values of inner diameter. This is indicated by the shift of the TL curves towards the Y-axis. Also a notable drop in the TL levels is observed due to the decreased area ratio by increasing the inner diameter.

### 5.6.2 Port diameter

The port diameter is another factor which has an effect on the TL characteristics. A change in the port diameter causes a change in the port cross-section area thereby causing an impedance mismatch. For the following cases, the port diameter is varied from 8 mm to 64 mm. These characteristics are plotted for an SISO configuration and the frequency range is changed to 5 to 2000 Hz since the analytical method has been validated.
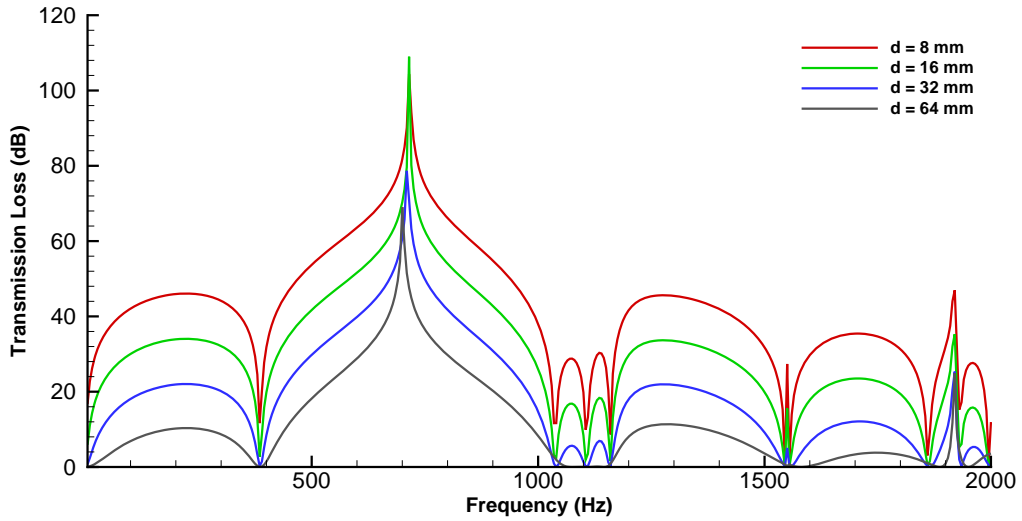


Figure 5.10: Analytical transmission loss for port diameter variation

Fig. 5.10 shows the effect of increasing port diameter on the transmission loss. All the parameters for the study are kept constant (Refer Sec. 5.3.1) except the port diameters of both, the inlet and the outlet ports. From this study, it can be seen that as the port diameter is increased, the difference in impedance of the annular cavity and the port reduces.Thus, the domes in the graph tend to get flatter and a considerable decrease is seen in the transmission loss.

# Chapter 6

# Conclusion

In this thesis, an optimum design methodology has been introduced for an EIEO muffler based on the idea of continuous jet formation. This approach has been performed for a one-dimensional case. This regression analysis based design has been used to calculate the modified dimensions of the muffler. This showed that the jet formation concept is ideal for short chamber mufflers, with $L/D$ ratio less than 1.

For a short chamber muffler, as the length and diameter are of comparable magnitude, the plane wave assumption does not hold. The high frequency waves, on account of their small wavelength, tend to have a three-dimensional propagation. Due to these reasons, it becomes essential to analyse the mufflers using a three dimensional study. Green's function method is one of the ways for a three-dimensional analysis, apart from FEM and BEM. An analytical approach has been developed for an annular cavity using the Green's function method. Using this study, the four pole parameters of the transfer matrix have been calculated. Based on the analytical derivations, a MATLAB code has been developed to estimate the transmission loss of an annular cavity with arbitrary locations of inlet and outlet ports.

These results were compared with those obtained by finite element method. LMS Virtual.Lab was used to numerically calculate the transmission loss of the annular cavity. Both, long-length and short-length cavities were studied as a part of this thesis. The analytical and FEM results were found to be in good agreement. The proposed formulation can also be used to calculate the transmission loss of circular chambers as well as the 1-D transfer matrix.

A parametric study was done for two parameters; the inner diameter of the cavity and the port diameter. The analytical TL curves for a=0.2b and a=0.4b match well with the numerical ones. As the inner diameter increases to 0.6b and above, the numerical method shows a deviation from the analytical TL prediction.

The port diameter affects the cross-sectional area of the ports to change with respect to the annular cross-sectional area. This causes an impedance mismatch between the cavity and the ports. The same variation is observed in the TL curves plotted for port diameters varying from 0.008 m to 0.064 m. There is a large difference in the impedance for small values of port diameter. This causes the domes in the TL curve to be elongated and the range of TL is high. Whereas, the graph for a higher port diameter show comparatively flatter TL curves due to a lesser difference in the impedance of the ports and the cavity.

# Chapter 7

# Future Scope

The three-dimensional analytical methodology for an annular cavity with various configurations has been established and validated with numerical methods as a part of this thesis. This provides a new approach to analyze the annular cavities where one-dimensional plane wave approximation cannot be used. The following points can be taken up as a future scope of this research work:

- Establishing a three-dimensional transfer matrix for EIEO muffler considering it as a combination of annular and circular cavities.

- Extending the same approach for analysis of an Extended Tube Concentric Resonator (ETCR) muffler.

# References

[1] D. A. Bies and C. H. Hansen. Engineering Noise Control: Theory and Practice. 4th edition. Taylor & Francis, New York, 2009.

[2] M. L. Munjal. IISc lecture notes series, volume 3 - Noise and Vibration Control. World Scientific, 2013.

[3] S. Mang. Investigation of Performance Evaluation and Design Techniques for Large Industrial Mufflers 2013.

[4] F. C. Karal. The analogous acoustical impedance for discontinuities and constrictions of circular cross sectioin. *The Journal of the Acoustical Society of America* 25, (1953) 233–237.

[5] Sahasrabudhe A. D. and Munjal M. L. Analysis of inertance due to the higher order mode effects in a sudden area discontinuity. *Journal of Sound and Vibration* 185, (1996) 515–529.

[6] J. W. Sullivan. Analysis of concentric-tube resonators having unpartitioned cavities. *The Journal of the Acoustical Society of America* 64, (1978) 207.

[7] P. Chaitanya and M. L. Munjal. Effect of wall thickness on the end corrections of the extended inlet and outlet of a double-tuned expansion chamber. *Applied Acoustics* 72, (2011) 65–70.

[8] S. N. Panigrahi and M. L. Munjal. Backpressure considerations in designing of cross flow perforated-element reactive silencers. *Noise Control Engineering Journal* 55, (2007) 504.

[9] J. Fang, Y. Zhou, P. Jiao, and Z. Ling. Study on Pressure Loss for a Muffler Based on CFD and Experiment. *2009 International Conference on Measuring Technology and Mechatronics Automation* 887–890.

[10] D. C. Wilcox. Turbulence Modelling for CFD. 2nd edition. DCW Industries, Inc., 1994.

[11] S. Aliakbar, H. Keskar, and B. Venkatesham. Optimum Design Methodology for Extended Inlet and Outlet Muffler. *National Symposium on Acoustics 2015* .

[12] M. K. Au-Yang. Pump-induced acoustic pressure distribution in an annular cavity bounded by rigid walls. *Journal of Sound and Vibration* 62, (1979) 577–591.

[13] J. Kim and W. Soedel. General formulation of four pole parameters for three-dimensional cavities utilizing modal expansion, with special attention to the annular cylinder. *Journal of Sound and Vibration* 129, (1989) 237–254.

[14] W. Zhou and J. Kim. Formulation of Four Poles of Three-Dimensional Acoustic Cavities Using Pressure Response Functions with Special Attention to Source Modeling. *Journal of Sound and Vibration* 219, (1999) 89–103.

[15] Y.-H. Kim. Greens solution of the acoustic wave equation for a circular expansion chamber with arbitrary locations of inlet, outlet port, and termination impedance. *The Journal of the Acoustical Society of America* 94, (1993) 473.

[16] B. Venkatesham, M. Tiwari, and M. L. Munjal. Transmission loss analysis of rectangular expansion chamber with arbitrary location of inlet/outlet by means of Green's functions. *Journal of Sound and Vibration* 323, (2009) 1032–1044.

[17] Wikipedia. Transmission loss (duct acoustics).

[18] M. L. Munjal. Acoustics of Ducts and Mufflers. John Wiley & Sons, 2014.

[19] I. L.Ver and L. L. Beranek. Noise and Vibration Control Engineering. John Wiley & Sons, 2007.

[20] The MathWorks Inc. MATLAB and Statistics Toolbox Release 2015a 2015.

[21] Wolfram-MathWorld. Green's Function–Helmholtz Differential Equation–from Wolfram MathWorld.

[22] Wolfram Research, Inc. Mathematica 9.0 2012.

[23] SIEMENS PLM Software. LMS Virtual.Lab Rev. 13, 2013.

# Appendix A

# Solutions of integrations

## A.1 Integration over elliptic surface (I)

Surface integration over the side port area of the cavity is performed over an elliptic surface area of the port as follows:

$$
\begin{aligned}
I_1 &= \int_{\text{port i}} \cos\theta \cos(m\theta) \cos(k_{zp}z) \, dS_A \\
&= \int_{\text{port i}} \cos\theta \cos(m\theta) \cos(k_{zp}z) \frac{b}{2} d\theta dz \\
&= \frac{b}{2} \int_{-b_i}^{+b_i} \left( \int_{\theta_2 - \left(\frac{2a_i}{bb_i}\right)\sqrt{(b_i^2-\eta^2)}}^{\theta_2 + \left(\frac{2a_i}{bb_i}\right)\sqrt{(b_i^2-\eta^2)}} \cos\theta \cos(m\theta) d\theta \right) \times \cos[k_{zp}(\eta + l_i)] d\eta \\
&= \pi a_i b_i \cos(k_{zp}l_i) \times \left[ F_{mp}\left(\frac{1}{2}, \cos[(m-1)\theta_2] \times \frac{J_1(b_i\beta_{m-1,i})}{b_i\beta_{m-1,i}}\right) + \cos[(m-1)\theta_2] \times \frac{J_1(b_i\beta_{m+1,i})}{b_i\beta_{m+1,i}} \right]
\end{aligned}
$$

$$(A.1)$$

where

$\quad a_i$ is the maximum radius of the elliptic area $i$

$\quad b_i$ is the minimum radius of the elliptic area $i$

$\quad \beta_{m,i} = \sqrt{(\frac{2ma_i}{bb_i})^2 + k_{zp}^2}$

$$
F_{mp}\{x_1, x_2\} : \text{conditional function} = \begin{cases} x_1, & m = 1, \ p = 0 \\ x_2, & \text{otherwise} \end{cases}
$$

## A.2 Integration over elliptic surface (II)

$$I_2 = \int_{\text{port i}} \cos(m\theta) \cos(k_{zp}z) \, dS_A$$

$$= \int_{\text{port i}} \cos(m\theta) \cos(k_{zp}z) \frac{b}{2} d\theta dz$$

$$= \frac{b}{2} \int_{-b_i}^{+b_i} \left( \int_{\theta_2 - \left(\frac{2a_i}{bb_i}\right)\sqrt{(b_i^2 - \eta^2)}}^{\theta_2 + \left(\frac{2a_i}{bb_i}\right)\sqrt{(b_i^2 - \eta^2)}} \cos\theta \cos(m\theta) d\theta \right) \times \cos[k_{zp}(\eta + l_i)] d\eta$$

$$= 2\pi a_i b_i \cos(k_{zp}l_i) \cos(m\theta_2) Q_{mp} \left( \frac{1}{2}, \frac{J_1(b_i\beta_{m,i})}{b_i\beta_{m,i}} \right)$$

(A.2)

where

$$Q_{mp}\{x_1, x_2\} : \text{conditional function} = \begin{cases} x_1, & \text{m} = 0, \text{p} = 0 \\ x_2, & \text{otherwise} \end{cases}$$

## A.3 Integration in local polar co-ordinates

$$I_3 = \iint J_m(\kappa_{mn}r) \cos(m\theta) f(r, \theta) r \, dr \, d\theta$$

$$= \frac{2\pi a_i^2}{(\kappa_{mn}a_i + 2\mu_{mn})} \left( J_1(\kappa_{mn}a_i) + \mu_{mn} \right) J_m(\kappa_{mn}\delta) \cos(m\theta_i) \cos(k_{zp}l_i)$$

(A.3)

where

$$\mu_{mn} = \begin{cases} 1, & m = 0, \ p = 0 \\ 0, & \text{otherwise} \end{cases}$$

*Note 1: The functions $f(r, \theta)$ and $f(z, \theta)$ used in the derivation are assumed to be equal to 1.*

*Note 2: The term $C_{mn}Y_m(\kappa_{mn}r)$ can be neglected from the integral as the port area is not annular; but circular in cross-section.*

# Appendix B

# Creating a hexahedral mesh in ANSYS workbench

This chapter explains the procedure to create an hexahedral mesh for use in LMS Virtual.Lab. As explained earlier, an hexahedral mesh is computationally more efficient. Thus, an emphasis has been given on meshing using hexahedral elements to reduce computation time.

1. Open ANSYS ®workbench. Create a new project using the *Mechanical Model* under the *Project Schematic* window
   *Project Schematic → RMB → New Component Systems → Mechanical Model*
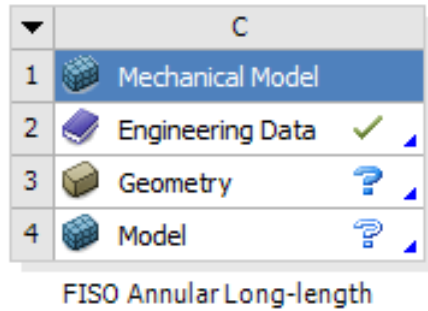


Figure B.1: Mechanical model

2. As shown in Fig. B.1, the *Engineering Data* is predefined and can be left as default. Open the *Geometry* tab to create the desired geometry.

3. The sketch for the annular cavity is shown in Fig. B.2. The dimensions are given according to the FISO long-length cavity model. Refer Fig. 3.3 and Sec. 5.3.3 for geometry dimensions. The inlet pipe will be constructed later for the ease of meshing. Using the *Extrude* command, extrude the following sketch to desired length (in this case 0.44 m). To create the outlet pipe, define a new plane at length 0.33 m. This plane will consist the sketch for the outlet pipe. Again, the *Extrude* command is used to extrude the outlet pipe section. The only difference is that the outlet pipe will be extruded upto the outer curved surface of the cavity.
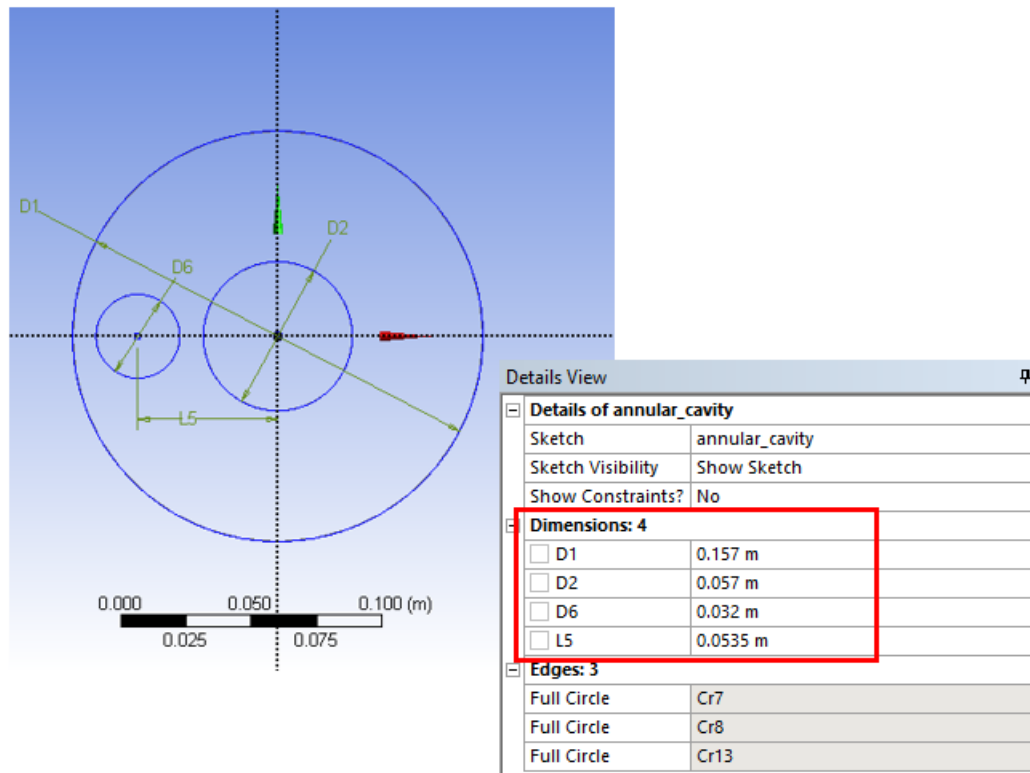
Figure B.2: Sketch for annular cavity
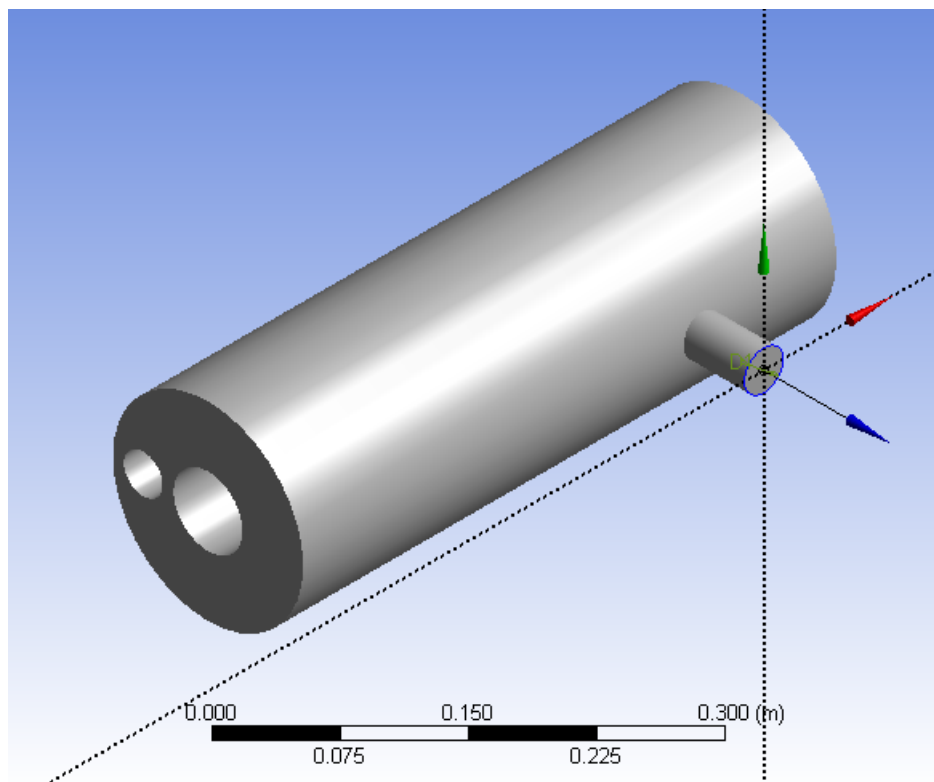


Figure B.3: Annular cavity with outlet
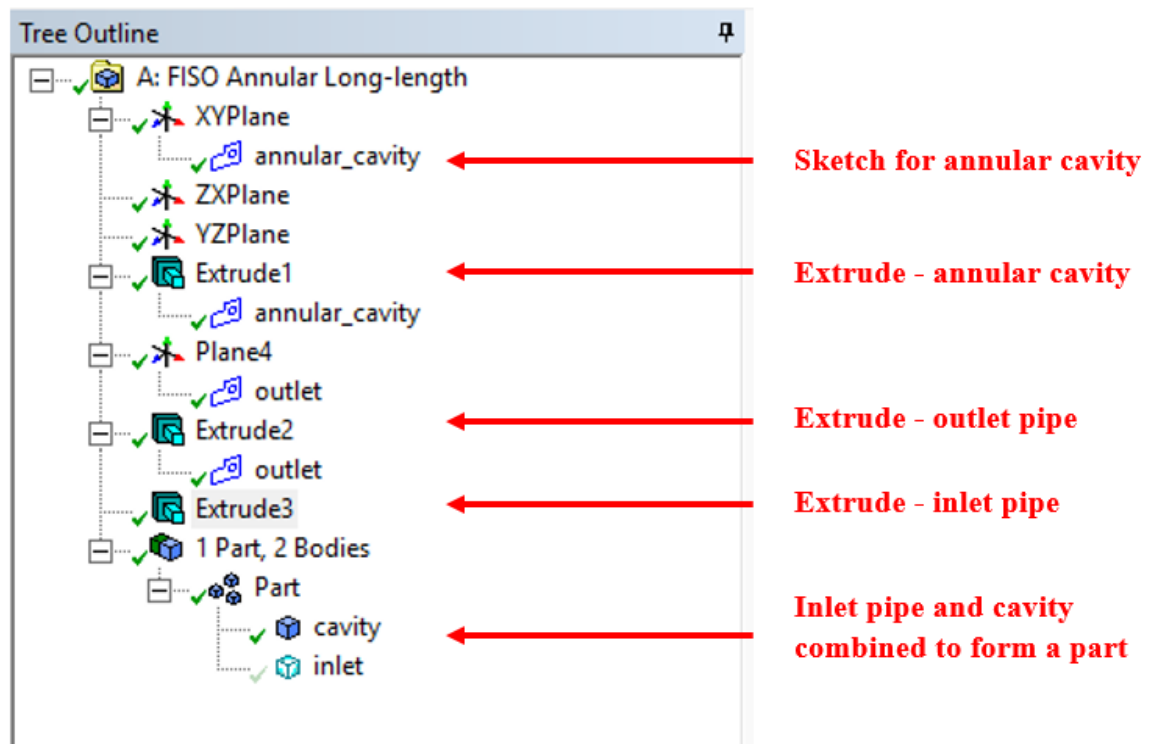
Figure B.4: The completed geometry tree
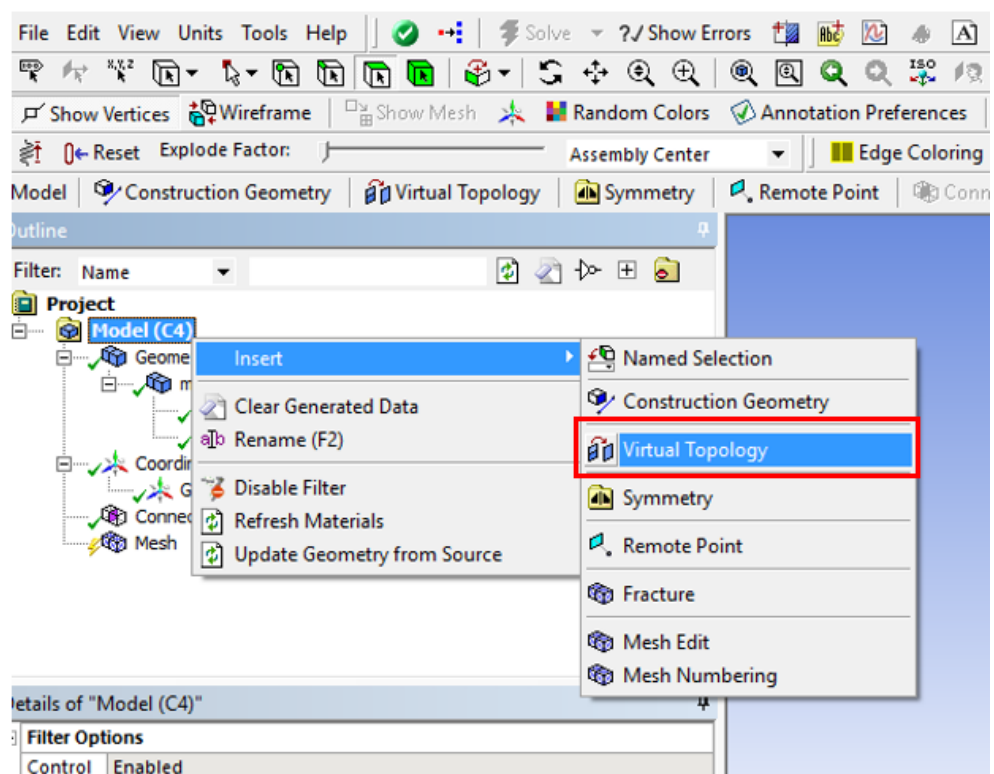


Figure B.5: Creating virtual topology

4. As shown in Fig. B.3, the annular cavity has a slot for the inlet pipe. To create the inlet pipe, select the slot edge on surface $S_C$ (refer Fig. 3.3) and use the *Extrude* command. Here, the operation *Add Frozen* is selected. Due to this option, the inlet pipe will be extruded as a separate body. Give the extrusion length as 0.5 m. After completing all the operations, the inlet pipe and the outlet pipe are combined together to form a new part. This makes sure that, although the inlet pipe is a separate body, it is a part of the annular cavity. The completed geometry tree will look like as shown in Fig. B.4. This completes the *Geometry* part of the module.

5. Now, the *Model* can be opened for meshing. (Refer Fig. B.1). The option of *Virtual Topology* is recommended for hexahedral meshing.
   *Model → RMB → Insert → Virtual Topology*
   This option enables the geometry to be split into a number of *Virtual Cells* by creating virtual vertices and splitting the edges. This becomes an important tool of use due to its property to split the geometry into several number of structured parts which is a feature of hexahedral mesh.
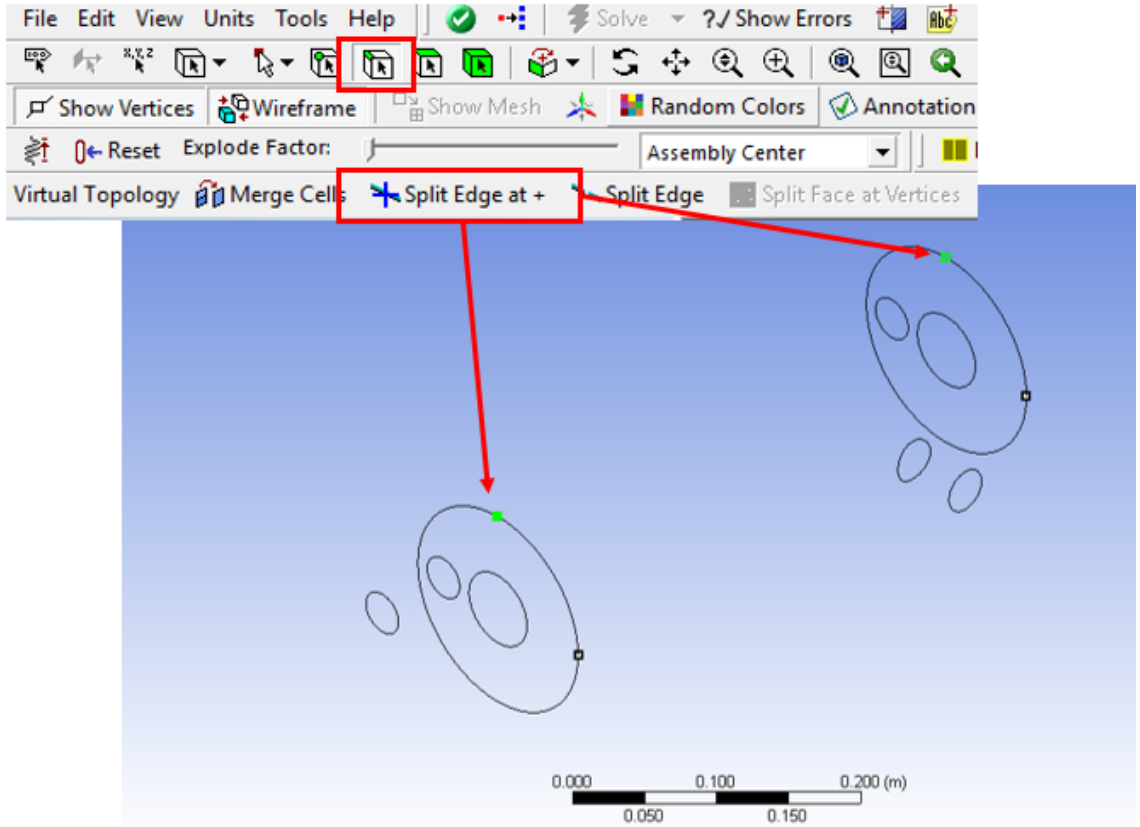


Figure B.6: Splitting the edge at "+"

6. Select the edge to be split. This will be denoted by a "+" symbol. Then, click on the *Split Edge at +* option as shown in Fig. B.6. Do this procedure for surfaces $S_B$ and $S_C$. Similarly all the edges can be split into different parts, as required. This operation will create virtual vertices which are then used to split the faces.
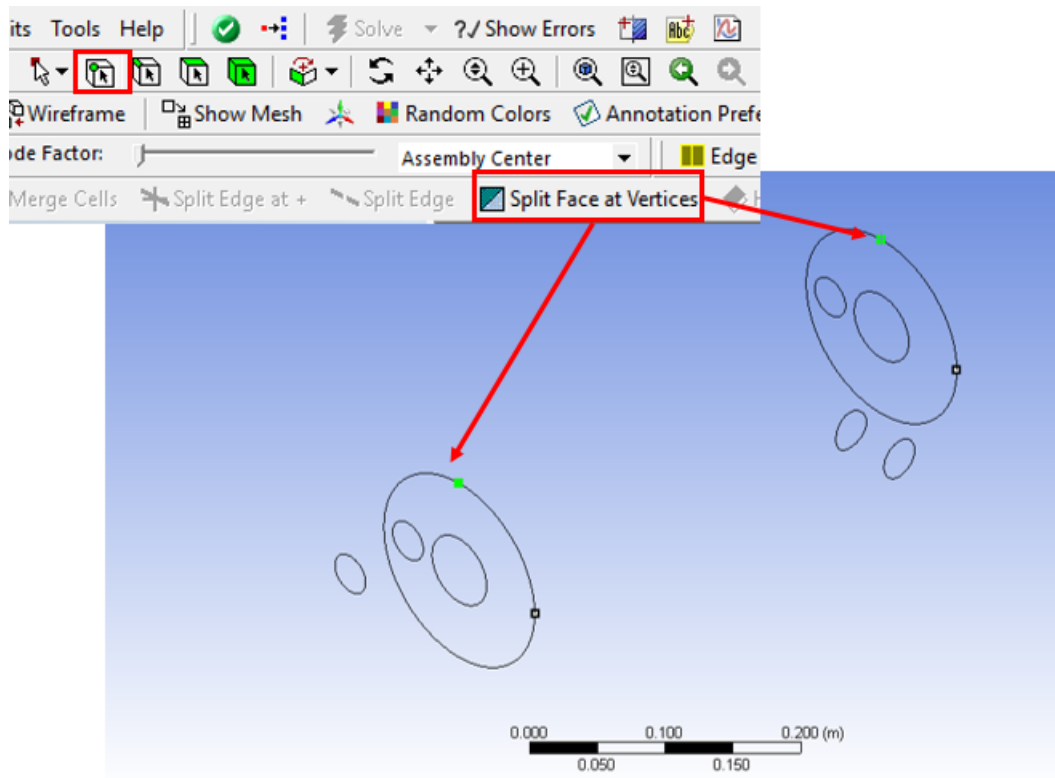
Figure B.7: Splitting the faces
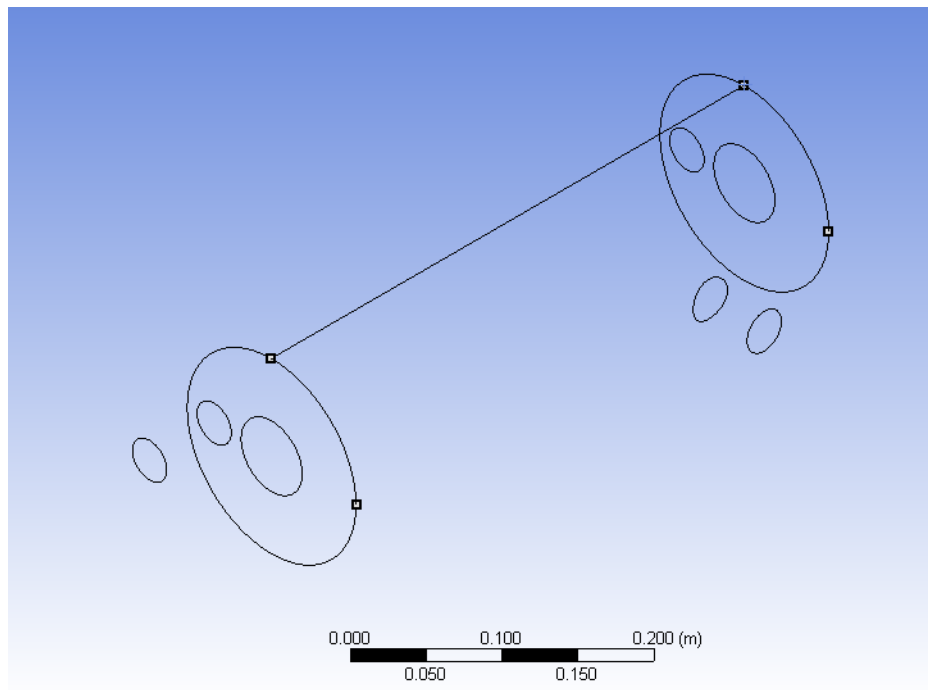


Figure B.8: Split curved surface $S_A$

7. Fig. B.7 shows the use of *Split Face at Vertices* command. After splitting the edges in the previous step, two virtual vertices will be formed. Select the two vertices at a time and click on the *Split Face at Vertices* button. This will split the curved surface $S_A$ into two different faces as shown in Fig. B.8. The above procedure is repeated for the complete geometry. The final stage, after splitting all the faces appropriately is shown in Fig. B.9 and Fig. B.10.
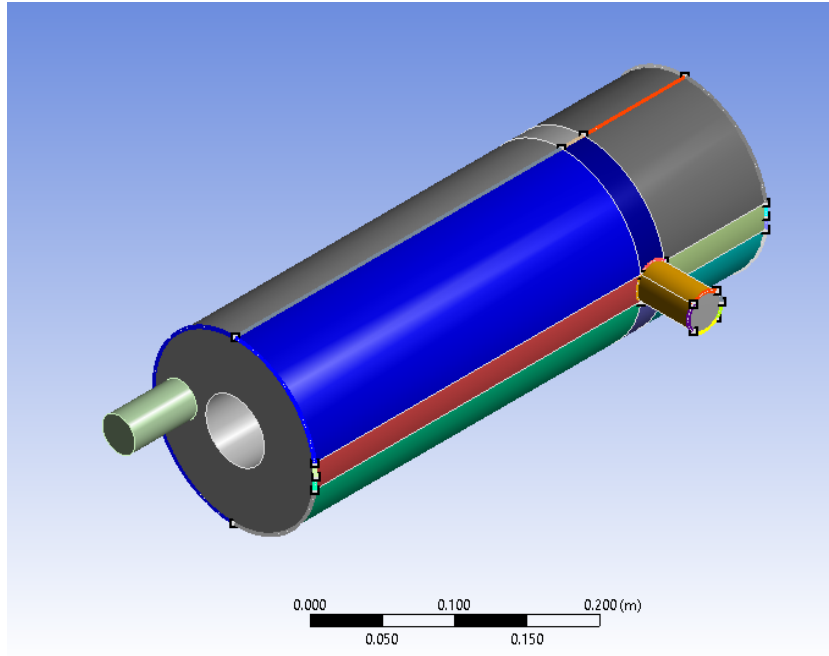


Figure B.9: Geometry split into faces (shaded exterior view)
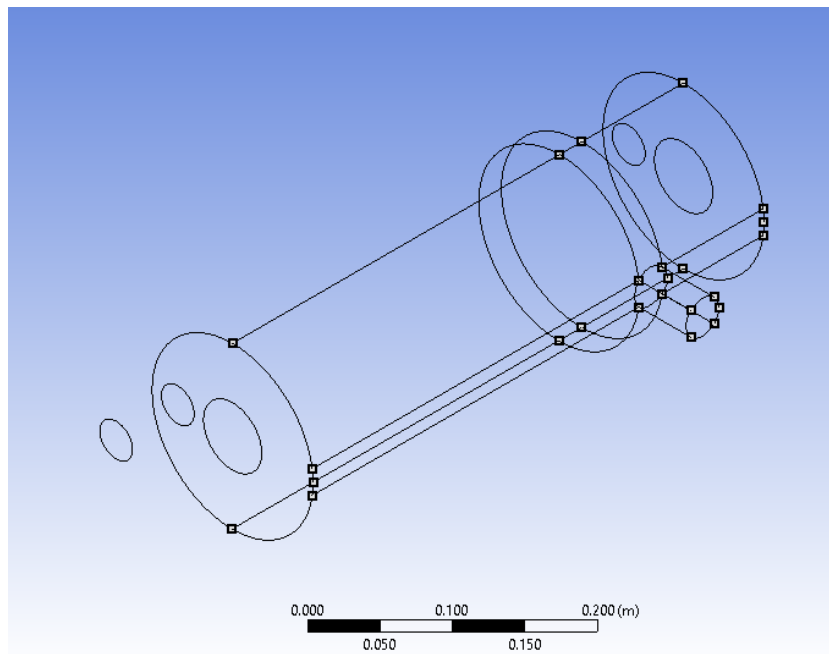


Figure B.10: Geometry split into faces (wireframe view)

8. The *MultiZone* method is a meshing tool which can be used to create a hexahedral mesh. The following steps will describe the procedure to define the parameters of this method.

   $Mesh \rightarrow Insert \rightarrow Method$
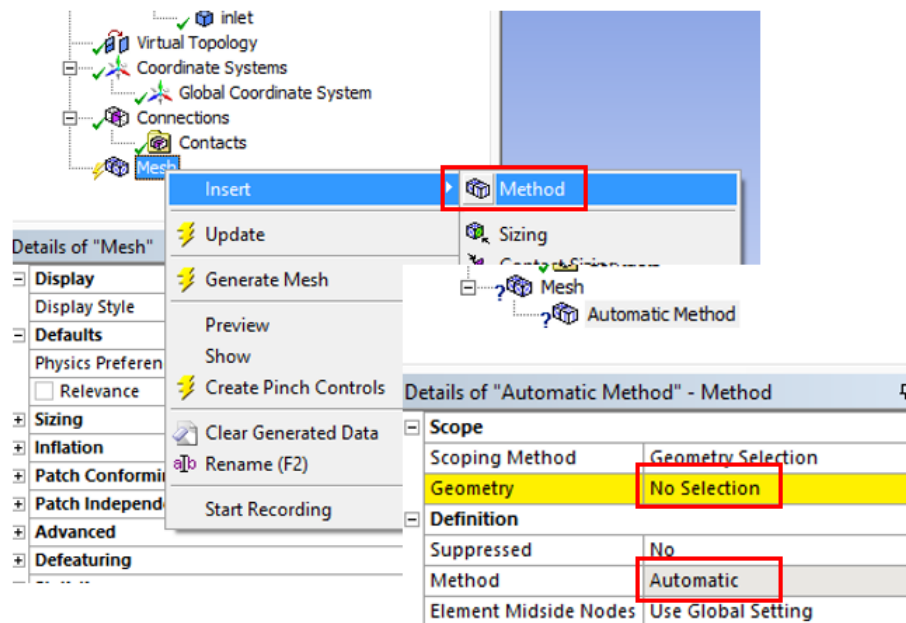


Figure B.11: Definition of multiZone method
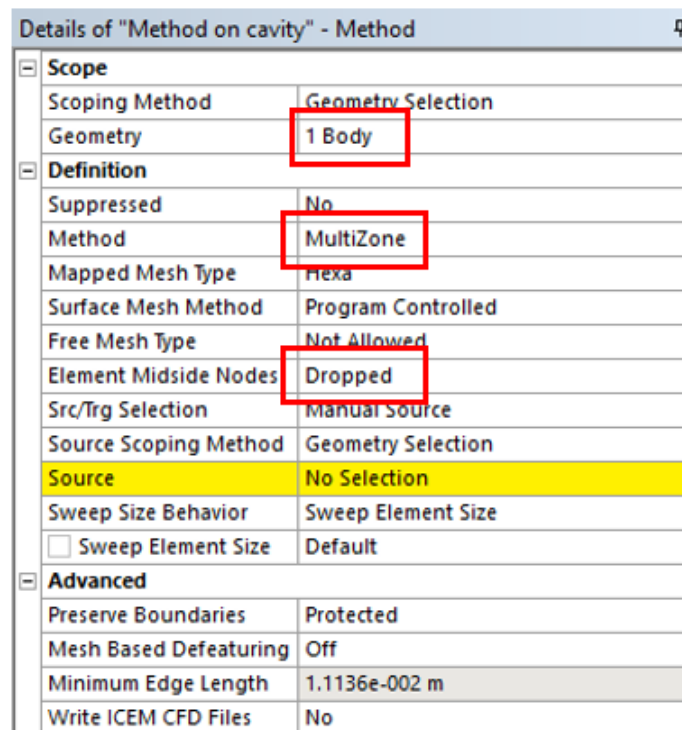


Figure B.12: MultiZone method for cavity

9. Fig. B.11 shows the definition of MultiZone method. Here, the geometry needs to selected for the method. Select the annular cavity and click *Apply*. The *Method* is changed to *MultiZone*. The *Element Midside Nodes* are dropped. The source and target selection is changed to select a manual source. Here, the end surfaces of the cavity ($S_B$ and $S_C$) are selected as the source. Rest of the parameters are left as default.

10. Similarly, another MultiZone method is defined for the inlet pipe. In this case, as the geometry is a simple cylinder, the source and target selection can be kept as automatic.
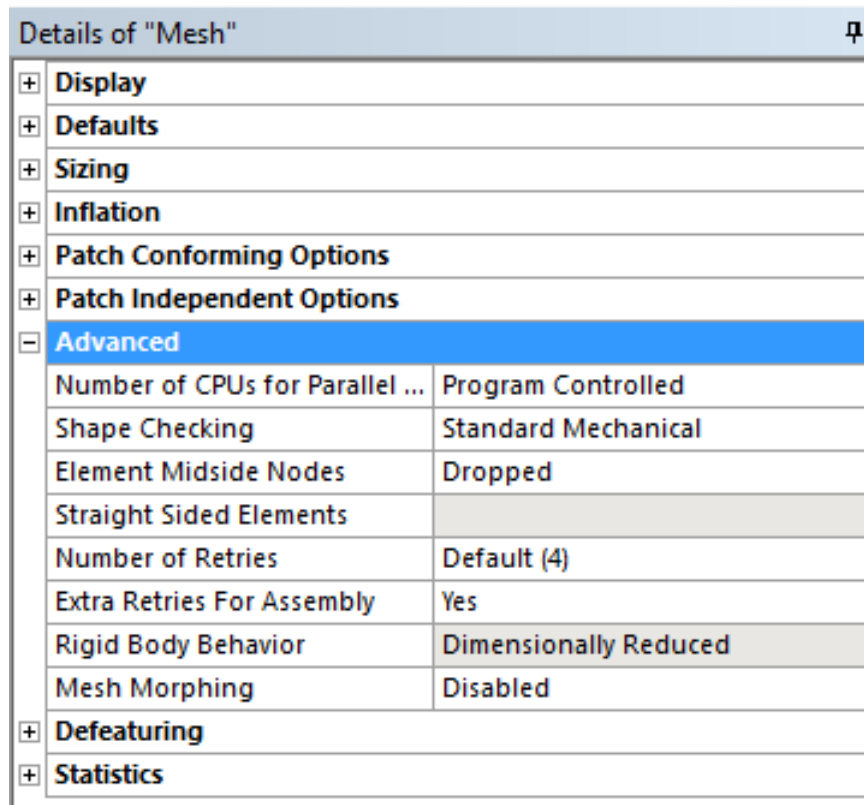


Figure B.13: Details of mesh

11. Fig. B.13 shows the detailed parameters of the mesh. The *Display* and *Defaults* options are set as default. The *Sizing* option consists of parameters which can be used to modify the element sizing, adjust the span angle, the relevance centre, etc.
The *Inflation* tab includes all the parameters required to define a inflation layer if required. These parameters are transition ratio, maximum layers, growth rate, etc. Inflation layers are particularly useful to capture the boundary layer effect by creating layers of fine elements near the boundary of the mesh.
The *Advanced* tab has the *Element Midside Nodes* option. This is a global setting for keeping or dropping the midside nodes. This is set to *Dropped*.
Apart from the meshing, there are also methods available for mesh control. These typically are the *Sizing*, *Inflation* and *Refinement* methods. These can be applied to faces or edges of a body as required.
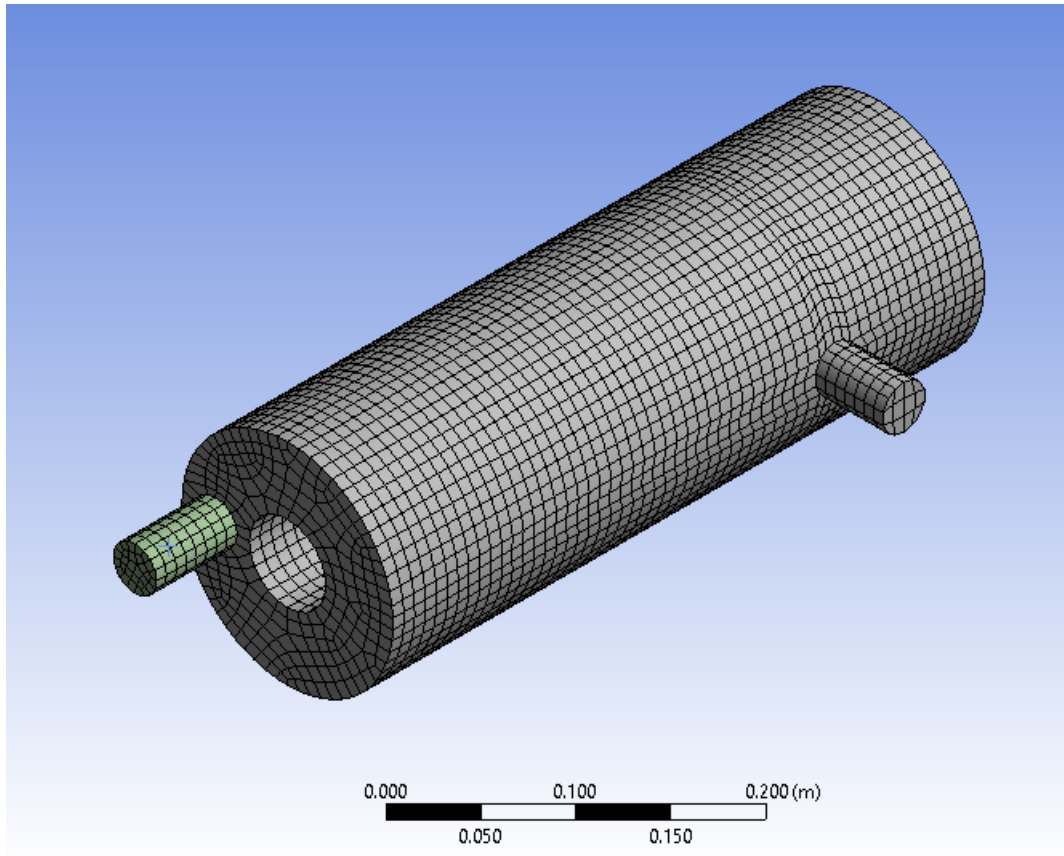
Figure B.14: The completed hexahedral mesh

12. After defining all the required parameters, update the mesh. Fig. B.14 shows the completed hexahedral mesh of the annular cavity. The inlet pipe being a separate body, is shown with a different colour.
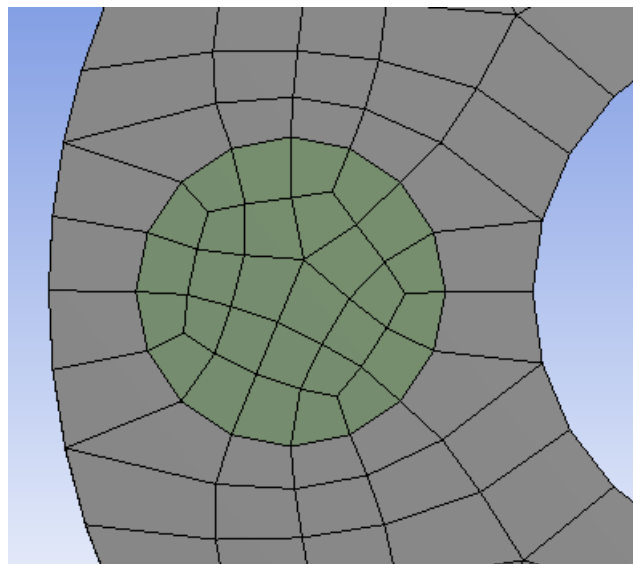


Figure B.15: Smooth connectivity

13. The inlet pipe, although being a separate body, has a smooth node-to-node connectivity with the annular cavity. The reason for this is shared topology. The inlet pipe shares its edge with the annular cavity. This makes it easier for the software to automatically adjust the position of nodes of two different bodies. Fig. B.15 shows the connectivity of the two bodies.
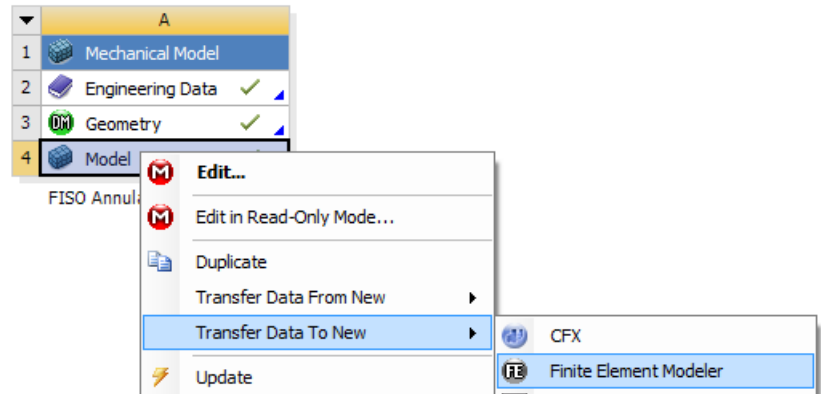


Figure B.16: The finite element modeler
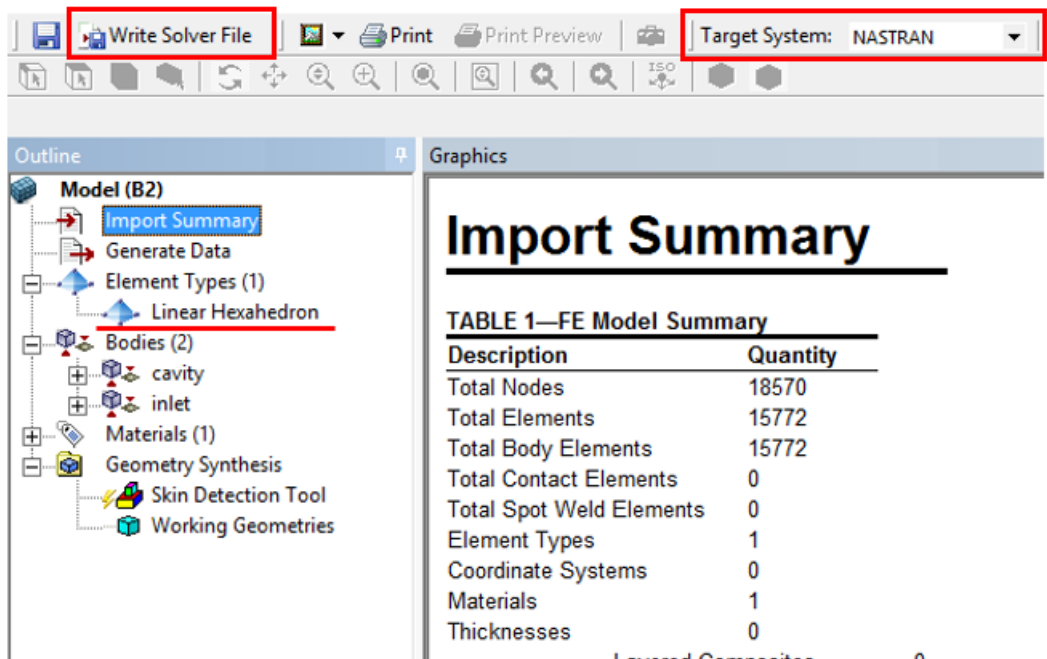


Figure B.17: Exporting the model for use in LMS Virtual.Lab

14. The finite element modeler is used to export the mesh in *.nas* format for analysis in LMS Virtual.Lab. As shown in Fig. B.16, transfer the model to finite element modeler and update the project. Fig. B.17 shows the import summary of the mesh. As indicated by the import summary, all the elements are of the same type i.e. linear hexahedrons. To export the mesh in *.nas* format, select the *Target System* as *NASTRAN*. Then click on *Write Solver File* and save the file to a desired location.

# Appendix C

# Calculation of transmission loss by LMS Virtual.Lab

This chapter explains the step-by-step procedure for calculation of transmission loss.

1. Open LMS Virtual.Lab. Start the Acoustic Harmonic FEM module. This will create a new analysis window with a pre-defined tree.
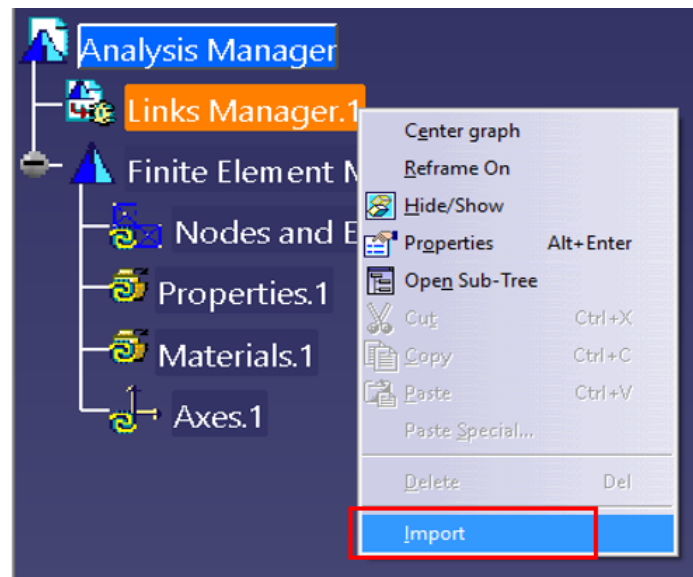   *Start → Acoustics → Acoustic Harmonic FEM*



Figure C.1: Importing the mesh

2. Import the desired mesh model with a compatible mesh file format as shown in Fig. C.1
   *Links Manager → RMB → Import*
   After selecting the desired file, a window will open as shown in Fig. C.2. Select the working units for *Length* and *Mass* as required. The rest of the units are preferably kept as defaults.

3. The imported mesh needs to be set as an acoustic mesh to carry out the acoustic analysis.
   *Nodes and Elements → Expand → (mesh-file-name) → RMB → Set Mesh Part Type → Set*
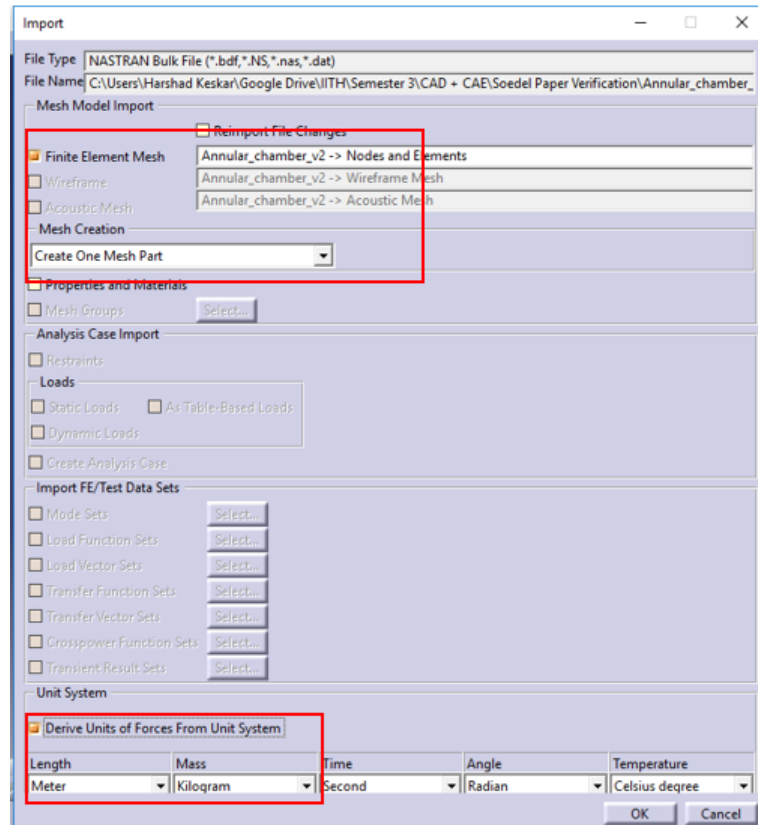
Figure C.2: Importing the mesh (2)
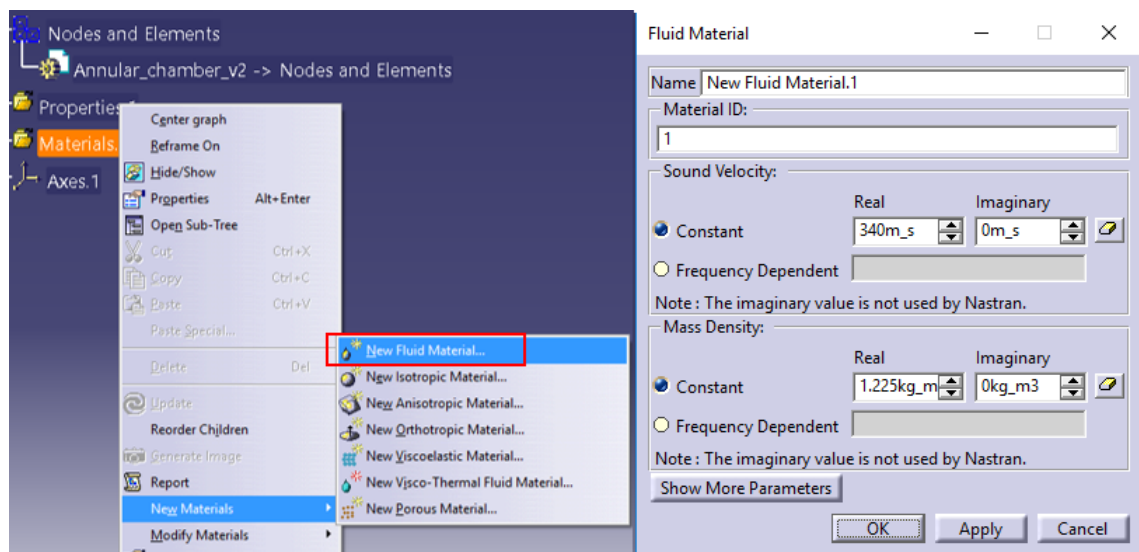


Figure C.3: Defining the acoustic material

*as Acoustical Mesh Part*

The displayed mesh changes its colour from green to blue after setting it as an acoustical mesh.

4. Define the acoustic material with properties *Sound Velocity* and *Mass Density*

*Materials* → *RMB* → *New Materials* → *New Fluid Material...*

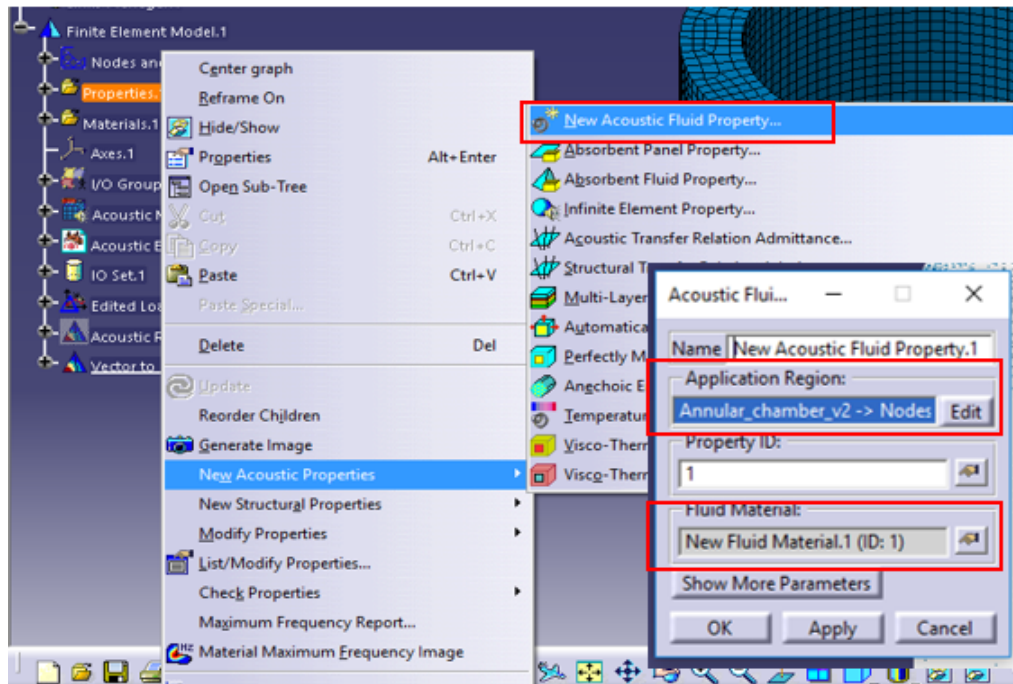A new window shows up to input the values of sound velocity and mass density as shown in Fig. C.3.



Figure C.4: New acoustic fluid property

5. The above created acoustic material needs to be assigned to the acoustic mesh. For this, a new acoustic fluid property has to be defined.

   *Properties* → *RMB* → *New Acoustic Properties* → *New Acoustic Fluid Property...*

   As shown in Fig. C.4, a small window will pop up. The *Application Region* is the acoustic mesh and the created material is applied in the *Fluid Material* selection.
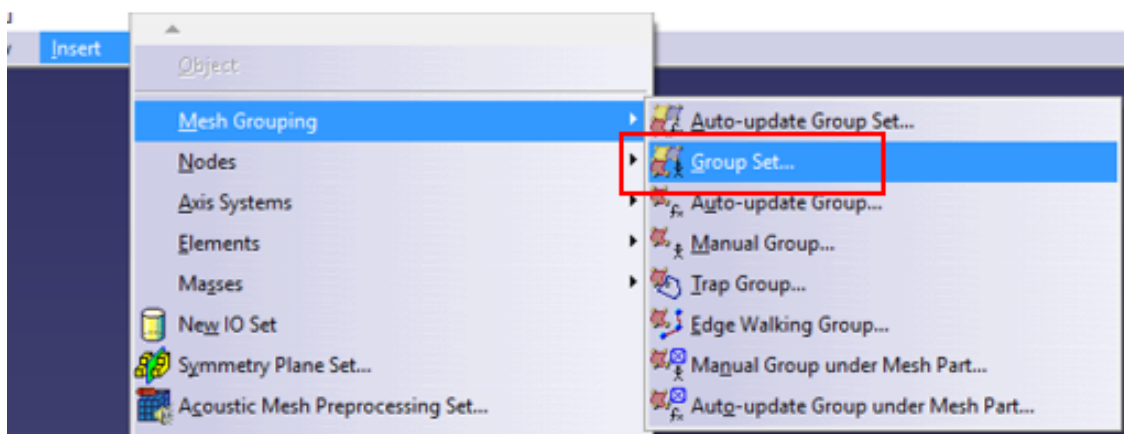


Figure C.5: Inserting a group set

6. The muffler cavity has an inlet and an outlet face. These faces need to be defined for further simulation. This can be done by inserting a group set in the tree as shown in Fig. C.5.
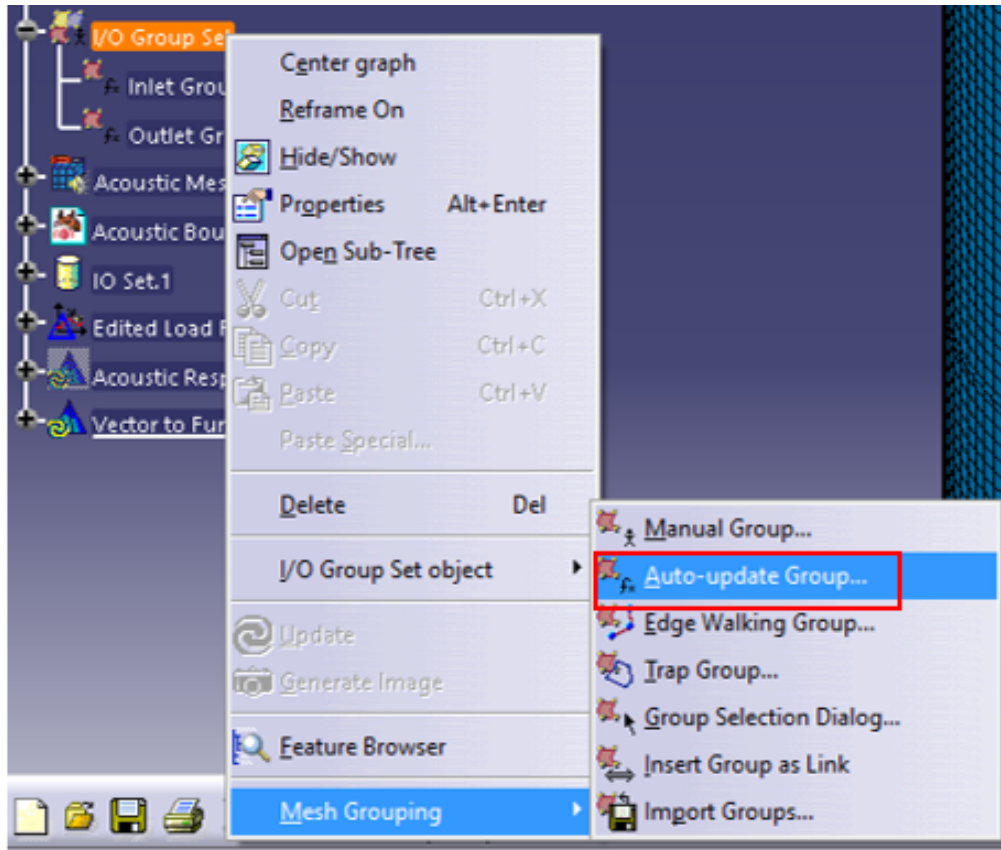   *Insert → Mesh Grouping → Group Set. . .*



Figure C.6: Creating a new group

7. New groups can be defined in the above created group set. Fig. C.6 shows the new group creation.
   *Group Set → RMB → Mesh Grouping → Auto-update Group. . .*

8. A new window will open to specify the type of the group to be defined. Here, under *Selection by Geometry* tab, *Feature Angle* method is selected. The inlet group parameters can be defined in the new window. As shown in Fig. C.7, under *Input Groups / Mesh Parts / CAD*, select the mesh under *Nodes and Elements* from the tree.
   The inlet face selection is done at the *Type Specific* tab. Here, the *Faces* option is selected to define the group. The *Feature Angle* is the angle between normals of two faces. By default, this value is 10 deg. From the displayed mesh, click on one of the faces on the inlet as a *Starting Element*. Then click on *Apply*. This will define the inlet group in the analysis tree. Follow the same procedure for the outlet group as shown in Fig. C.8.

9. Create the acoustic mesh preprocessing set.
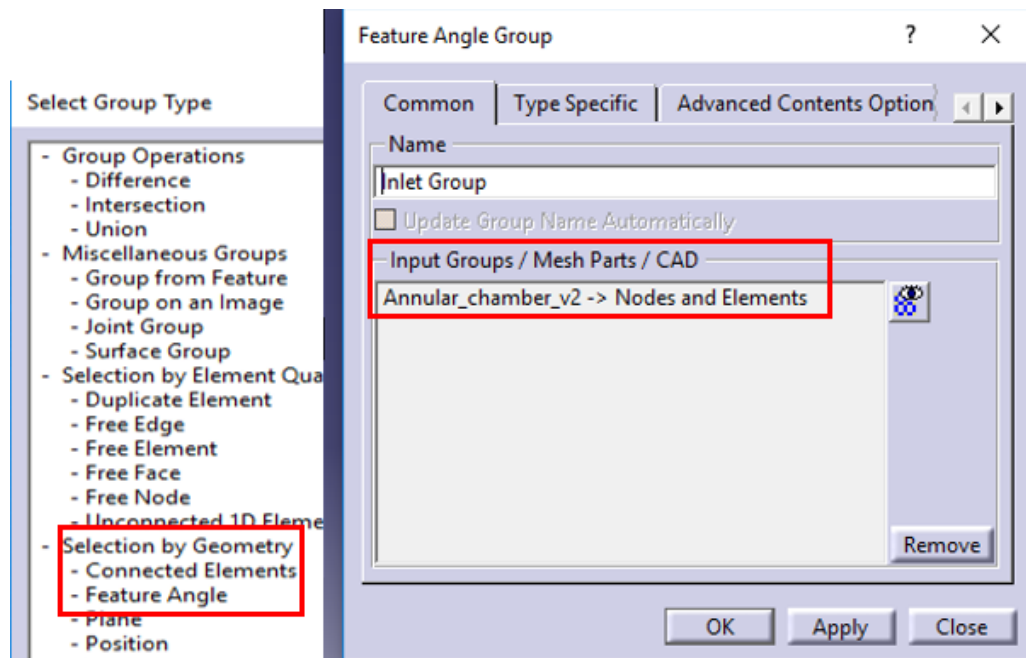   *Insert → Acoustic Mesh Preprocessing Set. . .*
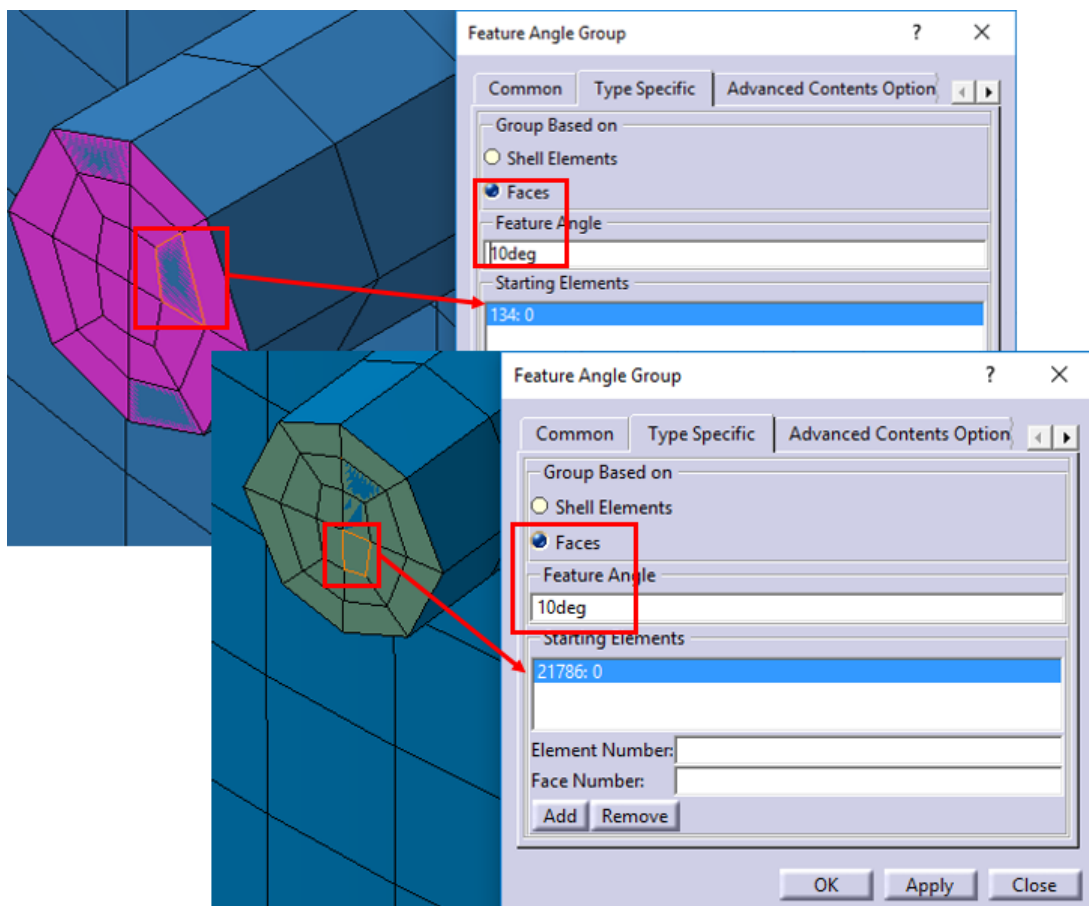
Figure C.7: Creating a new group (2)



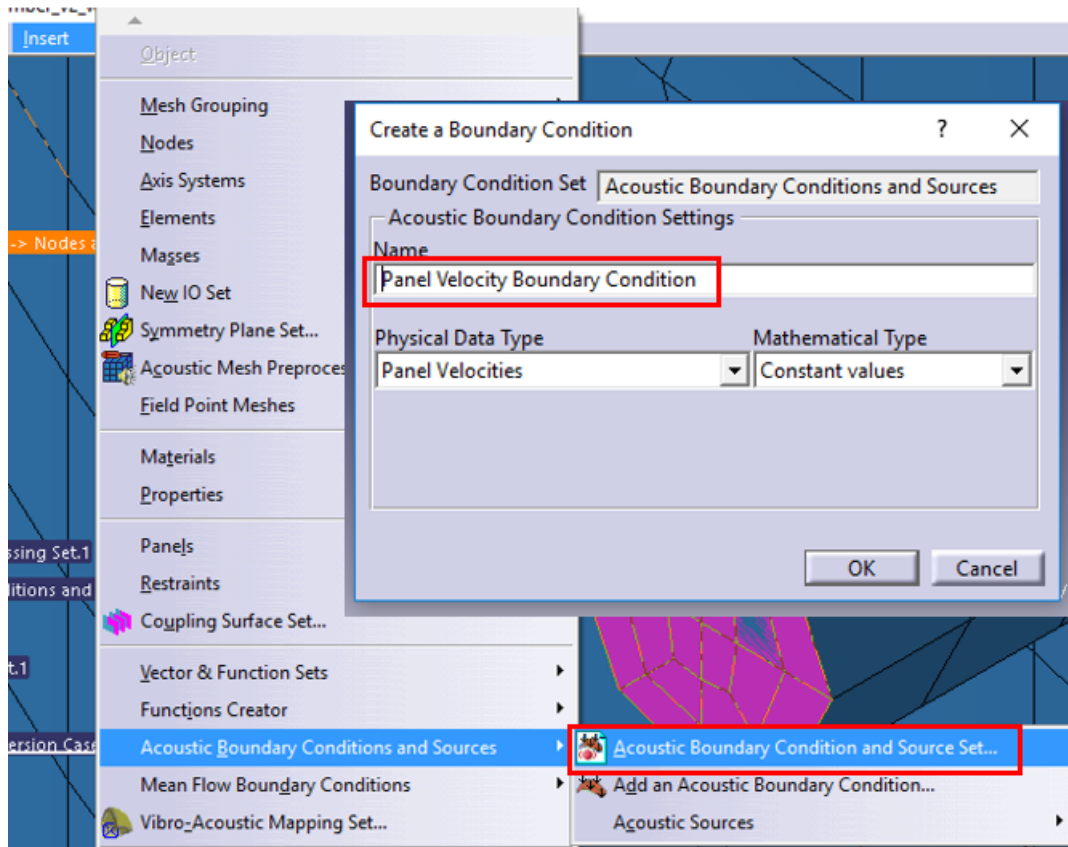Figure C.8: Defining the faces of the inlet and outlet groups

69

Figure C.9: Defining the boundary conditions

10. Proper boundary conditions must be given to the inlet and outlet faces. For this, a boundary conditions' set can be defined.
    *Insert → Acoustic Boundary Conditions and Sources → Acoustic Boundary Condition and Source Set...*
    In the simulation for transmission loss calculation, an input velocity (usually 1 $m/s$) is given. Thus, for the inlet face, a velocity boundary condition is defined. Locating the above created set in the analysis tree, a new boundary condition known as *Panel Velocity Boundary Condition* can be created as described in Fig. C.9.

11. After creating the *Panel Velocity Boundary Condition* the analysis tree will look as shown in Fig. C.10. In the *Faces* tab, the inlet face has to be selected as the application region of the velocity. The *Constant Values* tab specifies the magnitude of the velocity to be applied at the inlet. By default, the pre-set direction of velocity is into the inlet face (negative).
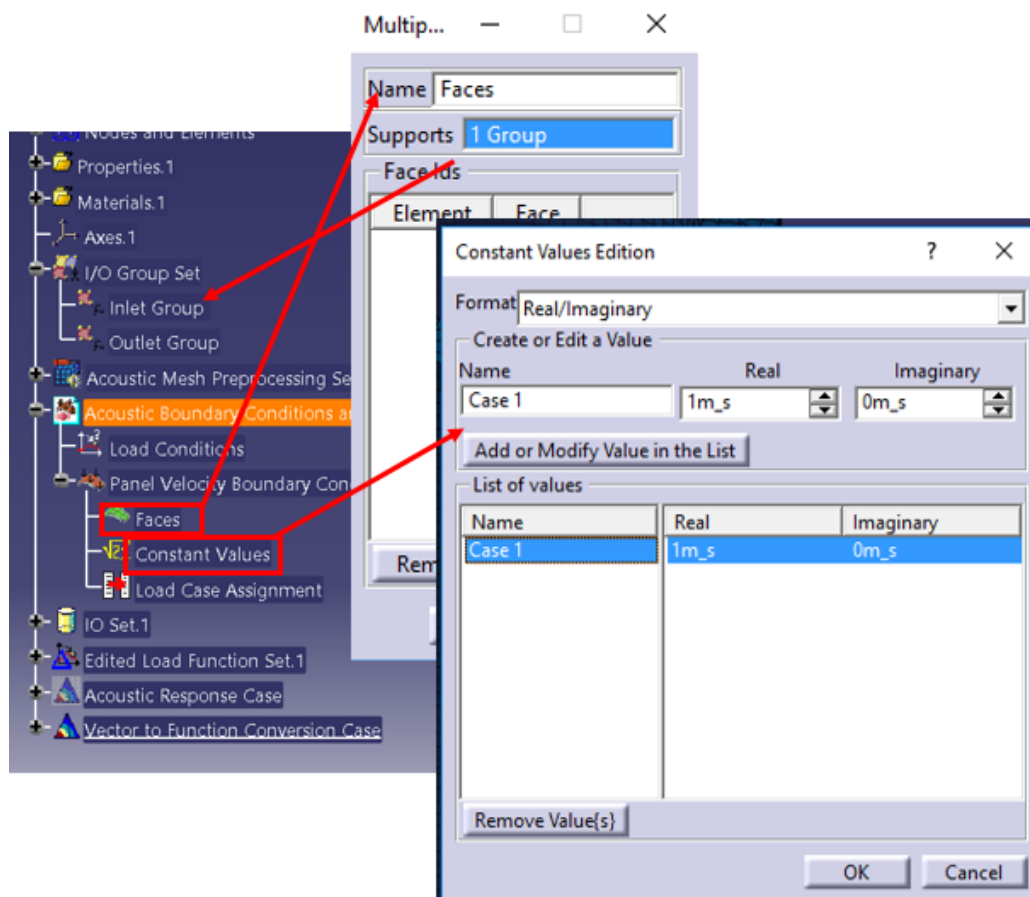
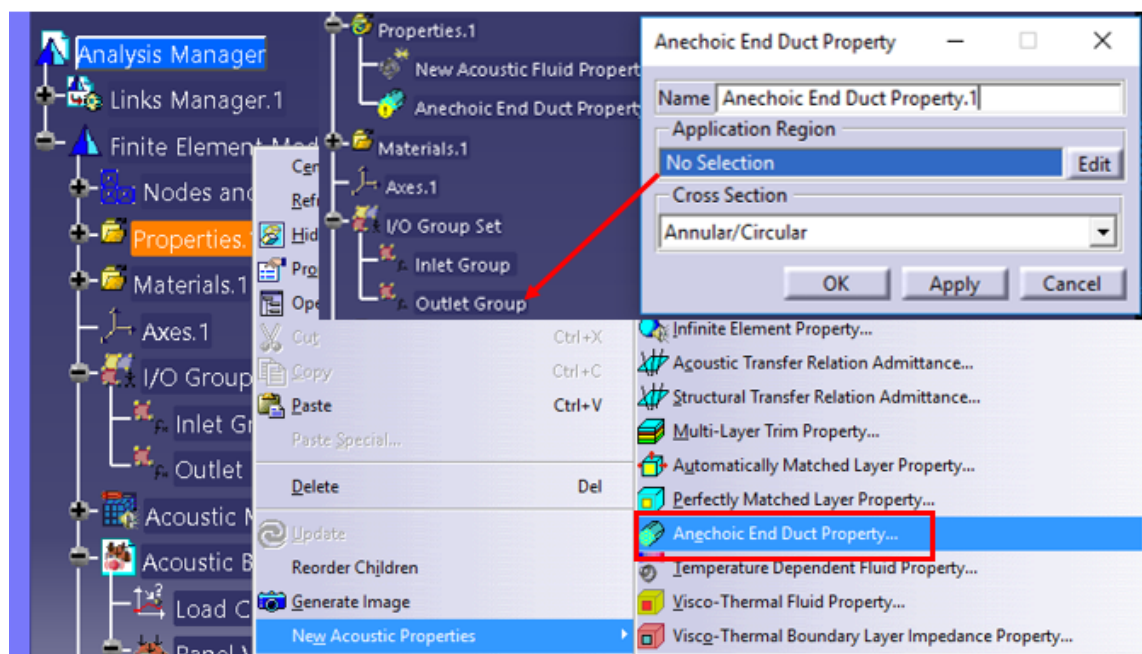Figure C.10: Defining the inlet boundary condition



Figure C.11: Defining the outlet boundary condition

12. For calculation of transmission the outlet is modelled with an anechoic termination. For this purpose, a new property is defined as the outlet boundary condition as shown in Fig. C.11.
*Properties → RMB → New Acoustic Properties → Anechoic End Duct Property...*
The *Application Region* is the outlet group defined in the analysis tree.

Note: This method of defining the outlet boundary condition is only applicable for circular/annular cross-sections. For other types of cross-sections, the *Absorbent Panel Property* is used. In this property the impedance value needs to be specified, which is the product of sound velocity and the mass density of the fluid.

13. This completes the pre-processing or the problem definition in the software. To solve the simulation, an analysis case known as *Acoustic Response Case* is created. The solution parameters of the case are enumerated in Fig. C.12.
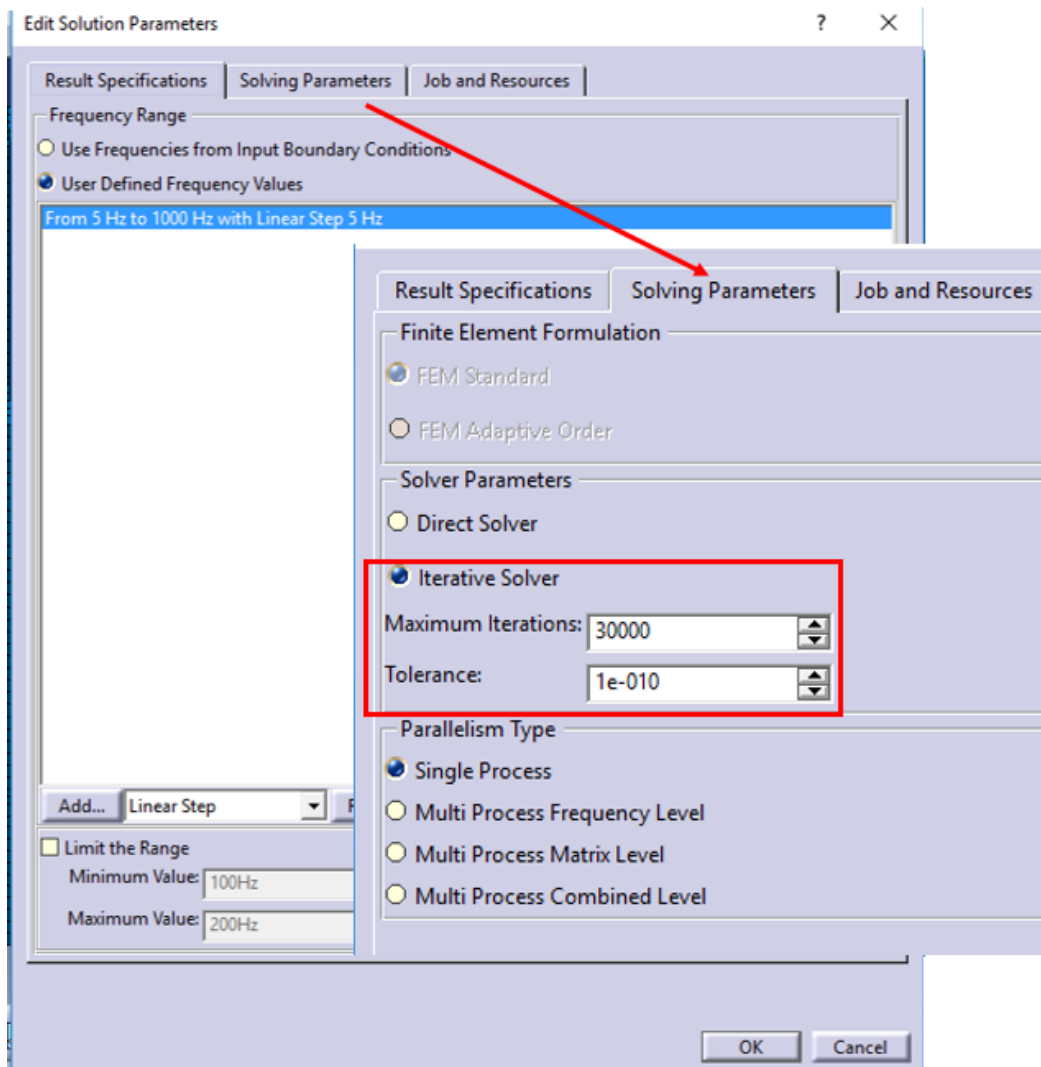*Insert → Acoustic Response → Acoustic Response Case...*



Figure C.12: Setting up the acoustic response case

14. The frequency range can be specified according to the users' requirement in the *Results Specifications* tab. Here the start value, the step size increment and the end value of the frequency needs to be defined.

    The *Solving Parameters* tab gives the choice for the type of solver and other multi-processing options.After setting up all the parameters, go to the analysis tree and start computing the solution.

    *Acoustic Response Case → Expand → Acoustic Response Solution Set → RMB → Update*
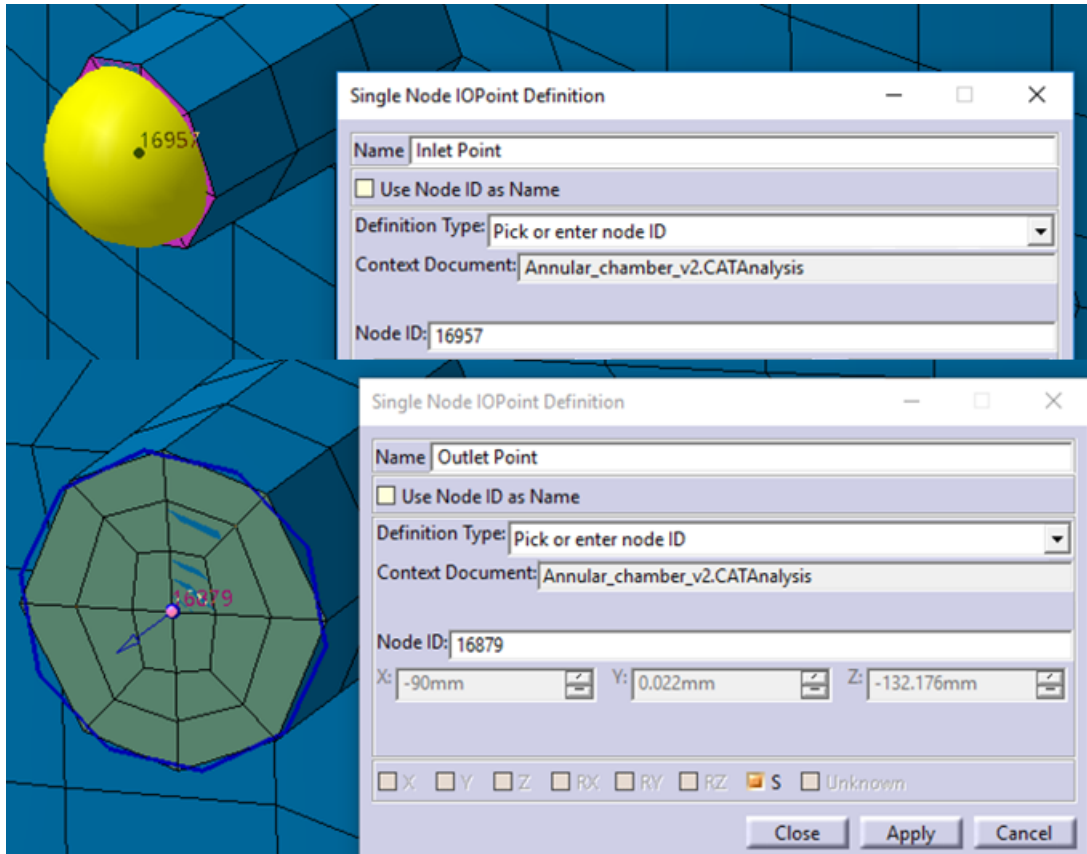


Figure C.13: Defining the IO set

15. The *Acoustic Response Case* calculates various properties like input power, acoustic power, radiation efficiency, absorptivity, etc. For further calculation, only the acoustic pressures at the inlet and outlet are required. To acquire these pressures, an *IO Set* needs to be defined.

    *Insert → New IO Set*

    *IO Set → RMB → Create Single IOPoint → New IOPoint...*

    Fig. C.13 shows how to pick a node ID on the corresponding face to create an IO point. These points will be used for calculation of acoustic pressure.
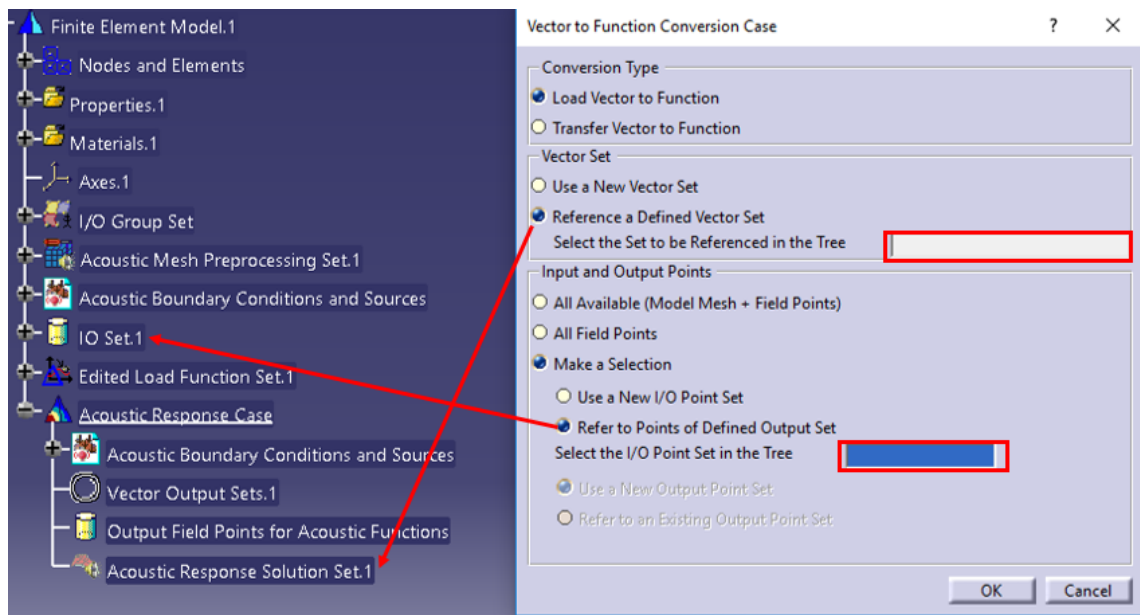
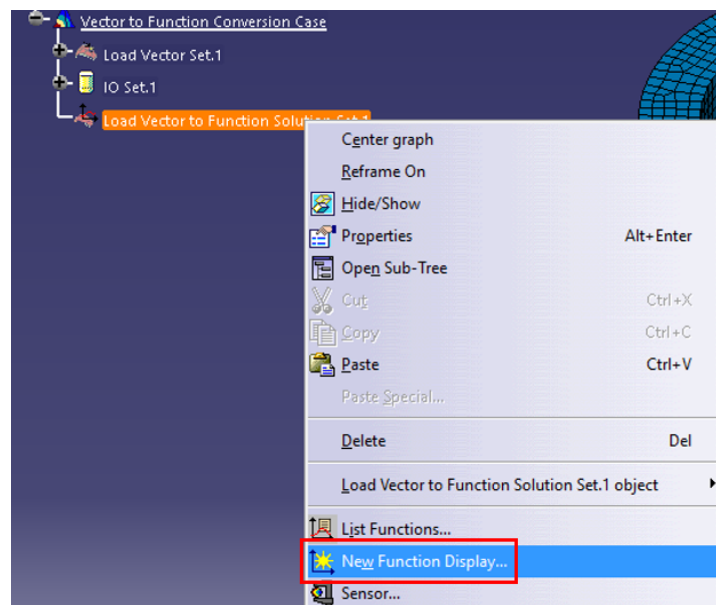Figure C.14: Creating a vector to function conversion case



Figure C.15: Plotting the acoustic pressures

16. A *Vector to Function Conversion Case* is used to convert the previously calculated properties to acoustic pressures at the inlet and outlet faces. Refer Fig. C.14.
    *Insert → Pre- and Post-Processing → Vector to Function Conversion Case...*
    *Vector to Function Conversion Case → Expand → Load Vector to Function Solution Set → RMB → New Function Display... → 2D Display → XY Plot* (Refer Fig. C.15).
    The values for acoustic pressure at inlet and outlet with real and imaginary components will be saved in the *Load Vector to Function Solution Set.*
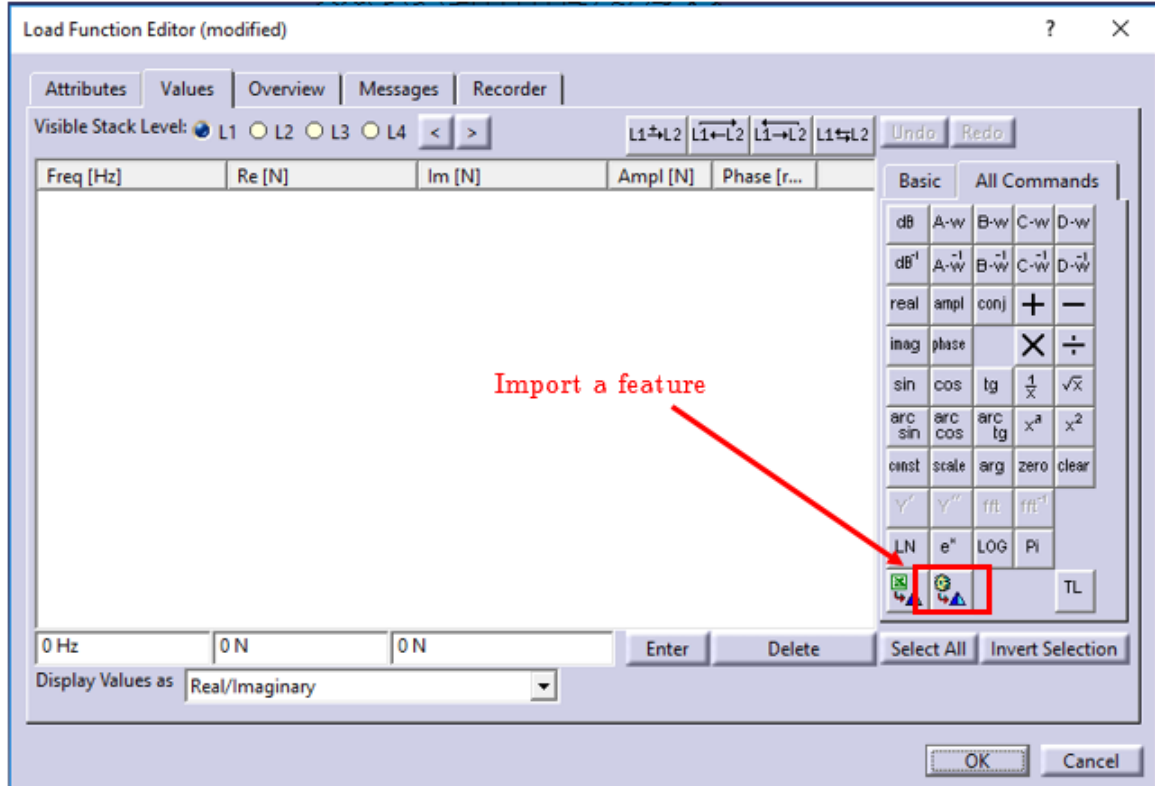
74

Figure C.16: The load function editor

17. The *Load Function Editor* is a tool used to calculate the transmission loss using the inlet and outlet acoustic pressures.

*Insert → Functions Creator → Edited Load Function...*

After selecting the above command, a new window will pop up. Click on the *Values* tab and select *Import a feature* as shown in Fig. C.16. Here the acoustic pressure needs to be imported. For this, select the *Load Vector to Function Solution Set* from the previously defined *Vector to Function Conversion Case* from the analysis tree. Fig. C.16 shows four stack levels L1 to L4. These will be used to store the acoustic pressure data. The transmission loss is calculated using Eq. C.1.

$$TL = 20 \log_{10} \left| \frac{P_{in} + \rho c V_{in}}{2 P_{out}} \right| \tag{C.1}$$

As stated before, the inlet velocity is considered negative by default setting. Thus, in the above formula $V_{in}$ will be equal to $-1$.

For ease of calculation, import the outlet pressure data first and multiply it by 2. Then, import the inlet pressure data, add $\rho c V_{in}$, and store in stack L1. This will be the numerator. The previous data in stack L1 will automatically move into stack L2. Then, using appropriate buttons according to the formula, arrive at the transmission loss values for the corresponding frequency values in a tabular form. The final edited function will look as shown in Fig C.17.
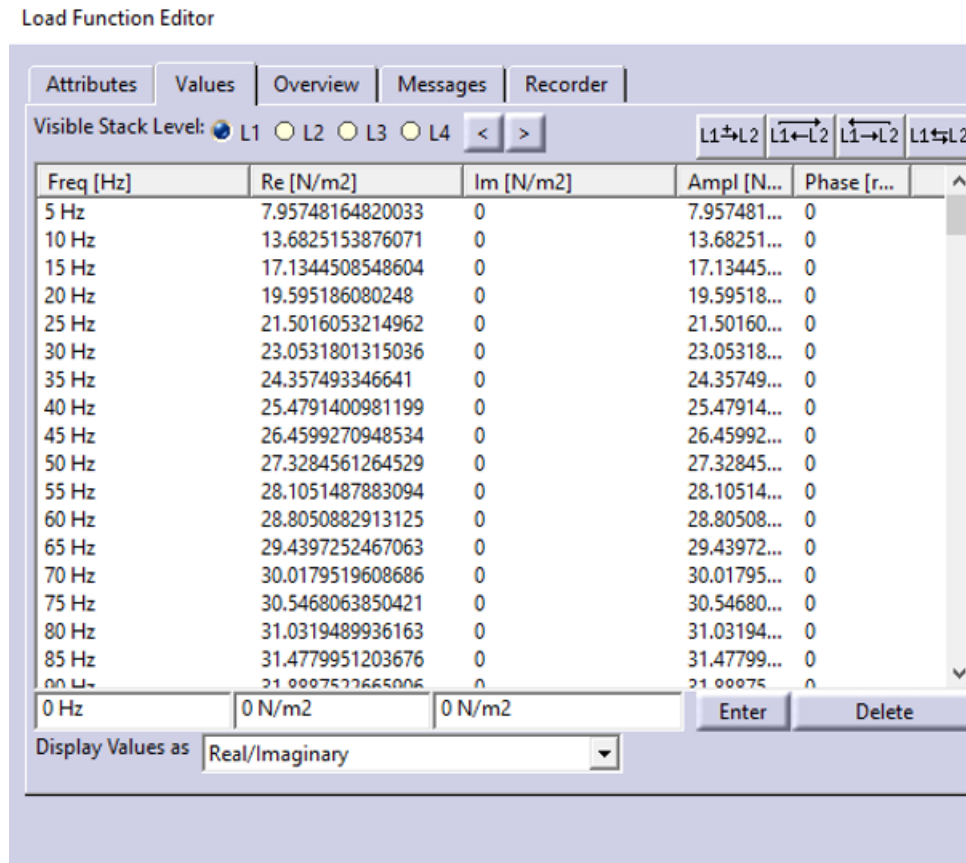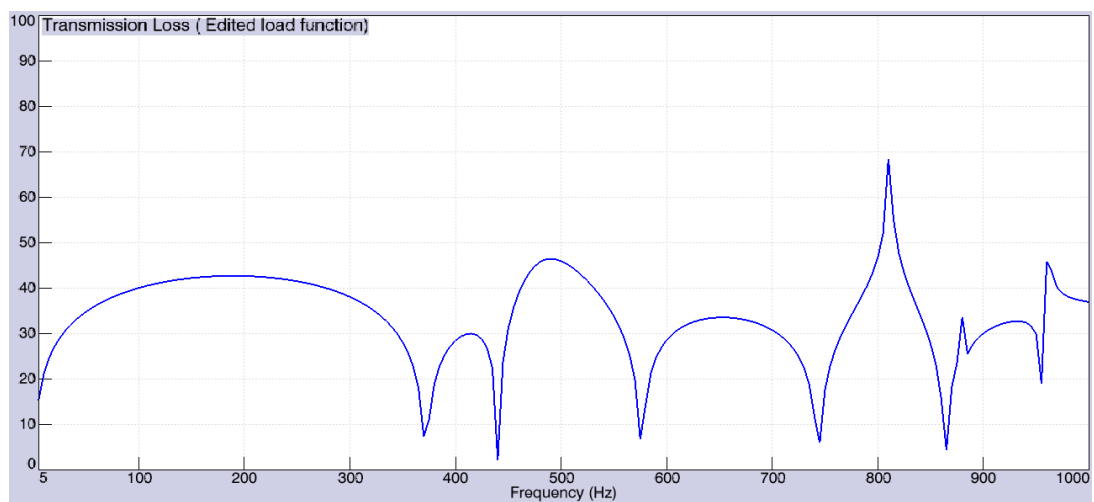
Figure C.17: Transmission loss values



Figure C.18: Transmission loss graph as a function of frequency

18. Plot the graph of transmission loss from the *Load Function Editor*.

    *Edited Load Function Set → Expand → Copy of Load Vector to Function Solution Set → RMB → New Function Display... → XY Display*